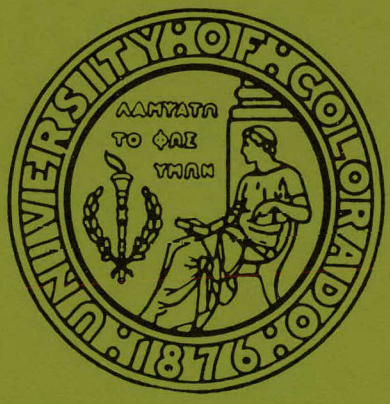

University of Colorado
Nuclear Physics Laboratory
Department of Physics
and Astrophysics

Technical Progress Report

Contract AT (11-1)-535

November 1, 1974
COO-535-710

DISCLAIMER

TECHNICAL PROGRESS REPORT

CONTRACT AT(11-1)-535

November 1, 1974

COO-535-710

TABLE OF CONTENTS

I. INTRODUCTION

This report summarizes the work carried out at the Nuclear Physics Laboratory of the University of Colorado during the period November 1, 1973, to November 1, 1974, under Contract AT(11-1)-535 between the University of Colorado and the United States Atomic Energy Commission.

A good deal of the work described in section II (Experimental Program) reflects the large influence of the theoretical group upon experimental studies. This close support has been a characteristic of the laboratory in previous years and continues to stand us in good stead.

Use of the rotating beam spectrometer facility (the swinger) has dominated the experimental studies this year. The improved resolution has allowed us to answer simple and fundamental nuclear structure questions which were heretofore obscured by unresolved multiplets. The neutron time-of-flight facility has allowed us to obtain a wide range of (^{3}He,n) data this year. This speed of data acquisition allows us to see global trends which stand out from the peculiarities of individual mass regions.

An increasing portion of our low-energy experiments either grows out of questions arising from medium-energy studies or supports proposed medium energy studies. Section B of this report details construction and field-mapping studies for EPICS which are carried out in Boulder.

This year's report reflects a continuing increase in our interaction with other research groups, both in the university and with other university and industrial research organizations. These collaborations include nuclear physics research, but also range from radiobiological studies to studies in support of deep space explorations.

The theoretical program has interacted strongly with the experimental work on the analysis and interpretation of two-step processes in transfer reactions. The paper on the (p,d)(d,n) contribution to the charge-exchange reaction was important in understanding the microscopic description of such reactions. Analogous two-step processes have been seen to be important in a wide variety of nuclear reactions reported here, including some in the medium energy field. Theoretical studies of intermediate energy proton and pion reactions are continuing, stimulated by the LAMPF facility.

II. EXPERIMENTAL PROGRAM

A. Nuclear Physics

1. Charged Particle Experiments

a. Single-Nucleon Transfer Reactions

i. A Study of the Higher Excited States of ^{10}Be from the ^{9}Be(d,p)^{10}Be Reaction - R. E. Anderson, J. J. Kraushaar, M. E. Rickey (on leave from Indiana University), and W. R. Zimmerman

Although much information about the low lying states of ^{10}Be is presently available from a variety of reactions, little is known of the properties of the higher lying states. Knowledge of the locations and properties of the higher lying states would be particularly useful in light of the recent data obtained[1] for the ^{9}Be(p,π^+)^{10}Be reaction.

The ^{9}Be(d,p)^{10}Be reaction was studied using 17.3 MeV deuterons and the emergent protons and deuterons were detected and separated with a counter telescope and standard particle identification electronics. Angular distributions over the range $10° \leq \theta_{cm} \leq 120°$ were obtained for the ground, 3.368, 5.958, 6.263, 7.37, 7.542, and 11.76 MeV states using a 2.60 mg/cm^2 ^{9}Be target. In addition, levels at 9.27, 9.40, and 10.57 MeV were identified but angular distributions could not be extracted. In order to obtain the natural line widths of some of these states, some spectra were also taken with a 240 μg/cm^2 target kindly supplied by R. H. Stokes of the Los Alamos Scientific Laboratory. A spectrum taken with the thin target is shown in the upper portion of fig. A1-a1.

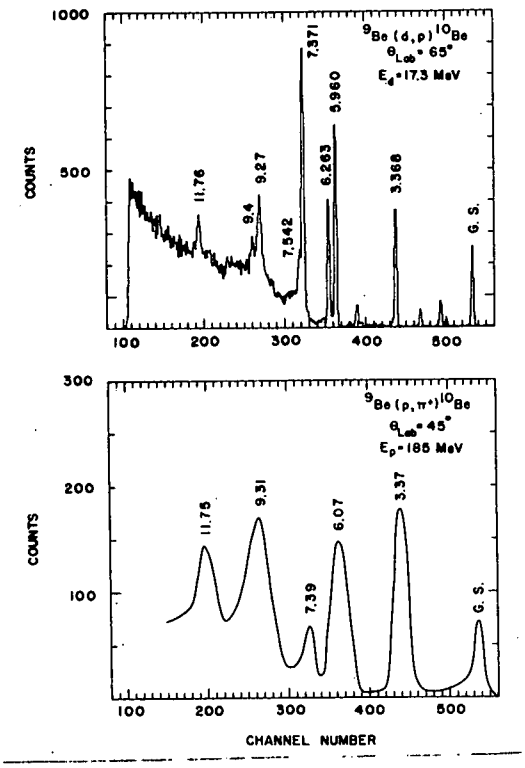

Fig. A1-a1. In the upper panel an energy spectrum is shown taken at 65° for the ^{9}Be(d,p)^{10}Be reaction. The energies shown, except for the state at 11.76 MeV, are from a data compilation. In the lower panel is shown an energy spectrum from the ^{9}Be(p,π^+)^{10}Be reaction at 185 MeV. The data are those of Dahlgren et al. (ref. 1) but have been replotted to conform with the ^{9}Be(d,p)^{10}Be energy scale.

DWBA calculations were carried out with the use of the code DWUCK using the deuteron parameters of Satchler.[2] Two sets of proton parameters were tried.[3,4] The experimental angular distributions along with the DWBA predictions are shown in fig. A1-a2 and fig. A1-a3. A better fit was obtained for the $^{9}Be(d,p_0)^{10}Be$ transition using the proton parameters of Perey[4] (set B) and these proton parameters were utilized for the remaining calculations. A satisfactory fit could not be obtained for the 11.76 MeV state. The spectroscopic factors obtained from this procedure are shown in table A1-I along with the predictions of Cohen and Kurath.[5] Spectroscopic factors obtained by Schiffer et al.[6] are also listed for comparison, and it can be seen that both the present work and that of Schiffer et al. yield values considerably below the theoretical predictions.

TABLE A1-I

Spectroscopic factors

Level Energy	J^{π}	ℓ_n	$S_{\ell j}$ (present work)	$S_{\ell j}$ (ref. 6)	Theo. $S_{\ell j}$ (ref. 5)	Percent $1p_{3/2}$ (ref. 5)
G.S.	0^+	1	0.94 (pot. A) 1.21 (pot. B)	1.67	2.357	100
3.368	2^+	1	0.17	0.24	0.274	17
5.958	2^+	1	0.54		0.421	47
6.263	2^-	0,2	0.33			
7.371	3^-	2	0.36			
7.542	2^+	1	0.20			

In addition to the single step DWBA analysis, a preliminary coupled channels analysis was performed for the $^{9}Be(d,p_0)^{10}Be$ transition. Using the code CHUCK only the 2.43 MeV state in ^{9}Be was considered in the coupling and the deuteron spin orbit potential was set to zero. The other optical parameters for both channels were identical to those used in the single step calculations. The results of the various calculations are shown in fig. A1-a4. Note that none of the calculations have been renormalized to the data. For calculation A the two spectroscopic factors have been set equal to 1.0 and for calculation B the spectroscopic factor for stripping from the 2.43 MeV state in ^{9}Be was reduced to 0.3. In calculation D the spectroscopic factor for stripping directly from the ground state of ^{9}Be was reduced to 0.3 and in calculation C this spectroscopic factor has been increased to 1.3. These results show that the calculation is most sensitive to the spectroscopic factor for stripping directly from the ^{9}Be ground state. In addition, the cross section is overestimated where the

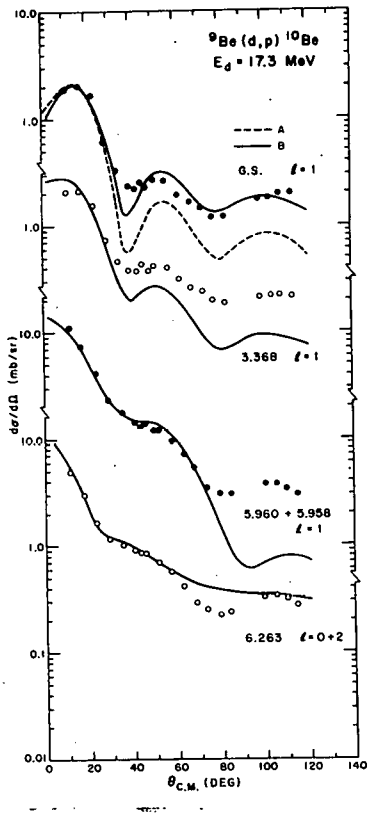

Fig. A1-a2. Experimental angular distributions for $^{9}Be(d,p)^{10}Be$. The relative uncertainties in the cross sections are generally smaller than the data points. The results of the DWBA calculations are shown as solid lines for proton parameters set A and as dashed lines for parameter set B.

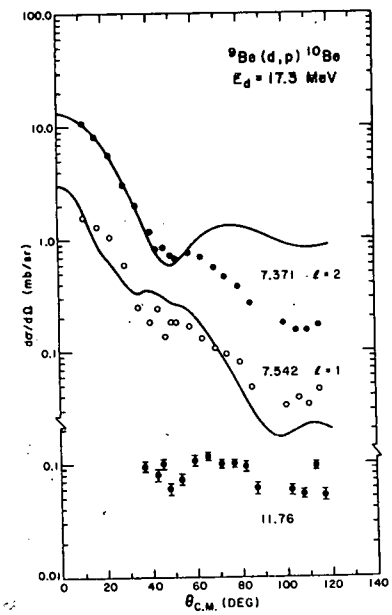

Fig. A1-a3. Experimental angular distributions for the higher excited states of ^{10}Be. The solid lines are the results of DWBA calculations.

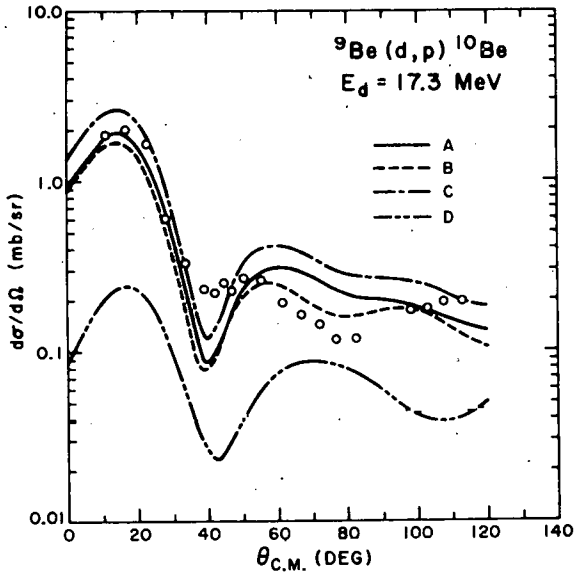

Fig. A1-a4. Comparison of experimental angular distributions for the ground state with various coupled channel calculations as detailed in the text.

spectroscopic factor obtained in the single step analysis is used thus indicating that perhaps a further reduction in the values listed in table A1-I is called for.

The natural line widths obtained in this work were 150±20, 291±20, and 121±10 keV respectively for the levels at 9.27, 9.4, and 11.76 MeV. In the bottom half of fig.a1 a spectrum obtained in the ^{9}Be(p,π^{+})^{10}Be reaction is shown for comparison with the present (d,p) work. The major differences appear to be the relatively weak population of the state at 7.37 and the relatively strong excitations of the states at 9.27, 9.4, and 11.76 MeV. One might expect a more exact correspondence on the basis of the one-nucleon model where a pion is emitted by the incoming proton and the neutron is captured into a vacant orbital. There could be a preferential population of the higher angular momentum states due to the greater angular momentum mismatch in the case of the (p,π^{+}) reaction, although this does not appear to agree with present observations.

This work is complete and has been submitted to Nuclear Physics for publication.

1 S. Dahlgren, P. Grafström, B. Höistad, and A. Åsberg, Nucl. Phys. A204 (1973) 53.
2 G. R. Satchler, Nucl. Phys. 85 (1966) 273.
3 B. A. Watson, P. P. Singh, R. E. Segel, Phys. Rev. 182 (1969) 977.
4 F. G. Perey, Phys. Rev. 131 (1963) 745.
5 S. Cohen and D. Kurath, Nucl. Phys. A101 (1967) 1.
6 J. P. Schiffer, G. C. Morrison, R. H. Siemssen, and B. Zeidman, Phys. Rev. 164 (1967) 1274.

ii. Proton Stripping on ^{24}Mg and ^{28}Si -
R. J. Peterson and R. A. Ristinen

The dominant background for the (^{3}He,t) reactions on ^{24}Mg and ^{28}Si reported in section II-A-1-c are the peaks from the (^{3}He,d) reaction. Ungated spectra were taken at each angle to subtract this background, and these ungated spectra have proven to provide useful data on the proton stripping to ^{25}Al and ^{29}P. Studies of the reaction mechanism at 38 MeV will be aided by the stripping to states of known Nilsson structure in ^{25}Al, and particularly to the $7/2^+$ state at 1.61 MeV. The angular distribution to this state is observed to peak at 20 deg, with a magnitude just 1% of the ground state strength. Analysis and DWBA interpretation are continuing.

5450

iii. Proton Spectroscopy of ^{105}Ag from the (^{3}He,d) Reaction - R. E. Anderson and J. J. Kraushaar

Multiple quasirotational bands built on $5/2^+$, $7/2^+$, and $11/2^-$ states have recently been reported[1] in ^{101}Pd, ^{103}Pd, and ^{105}Pd. Although the even-even cores of these nuclei display similar quasirotational structure[2] the well developed $5/2^+$ band in ^{101}Pd is not observed in ^{103}Pd and ^{105}Pd. Subsequent study[3] of the single-particle nature of the bandhead states with the (d,p) and (d,t) reactions showed that a close correlation exists between the existence of a quasirotational band and the single-particle purity of the bandhead state. This study showed that a pure single-particle state could act as a bandhead while fragmentation of the single-particle strength over several states resulted in breakup of the quasirotational band.

The neutron deficient silver isotopes ^{101}Ag, ^{103}Ag, and ^{105}Ag may be compared with ^{101}Pd, ^{103}Pd, and ^{105}Pd since they involve the same even-even cores but different valence particles. In this case the valence particle is a proton rather than a neutron and different single-particle orbits are thus involved.

The (^{3}He,d) reaction provides the means to observe the single-particle characteristics of some excited states of ^{105}Ag. In addition, there is no experimental information presently available for the existence or properties of excited states of ^{105}Ag other than the ground, 25 keV, and 53 keV states. Thus the $^{104}Pd(^3He,d)^{105}Ag$ reaction can provide much new knowledge in this area.

The $^{104}Pd(^3He,d)^{105}Ag$ reaction was studied with incident 33.24 MeV ^{3}He ions. The deuterons were detected in the energy-loss spectrometer. A typical spectrum is shown in fig. A1-a5. Peak areas and centroids were extracted from each spectrum and relativistic kinematics were used to obtain the appropriate excitation energies. The energy calibration was obtained by comparison with the $^{56}Fe(^3He,d)^{57}Co$ reaction. The excitation energies of the states of ^{57}Co were taken from the literature.[4]

The experimental angular distributions were compared with the

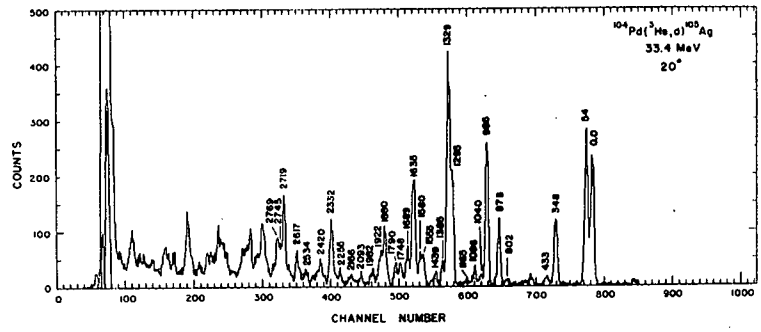

Fig. A1-a5. An energy spectrum taken at 20° for the $^{104}Pd(^{3}He,d)^{105}Ag$ reaction.

DWBA predictions in order to extract ℓ-values and spectroscopic factors. These comparisons are shown in figs. A1-a6, A1-a7, A1-a8, and A1-a9. The code DWUCK was utilized along with the optical parameters[5] of Auble et al. and the calculations included both non-locality and finite range corrections. The excitation energies and spectroscopic factors of the states of ^{105}Ag seen in the (^{3}He,d) reaction are seen in table A1-II. Since j values could not be determined in this experiment two values are quoted for each spectroscopic factor. The ground, 53 keV, 347 keV, and 876 keV states appear to exhaust all of the $p_{1/2}$, $p_{3/2}$, and $g_{9/2}$ strength in ^{105}Ag and the simple shell model predicts that the sum of their spectroscopic factors should be 4.0. However, from table A1-II, this sum is seen to be 2.3. When the local, zero range (LZR) approximation was utilized in making the DWBA calculations, this sum increased to 4.2. It may be that the LZR approximation to the DWBA yields a better description of absolute spectroscopic strengths for ^{105}Ag than does the DWBA with the non-local and finite range corrections.

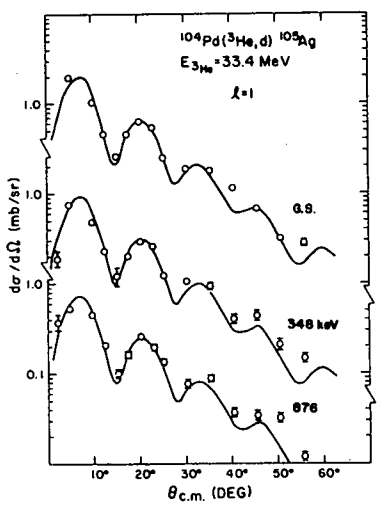

Fig. A1-a6. Angular distributions for states described by an ℓ-transfer of 1 seen for the $^{104}Pd(^{3}He,d)^{105}Ag$ reaction. The solid curves are the DWBA predictions.

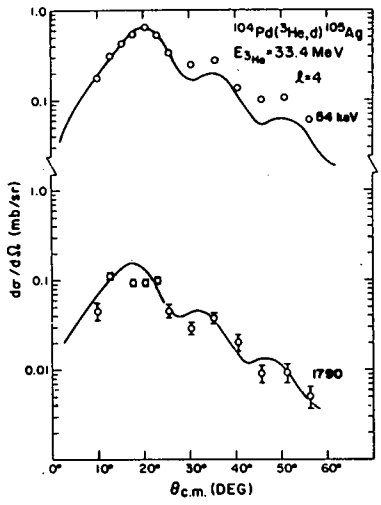

Fig. A1-a7. Angular distributions for those states described by an ℓ-transfer of 4.

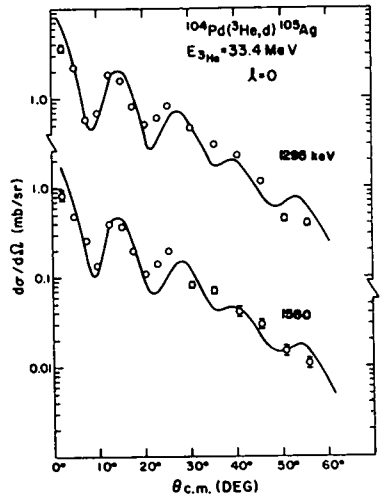

Fig. A1-a8. Angular distributions for those states described by an ℓ-transfer of 0.

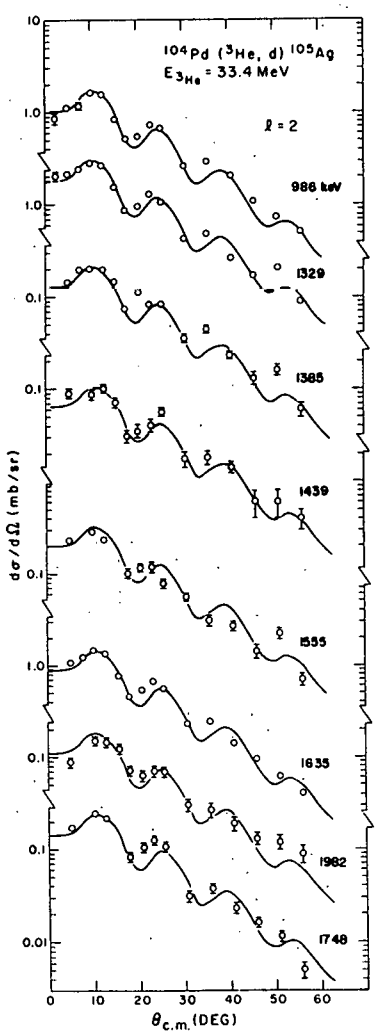

Fig. A1-a9. Angular distributions for those states described by an ℓ-transfer of 2.

TABLE A1-II

Summary of the information obtained for the levels of ^{105}Ag.

Energy	ℓ	J^π	$C^2S(2J+1)$	
			$J_<$	$J_>$
0.0	1	$1/2^-$	0.46	
53	4	$9/2^+$		1.57
348	1	$(3/2^-)$	(0.21)	0.16
433				
802				
876	1	$(3/2^-)$	(0.19)	0.14
986	2	$(5/2^+)$	(0.69)	0.52
1040				
1096				
1165				
1295	0	$1/2^+$		0.17
1329†	2		1.14	0.86
1385	2		0.08	0.06
1439	2		0.04	0.03
1555	2		0.12	0.09
1580	0	$1/2^+$		0.04
1635	2		0.16	0.12
1689				
1748	2		0.11	0.08
1790	4		0.45	0.23
1880	(4)		(1.21)	(0.61)
1922	(4)		(0.67)	(0.34)
1982	2		0.07	0.05
2093				
2166				
2255				
2332	(2,4)		{ 0.11 if 2	0.08 if 2
2420			{ 0.63 if 4	0.31 if 4
2534				
2617*				
2719*				
2745*				
2769*				

†This level appears to be a doublet at about 1327 keV and 1335 keV. Both transitions appear to be $\ell=2$.

*These levels are multiplets of predominantly $\ell=2$ character.

An interesting comparison can be made with the studies[5,6] of the $^{106,108}Pd(^{3}He,d)^{107,109}Ag$ reactions. There is a progressive lowering of the excitation energies of analogous states in going from ^{105}Ag to ^{107}Ag and finally to ^{109}Ag. For example, the strong lowest lying $\ell=2$ transitions are seen with the same spectroscopic strengths in all three of these residual nuclei. However, the excitation energy for this state drops from 986 keV in ^{105}Ag to 911 keV in ^{107}Ag to 727 keV in ^{109}Ag. Similar behavior can be noted for other analogous states seen in these nuclei.

In terms of the possible existence of quasirotational bands in ^{105}Ag, the strong single particle states are the ones of importance. The $\ell=2$ strength appears to be spread over many states. Even if one were to assume that the 986 and 1327 keV transitions represent different single particle orbitals (i.e. $d_{3/2}$ and $d_{5/2}$) then about 82% of the $\ell=2$ strength is still missing. Similarly, the 1295 and 1580 keV transitions constitute only a small fraction of the available $3s_{1/2}$ strength. Finally, the $p_{3/2}$ strength is most likely split evenly between the 347 and 876 keV levels (systematics observed in ^{107}Ag and ^{109}Ag suggest that these levels have a spin-parity of $3/2^-$). Thus the only likely candidates for quasirotational bandhead states in ^{105}Ag are the ground and 53 keV states which contain all the available $p_{1/2}$ and $g_{9/2}$ strengths respectively.

---

1 F. A. Rickey and P. C. Simms, Phys. Rev. Lett. 31 (1973) 404.
2 G. Scharff-Goldhaber, M. McKeown, A. M. Lumpkin, and W. F. Piel, Jr., Phys. Lett. 44B (1973) 416.
3 F. A. Rickey, R. E. Anderson, and J. R. Tesmer, to be published.
4 B. Rosner and C. H. Holbrow, Phys. Rev. 154 (1967) 1080.
5 R. L. Auble, F. E. Bertrand, Y. A. Ellis, and D. J. Horen, Phys. Rev. C 8 (1973) 2308.
6 R. E. Anderson, R. L. Bunting, J. D. Burch, S. R. Chinn, J. J. Kraushaar, R. J. Peterson, D. E. Prull, B. W. Ridley, and R. A. Ristinen, to be published.

54,451

iv. A Study of the $^{106}Pd(p,d)^{105}Pd$ and $^{106}Pd(^{3}He,d)^{107}Ag$ Reactions — R. E. Anderson, R. L. Bunting, J. D. Burch, S. R. Chinn, J. J. Kraushaar, R. J. Peterson, D. E. Prull, B. W. Ridley, and R. A. Ristinen

In one of the initial investigations with the energy-loss spectrograph a series of reactions was investigated to provide information about the excited states of ^{106}Ag. In order to obtain energy calibration data for the $^{107}Ag(p,d)^{106}Ag$ and $^{105}Pd(^{3}He,d)^{106}Ag$ reactions that were involved in that study, data were obtained for the $^{106}Pd(p,d)^{105}Pd$ and $^{106}Pd(^{3}He,d)^{107}Ag$ reactions. In the process of obtaining these calibration data it became clear that it would be useful to obtain complete angular distributions as there is considerable interest in the level structure of both ^{105}Pd and ^{107}Ag and the present data could add to our knowledge of these nuclei because of the

relatively good energy resolution. Information on the level structure of these two nuclei can also aid in the interpretation of the ^{106}Ag results.

Data were accumulated from 2.5° to 70° in the case of the (p,d) reaction and from 2.5 to 50° for the (^{3}He,d) reaction. Beam currents of several microamperes of 22.5 MeV protons and 32.8 MeV ^{3}He ions were used. About 10^{4} μc of charge was collected at each angle.

A sample spectrum for the ^{106}Pd(p,d)^{105}Pd reaction is shown in fig. A1-a10. As stated earlier, the ^{105}Pd spectra were used as a calibration for the ^{107}Ag(p,d)^{106}Ag reaction. For this purpose and as an internal calibration for the ^{105}Pd states, the states indicated in table A1-III were used as calibration points. The energies are those of Kawakami and Histake.[1] A non-linear least squares fit to a third degree polynomial of lab momentum versus channel number was made and the resulting parameters were used for computing the deuteron momenta for the other states in ^{105}Pd and all of the states in ^{106}Ag. The corresponding excitation energies are shown in fig. A1-a10 and in table A1-III for the ^{105}Pd states.

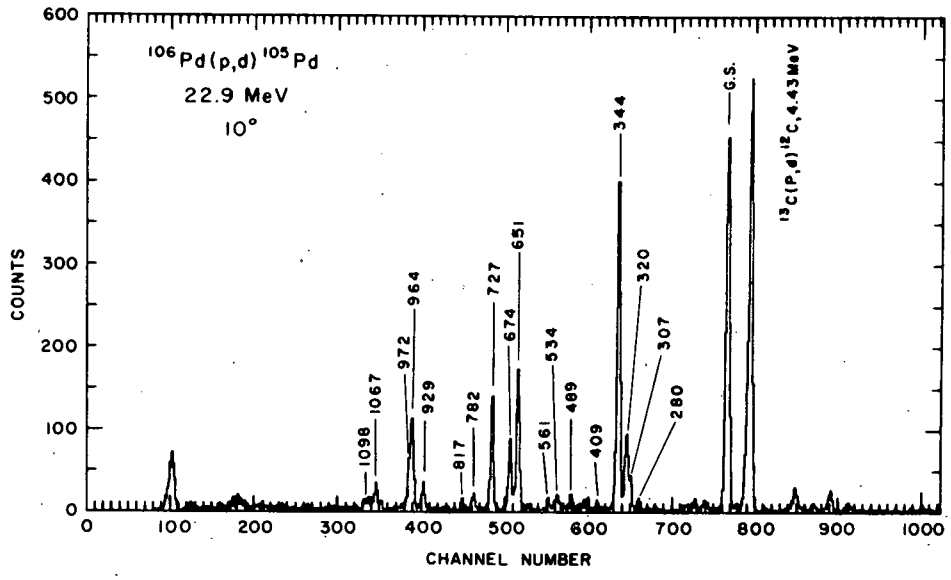

Fig. A1-a10. Deuteron spectrum from the ^{106}Pd(p,d)^{105}Pd reaction. Most of the small unlabeled peaks are from the presence of ^{108}Pd in the target.

In fig. A1-a11 is shown a sample spectrum for the ^{106}Pd(^{3}He,d)^{107}Ag reaction taken at 20°. The small peaks, to the right of the ^{107}Ag ground state are primarily due to the ^{108}Pd(^{3}He,d)^{109}Ag reaction. The presence of ^{105}Pd (11.25%) in the target resulted in some small peaks in the spectra that were due to the ^{105}Pd(^{3}He,d)^{106}Ag reaction. Some of these peaks are indicated in fig. A1-a11. Because this reaction was studied in detail at the same time as the reaction leading to ^{107}Ag, it was

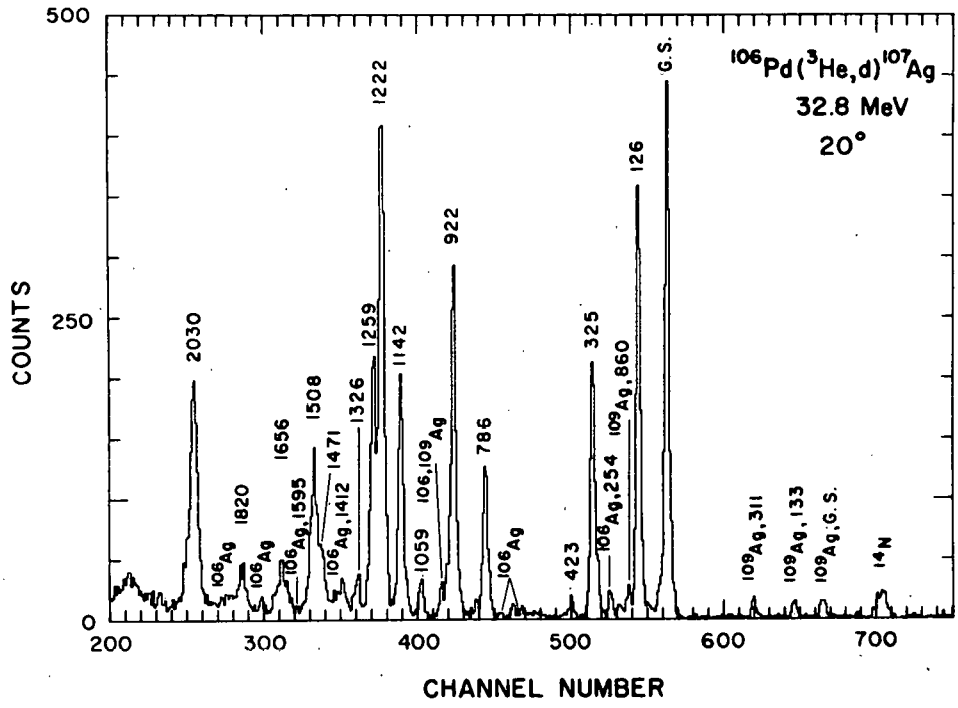

Fig. A1-a11. Deuteron spectrum from the $^{106}Pd(^{3}He,d)^{107}Ag$ reaction. The peaks marked ^{106}Ag were due to the presence of ^{105}Pd in the target and their contribution was subtracted out using data from an enriched ^{105}Pd target.

possible to subtract a computed fraction of the ^{106}Ag spectrum from the ^{107}Ag spectrum on an angle by angle basis. The data in fact were taken by alternating targets at each angle.

The angular distributions for the $^{106}Pd(p,d)^{105}Pd$ reaction are shown in figs. A1-a12, A1-a13, and A1-a14. In fig. A1-a12 the $\ell=2$ angular distributions are described very adequately by the distorted wave calculations except for the data at 2.5° and 5.0°. The $\ell=2$ assignments are quite consistent with the J^{π} assignments from the decay scheme studies of others shown in table A1-III. In previous neutron pickup studies[2,3] an angular distribution was not obtained for the state at 280 keV but, as shown in fig. A1-a12, an $\ell=2$ assignment is quite clear from the present work.

Three angular distributions that can be rather clearly assigned $\ell=0$ are shown in fig. A1-a13. There is good agreement on the assignment to the 344 keV state but Rickey et al.[3] assign the 674 keV state as $\ell=2$. A $1/2^{+}$ spin and parity assignment has been given this state by gamma-gamma directional correlation measurements[4] which of course is compatible only with $\ell=0$.

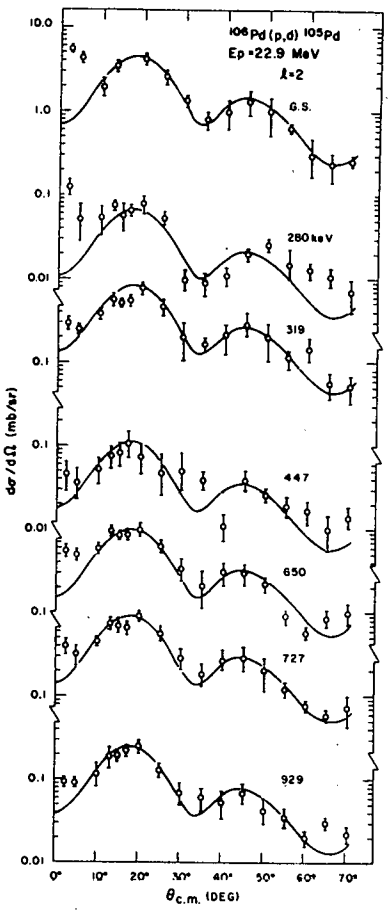

Fig. A1-a12. Angular distributions for $\ell=2$ for the $^{106}Pd(p,d)^{105}Pd$ reaction.

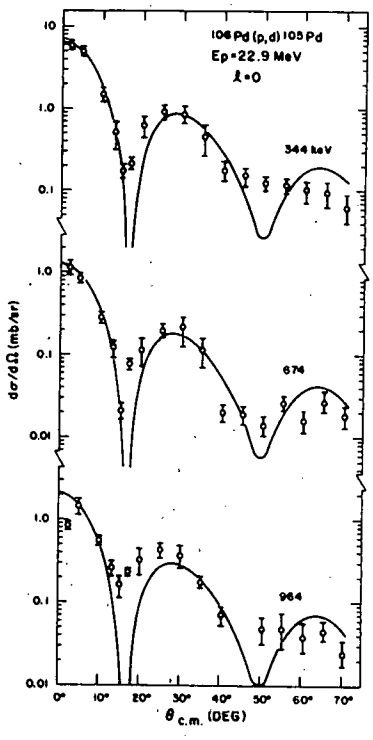

Fig. A1-a13. Angular distributions for $\ell=0$ for the $^{106}Pd(p,d)^{105}Pd$ reaction.

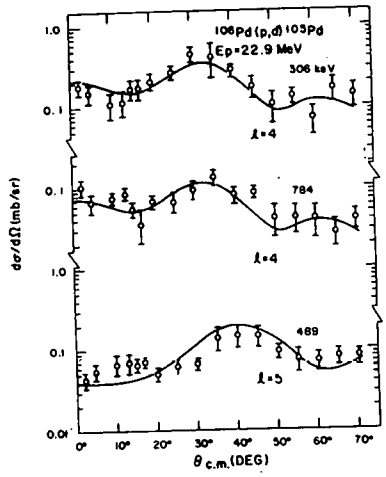

Fig. A1-a14. Angular distributions for ℓ=4 and ℓ=5 for the $^{106}Pd(p,d)^{105}Pd$ reaction.

In fig. A1-a14 are shown angular distributions for the states at 306 and 784 keV that appear to have ℓ=4 angular distributions. There is general agreement on the 306 keV state but the 784 keV state was assigned ℓ=2 [3] and ℓ=0 [2] by others. Only the ℓ=4 assignment is consistent with $9/2^+(7/2^+)$ assignment from the decay scheme studies,[1] but the assignment from the nuclear data compilation was $(5/2)^+$. The ℓ=5 assignment for the 489 keV state is consistent with previous measurements.

Differences of up to a factor of two in the magnitudes of the spectroscopic factors determined in this work (and shown in table A1-III) and ref. 3 are seen. This is probably due to the inclusion of the strengths of several unresolved states in the (d,t) cross sections due to the poorer energy resolution of the (d,t) experiment. The inclusion of states at 280 and 319 keV, for example, with the 307 keV ℓ=4 transition no doubt mainly accounts for the (d,t) spectroscopic factors being appreciably higher than they are from the present (p,d) experiment.

The angular distributions obtained for the $^{106}Pd(^3He,d)^{107}Ag$ reaction are shown in figs. A1-a15, A1-a16, A1-a17. Here again the description of the data by the distorted wave calculations appears excellent with the exception of the possible weak ℓ=3 transition to the state at 423 keV and the unresolved doublet at 1471 keV. As can be seen in table A1-IV, neither of the ℓ=0 transitions have been assigned previously. The angular distribution for the level at 1142 keV shown in fig. A1-a15 rather clearly requires an ℓ=0 assignment and hence a spin and parity of $1/2^+$.

The values of $(2J+1)C^2S$ are listed in table A1-IV and where comparisons can be made there is reasonable agreement between the two (^{3}He,d) experiments. If one assumes that the ground, 322 and 786 keV states contain all of the $2p_{1/2}$ and $2p_{3/2}$ strength and that the 126 keV

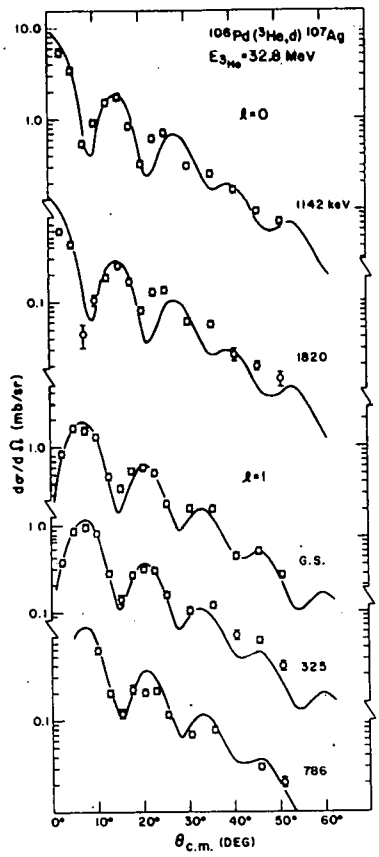

Fig. A1-a15. Angular distributions for ℓ=0 and ℓ=1 for the $^{106}Pd(^{3}He,d)^{107}Ag$ reaction.

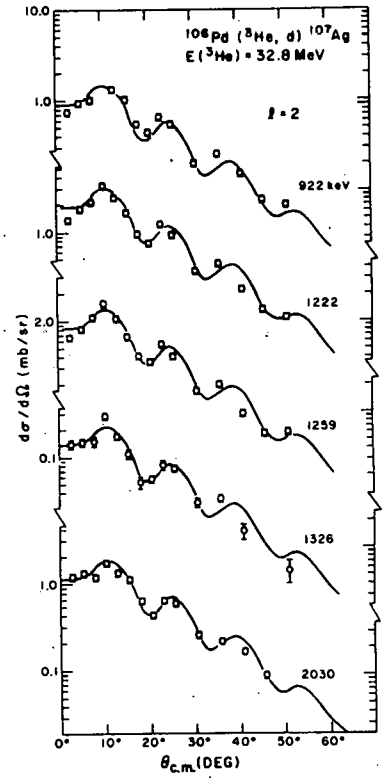

Fig. A1-a16. Angular distributions for ℓ=2 for the $^{106}Pd(^{3}He,d)^{107}Ag$ reaction.

TABLE A1-III

Summary of information on the levels of ^{105}Pd

Nuclear Data Sheets		Present work (p,d)			Rickey et al.[a] (d,t)			Cujec[b] (d,p) and (d,t)	
Energy (keV)	J^π	Energy (keV)	ℓ	C^2S'	Energy (keV)	ℓ	C^2S'	Energy (keV)	ℓ
0.0	$5/2^+$	0.0	2	1.78	0.0	2	1.85	0.0	2
280.51 c)	$3/2^+$	280	2	0.44				280	2
306.25 c)	$(7/2)^+$	306	4	2.52	307	4	5.46		
319.18 c)	$(5/2)^+$	319	2	0.36				321	2
344.52 c)	$(1/2)^+$	344	0	0.31	343	0	0.70	340	0
442.23	$(5/2)^+$	447	2	0.04	451	(1)	0.07	441	
489.11 c)	$(11/2)^-$	489	5	0.85	488	5	1.63	486	5
		535			538	2	0.11		
560.75	$(5/2)^+$	561						565	2
644.50	$(7/2)^-$								
650.69 c)	$3/2^+$	650	2	0.61	646	2	0.70	651	2
673.18 c)	$(1/2)^+$	674	0	0.05	674	2	0.15		
694.00	$(7/2^+,9/2^+)$							692	4
727.17 c)	$(5/2)^+$	727	2	0.47	724	2	0.52	721	2
781.30	$(5/2)^+$	784	4	0.54	778	2	0.14	785	0
		808			816	2	0.05		
929.4 c)		929	2	0.14	925	2	0.15		
939.0	$(1/2^+)$							939	0
962.37	$(1/2,3/2)^+$	964	0	0.09	962	2	0.34		
979.0	$(3/2^+,5/2^+)$	972						979	2
1072.2	$(5/2^+)$							1068	0
1087.93	$3/2^-$				1090	1	0.08		
1098.4 c)	$(5/2^+)$	1098						1105	2

a) See ref. 3. Nine additional states above 1 MeV were observed but are not listed here.

b) See ref. 2. Fifteen additional states above 1 MeV were observed but are not listed here.

c) These energies were assumed for calibration purposes.

TABLE A1-IV

Summary of information on the levels of ^{107}Ag

Nuclear Data Sheets and Kuhfeld and Hintz[a] (p,t)		Present work (^3He,d)			Kuhfeld and Hintz[a] (^3He,d)	
Energy (keV)	J^π	Energy (keV)	ℓ	$(2J+1)C^2S$	ℓ	$(2J+1)C^2S$
0.0	$1/2^-$	0.0	1	0.50	1	0.38
93.08	$7/2^+$	93				
125.7 [c]	$(9/2)^+$	126	4	1.46	4	0.90
324.6 [c]	$3/2^-$	325	1	0.19	1	0.26
422.6	$5/2^-$	423	(3)	0.056	(3)	<0.4
786.5 [c]	$3/2^-$	786	1	0.15	1	0.18
922.0 [c]	$(5/2^+)$	922	2	0.47		
949.0	$5/2^-$				strong	
973.2						
		1059	4	0.19(0.10)		
1142.4 [c]		1142	0	0.32	not observed	
1160.0						
1222.4 [c]	$(5/2^+)$	1222	2	0.82	strong	
1250.0						
(1262.0)		1259	2	0.48(0.35)		
1325.0		1326	2	0.08(0.06)		
1464.5 [b]	$3/2^-$	1471(D)	(1,2)		seen	
1482						
1500		1508	4	1.52(0.77)		
1574						
1615	$1/2^-$					
1653(D)	$7/2^+,1/2^-$	1656	4	0.30(0.16)	4	0.75
1688						
1836		1820	0	0.05		
1840	$5/2^+$				2	0.06
1854	$1/2^-$					
1880	$(5/2^+)$	1880				
1911	$(5/2^+)$	1917				
1957						
2030 [c]	$5/2^+$	2030	2	0.43	2	0.23
2066	$(7/2^+)$					
		2095				
		2105				
2119						
2144	$(5/2^+)$					
2182	$(7/2^+)$					
2190	$5/2^+$	2197			2	0.05
2203	$(5/2^+)$					
2229	$(7/2^+)$					

a) See ref. 5.

b) The energies and assignments for the 1482 keV state and higher were taken from ref. 5 and are mostly based on the results of study of the $^{109}Ag(p,t)^{107}Ag$ reaction.

c) These energies were assumed for calibration purposes.

(D) implies the existence of two or more unresolved levels.

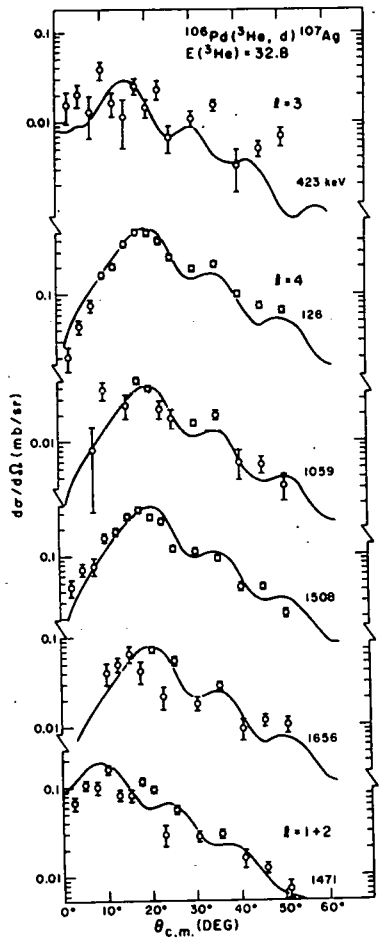

Fig. A1-a17. Angular distributions for ℓ=3 and ℓ=4 for the $^{106}Pd(^{3}He,d)^{107}Ag$ reaction. The theoretical ℓ=3 angular distribution for the 423 keV is shown for comparison only. The assignment is based on other data.

level contains the $1g_{9/2}$ strength, one might expect the sum of the spectroscopic factors for these states to be four, since four protons are needed to close the shell at 50. The experimental sum for these four states is 2.30. The data of Kuhfeld and Hintz[5] indicate a value of 1.72 for the same sums.

---

1 H. Kawakami and K. Histake, Nucl. Phys. A149 (1970) 523.
2 B. Cujec, Phys. Rev. 131 (1963) 735.
3 F. A. Rickey, R. E. Anderson, and J. R. Teamer, to be published.
4 M. Behar and Z. W. Grabowski, Nucl. Phys. A196 (1972) 412.
5 A. Kuhfeld and N. M. Hintz, to be published.

54,452

v. Level Structure of ^{106}Ag - R. E. Anderson, R. L. Bunting, J. D. Burch, S. R. Chinn, J. J. Kraushaar, R. J. Peterson, D. E. Prull, B. W. Ridley, and R. A. Ristinen

The only available information on the levels of ^{106}Ag concerns the 24.1 min ground state and the 8.4 d isomer. By using atomic beam methods the spin of the ground state has been determined to be 1 and that of the 8.4 d isomeric level 6. Even parity for both the ground and isomeric states has been established from the allowed nature of the beta decays.

The level structure of even mass odd nuclei such as ^{106}Ag is of great interest since they provide information on the effective nucleon-nucleon interaction in nuclear matter from the observation of the configuration multiplets formed by the odd proton and odd neutron.

In order to obtain information on the excited states of ^{106}Ag the help of a number of nuclear reactions has been enlisted. Initially the ^{103}Rh(α,nγ)^{106}Ag reaction was studied at several bombarding energies and the intensities and energies of the prompt γ-ray transitions between the levels of ^{106}Ag were determined. Unfortunately, because of the great number of lines observed, the construction of a unique level scheme without coincidence measurements appeared impossible. In order to determine the position of the levels the two single nucleon transfer reactions available, namely ^{107}Ag(p,d)^{106}Ag and ^{105}Pd(^{3}He,d)^{106}Ag, were investigated. Angular distributions were obtained with a resolution of about 12 keV for the (p,d) reaction and about 20 keV for the (^{3}He,d) reaction using the energy-loss spectrograph. In order to obtain calibration spectra for these reactions the ^{106}Pd(p,d)^{105}Pd and ^{106}Pd(^{3}He,d)^{107}Ag reactions were also studied and the results of that investigation are reported in the preceding contribution.

It shortly became evident that while the ^{107}Ag(p,d) and ^{105}Pd(^{3}He,d) reactions provided a great deal of information on the relative positions of the levels and the ℓ-values of the transferred nucleons, they populated only a fraction of the total number of states and in fact did not populate the ground state with any observable intensity. A similar situation has occurred with the ^{107}Ag(d,p)^{108}Ag reaction where the absence of the ground state transition caused confusion in understanding the levels of ^{108}Ag. The ground state of ^{108}Ag, which also has a spin and parity of 1+, must be very similar in structure to the ground state of ^{106}Ag.

Because the Q-values for the reactions leading to ^{106}Ag are not known with sufficient precision, it was impossible to determine the absolute positions of the levels with the needed accuracy. The ^{106}Pd(^{3}He,t)^{106}Ag reaction was next investigated as a means of overcoming these difficulties. The very low cross sections for this reaction, however, meant that prohibitively long running periods would be required to accumulate good spectra.

The final reaction investigated was $^{104}Pd(^{3}He,p)^{106}Ag$. This reaction was selected over $^{106}Pd(\alpha,d)^{106}Ag$ on the basis of the less restrictive isospin selection rule. The $(^{3}He,p)$ reaction did in fact populate the ground state as well as a sufficient number of other states so that information from the other reactions could be combined into a coherent level scheme. A spectrum taken with this reaction is shown in fig. A1-a18.

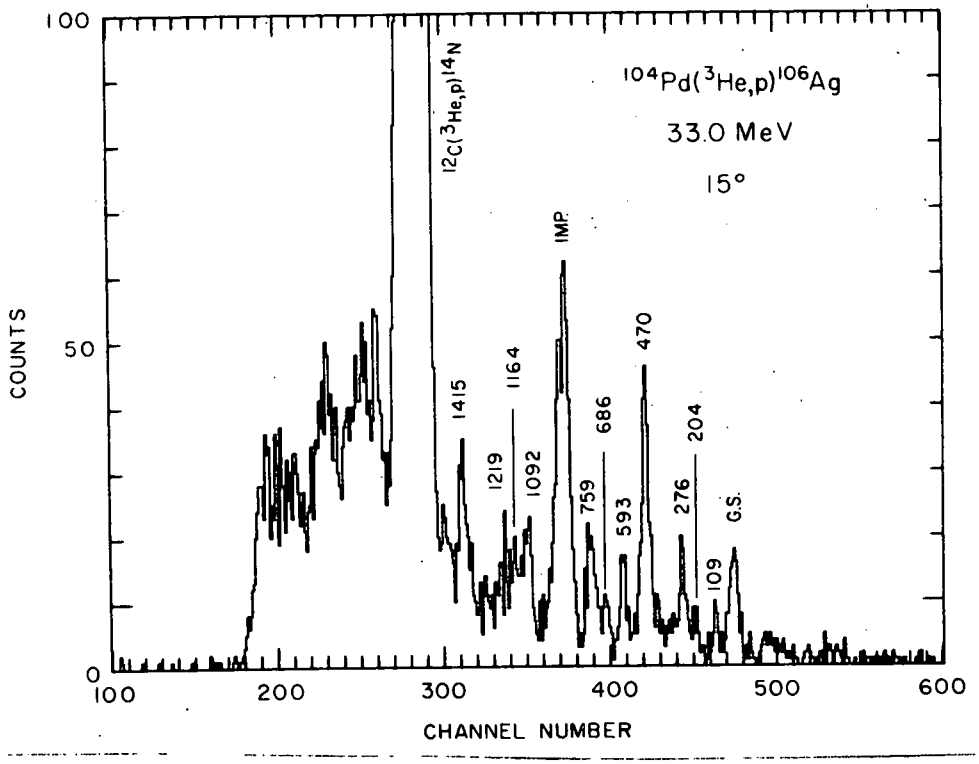

Fig. A1-a18. A spectrum taken at 15° for the $^{104}Pd(^{3}He,p)^{106}Ag$ reaction.

The angular distributions for the various states reached in the $^{107}Ag(p,d)^{106}Ag$ reaction are shown in figs. A1-a19, A1-a20, A1-a21, and A1-a22. The error bars for the most part are smaller than the data points. The solid lines are the results of distorted wave calculations. Twelve angular distributions (figs. A1-a19 and A1-a20) appear to be well described by an ℓ-transfer of 2. This would correspond to the pickup of a 2d neutron. In fig. A1-a21 are shown five angular distributions that are ℓ=0 transfer. Finally, in fig. A1-a22 are shown the remaining angular distributions. The state at 517 keV appears to require an ℓ=4 transfer and the state at 886 keV an ℓ=5 or 6. From the viewpoint of the shell model the ℓ=5 choice is, of course, preferred.

The angular distributions for the $^{105}Pd(^{3}He,d)^{106}Ag$ reaction are

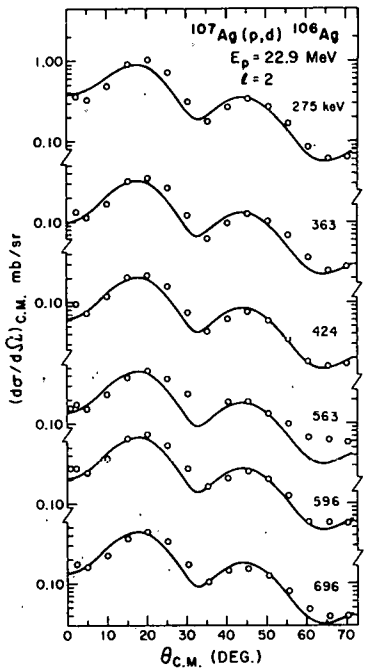

Fig. A1-a19. Angular distributions for the ^{107}Ag(p,d)^{106}Ag reaction that involve an ℓ-transfer of 2. In fig. A1-a19 through fig. A1-a26 the solid curves are the results of the DWBA calculations.

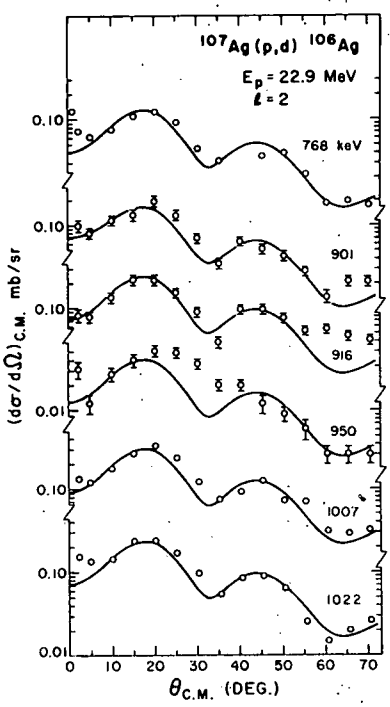

Fig. A1-a20. Angular distributions for the ^{107}Ag(p,d)^{106}Ag reaction that involve an ℓ-transfer of 2.

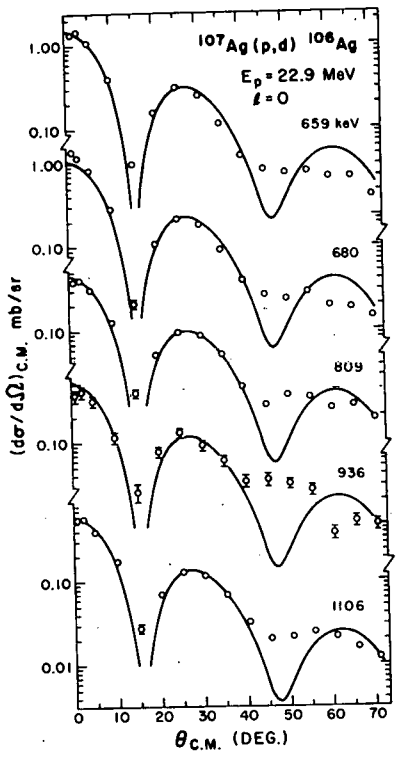

Fig. A1-a21. Angular distributions for the ^{107}Ag(p,d)^{106}Ag reaction that involve an ℓ-transfer of 0.

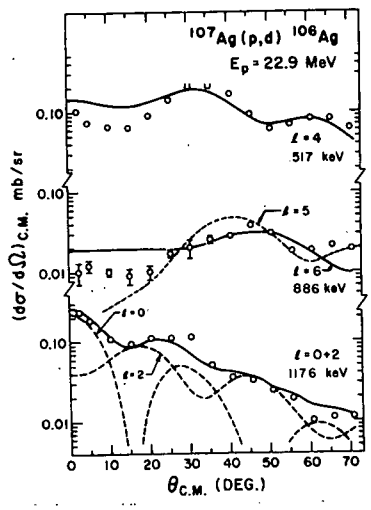

Fig. A1-a22. Angular distributions for the ^{107}Ag(p,d)^{106}Ag reaction.

shown in figs. A1-a23, A1-a24, A1-a25, and A1-a26. The ℓ=1 angular distributions are shown in figs. A1-a23 and A1-a24 and the distorted wave calculations appear to describe most of the angular distributions quite adequately. The ℓ=2 angular distributions are shown in fig. A1-a25 where eight higher lying states would appear to involve a proton being stripped into a 2d orbital. Lastly, fig. A1-a26 shows five angular distributions that are described very well by distorted wave calculations involving ℓ=4 proton stripping.

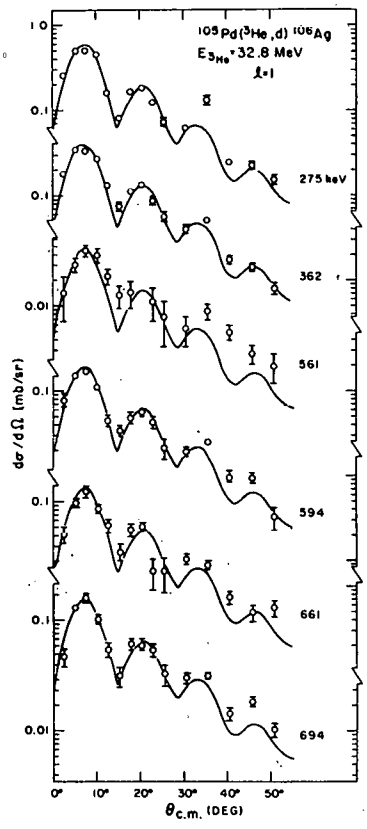

Fig. A1-a23. Angular distributions for the $^{105}Pd(^{3}He,d)^{106}Ag$ reaction that involve an ℓ-transfer of 1.

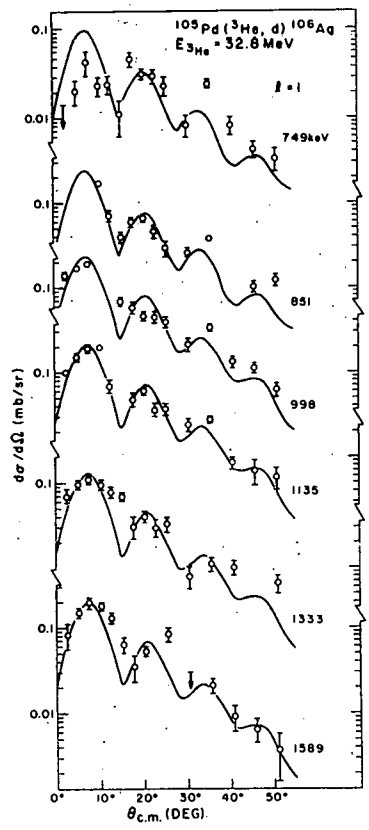

Fig. A1-a24. Angular distributions for the $^{105}Pd(^{3}He,d)^{106}Ag$ reaction that involve an ℓ-transfer of 1.

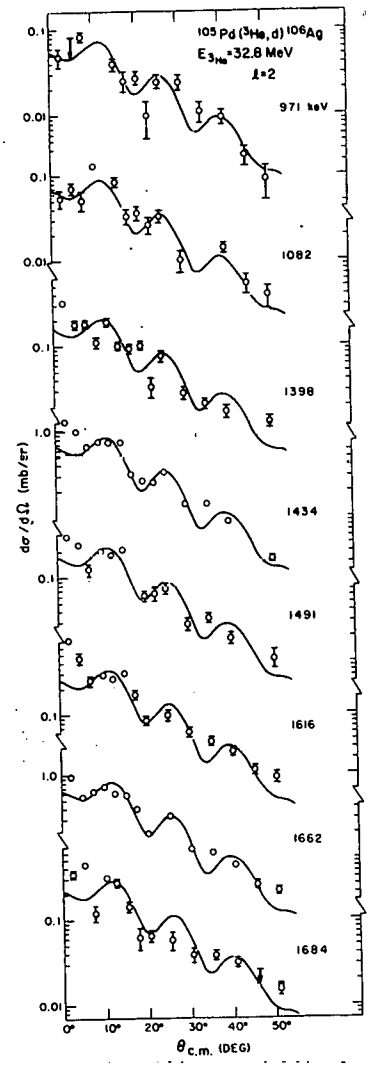

Fig. A1-a25. Angular distributions for the $^{105}Pd(^{3}He,d)^{106}Ag$ reaction that involve an ℓ-transfer of 2.

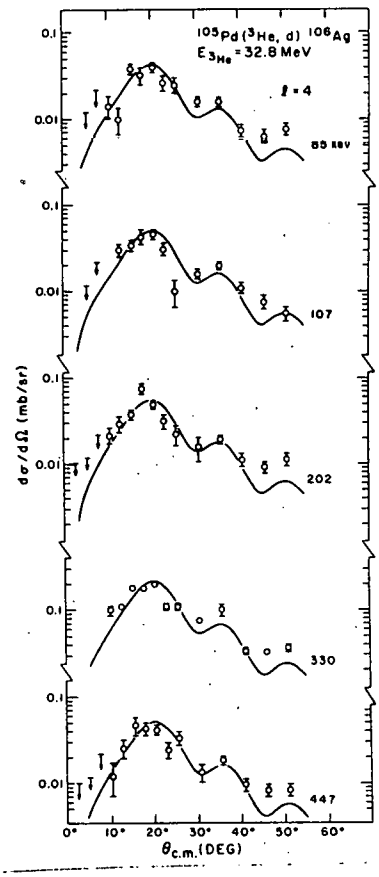

Fig. A1-a26. Angular distributions for the $^{105}Pd(^{3}He,d)^{106}Ag$ reaction that involve an ℓ-transfer of 4.

The spectroscopic factors were extracted for the states observed in both reactions. The energies of the levels of ^{106}Ag as determined by various reactions are shown in table A1-V. The uncertainties in the energies are shown in parentheses and reflect the uncertainty in determining the position of the peaks as well as the uncertainty introduced by the calibration procedure. Since the ground state transitions were not observed in the (p,d) and (^{3}He,d) reactions a constant had to be added to the relative energies from those two reactions to obtain absolute level positions.

An attempt was made to place the γ-rays observed in a self consistent decay scheme for ^{106}Ag which incorporated the energy levels seen in the $^{105}Pd(^3He,d)^{106}Ag$, $^{107}Ag(p,d)^{106}Ag$ and $^{104}Pd(^3He,p)$ reactions and shown in table A1-V. With the aid of a computer program the γ-ray list was studied for recurring sums and differences of two or more transitions. Several criteria were applied to the resulting list of possible energy levels in order to eliminate the large number of accidental sums. Only levels which were populated and depopulated by three or more transitions were kept and the error in the closure of the sums was required to be within the uncertainty in the energies of the γ-rays involved. With the exception of the 1195.54 keV level, only levels which appeared to correspond with the energy levels seen in the charged particle reactions, consistent with the energy uncertainties quoted, were kept. In addition, the criterion of intensity balance for a given level was applied to the placement of γ-rays. This procedure was iterated--the energy levels and γ-ray placements were first established at low excitations; then, using these level energies and the unplaced transitions, the level search procedure was repeated, additional placements made, and so on. This procedure was carried out until there appeared to be no additional placements that could be made consistent with the above requirements. The result is shown in fig. A1-a27.

The Q-values were also determined for the three reactions studied and these results along with the resulting mass of ^{106}Ag is listed in table A1-VI.

It appears reasonable to expect a set of at least 6 even parity states in ^{106}Ag ranging in spin from 1^+ to 6^+ from the $[\pi(1g_{9/2})^{-3}_{7/2},\nu(2d_{5/2})]$ configuration. Since the ground state of ^{107}Ag has predominantly a $[\pi(2p_{1/2})^1(1g_{9/2})^{-2}_0,\nu(2d_{5/2})^2_0]$ configuration these states should not be reached by the $^{107}Ag(p,d)$ reaction. If on the other hand ^{105}Pd has at least partially a $[\pi(1g_{9/2})^{-4}_0,\nu(d_{5/2})]$ configuration the (^{3}He,d) reaction should reach these six states with ℓ=4 transitions. The five states that meet these criteria are the states at 85, 107, 202, 330, and 447 keV. It is tempting to include the ground state as the sixth component with a spin and parity of 1^+ except that no deuteron group in the (^{3}He,d) reaction was seen to the ground state. The non-observation of such a transition to the ground state of ^{106}Ag may be largely caused by the fact that Q-values of (^{3}He,d) reactions to ^{106}Ag and ^{107}Ag differ only by 10 keV and because of the rather large amount of ^{106}Pd in the ^{105}Pd target. Because of a large cross section to the ground state of ^{107}Ag it was difficult using the subtraction method outlined to see a weak transition in that energy region.

TABLE A1-V

Summary of level information for ^{106}Ag

$^{107}Ag(p,d)$ E(keV)	ℓ	$^{105}Pd(^{3}He,d)$ E(keV)	ℓ	$^{104}Pd(^{3}He,p)$ E(keV)	$^{103}Rh(\alpha,n\gamma)$ E(keV)	J^{π}
				0.0	0.0	1^{+}
		85(2)	4		87.95	6^{+}
		107(2)	4	109(5)	110.60	$(2)^{+}$
		202(2)	4	204(6)	205.83	$(3)^{+}$
		257(3)			257.95	
275(1)	2	275(1)	1	276(4)	277.00	$(2)^{-}$
		330(1)	4		330.88	$(5)^{+}$
				335(6)	337.70	
363(1)	2	362(1)	1		364.26	$(3)^{-}$
		382(6)			384.60	
		429(3)				$(1,2,3)^{-}$
424(1)	2	447(2)	4		444.71	$(4)^{+}$
472(2)				470(4)	471.89	
517(1)	4	517(4)			520.04	$(3,4,5)^{-}$
563(2)	2	561(2)	1		558.06	$(1,2,3)^{-}$
596(1)	2	594(1)	1	593(4)	597.90	$(1,2,3)^{-}$
659(1)	0	661(2)	1		657.80	1^{-}
680(1)	0			} 686(7)		
696(1)	2	694(2)	1			$(1,2,3)^{-}$
		749(2)	(1)	} 759(5)		
768(2)	2	769(2)			768.12	$(1,2,3)^{-}$
809(2)	0					$(0,1)^{-}$
859(4)	4,5	851(2)	1			$(4,3)^{-}$
		874(3)				

(TABLE A1-V is continued on next page)

TABLE A1-V (continued)

^{107}Ag(p,d) E(keV)	ℓ	^{105}Pd(^{3}He,d) E(keV)	ℓ	^{104}Pd(^{3}He,p) E(keV)	^{103}Rh(α,nγ) E(keV)	J^{π}
886(2)	5,6				883.27	
901(1)	2	898(2)			899.09	$(1,2,3)^{-}$
916(1)	2				911.43	$(1,2,3)^{-}$
936(2)	0			939(7)		$(0,1)^{-}$
950(2)	2					$(1,2,3)^{-}$
		971(2)	2		968.86	$(0\text{-}5)^{+}$
		998(2)	1			$(1\text{-}4)^{-}$
1007(1)	2				1009.17	$(1,2,3)^{-}$
1022(1)	2	1018(4)				$(1,2,3)^{-}$
		1082(2)	2	1092(6)		$(0\text{-}5)^{+}$
1106(2)	0					$(0,1)^{-}$
		1135(2)	1	1163(5)	1130.49	$(1\text{-}4)^{-}$
1176(2)	0+2				1195.54	
				1219(6)		
		1333(2)	1		1337.55	$(1\text{-}4)^{-}$
		1398(3)	2	1415(4)	1397	$(0\text{-}5)^{+}$
		1434(2)	2			$(0\text{-}5)^{+}$
		1491(2)	2			$(0\text{-}5)^{+}$
		1589(2)	1			$(1\text{-}4)^{-}$
		1616(2)	2			$(0\text{-}5)^{+}$
		1662(2)	2			$(0\text{-}5)^{+}$
		1684(2)	2			$(0\text{-}5)^{+}$

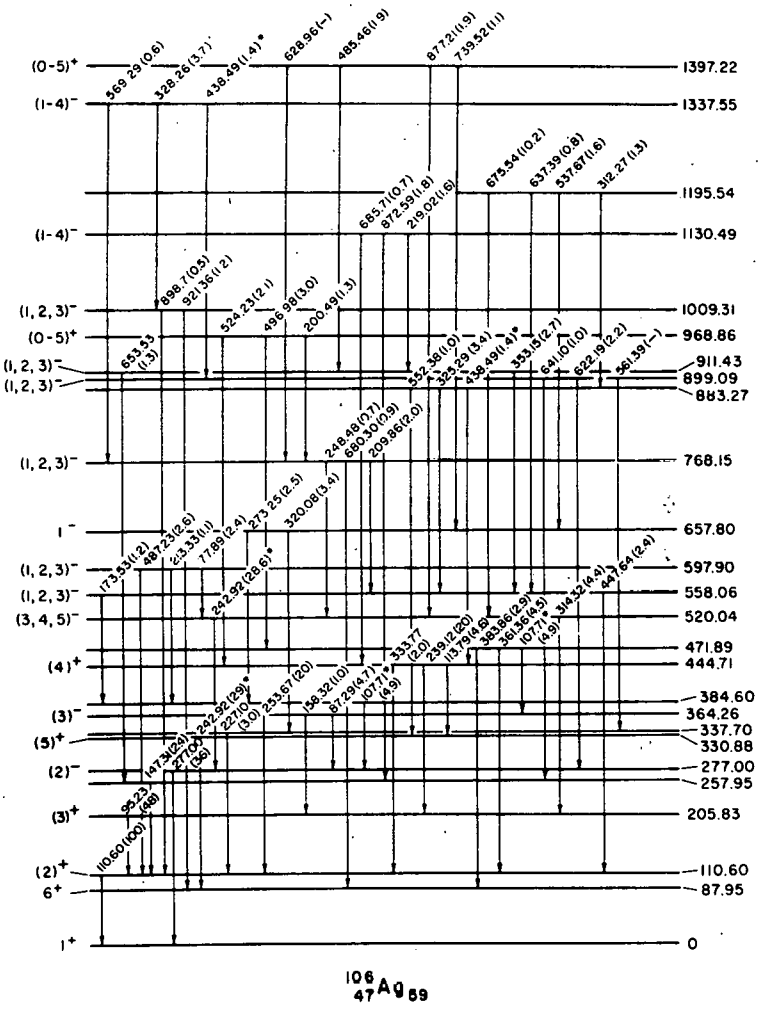

Fig. A1-a27. Partial level diagram for ^{106}Ag and γ-ray transitions from the ^{103}Rh(α,nγ)^{106}Ag reactions. The placement of the transitions between levels over about 400 keV is tentative. With the exception of the 1195.54 state the levels are from the charged particle reactions, but the precise energies listed are based on the γ-ray data. Relative gamma ray intensities as observed at 13.76 MeV are shown in parentheses. The transitions marked with an asterisk appear twice in the scheme and the 561.39 and 628.96 keV γ-rays had measurable intensity only at 17 MeV bombarding energy.

TABLE A1-VI

Q-values and mass of ^{106}Ag for the various reactions studied

Reaction	Q-value (keV)			Mass of ^{106}Ag (μu)
	1971 Survey[a]	1972 Survey[a]	Present Work	Present
$^{106}Pd(^{3}He,d)^{107}Ag$	301±7	297±9		
$^{106}Pd(p,d)^{105}Pd$	-7336±10	-7337±10		
$^{105}Pd(^{3}He,d)^{106}Ag$	311±11	311±15	322±8	105.906668±11
$^{107}Ag(p,d)^{106}Ag$	-7327±13	-7323±14	-7305±11	105.906656±13
$^{104}Pd(^{3}He,p)^{106}Ag$	5159±15	5181±15	5153±6	105.906687±13
$^{54}Fe(^{3}He,p)^{56}Co$	7430±4	7430±4		

[a]) See ref. 2).

There should be two negative parity states in ^{106}Ag, i.e. 2^- and 3^- formed by the $[\pi(2p_{1/2})^1(1g_{9/2})^{-2}_0,\nu(2d_{5/2})]$ configuration and these should be readily reached by the (p,d) reaction on ^{107}Ag with $\ell=2$ transitions. To the extent that the ground state of ^{105}Pd has a $[\pi(2p_{1/2})^{-2}_0(1g_{9/2})^{-2}_0,\nu(2d_{5/2})]$ configuration these states should also be reached by the $^{105}Pd(^3He,d)^{106}Ag$ reaction with $\ell=1$ transitions. There are five states that meet these requirements but it is possible that the lowest energy state at 275 keV of this group is the 2^- member of the doublet and the 3^- member is at 362 keV. From the empirical rules and from systematics in this mass region one might expect the 2^- state to be nearest the ground state.

From a number of considerations the spin and parity assignments shown in fig. Al-a28 for these two configurations were arrived at. The 8.4 d isomeric state is thus at 88.00 keV.

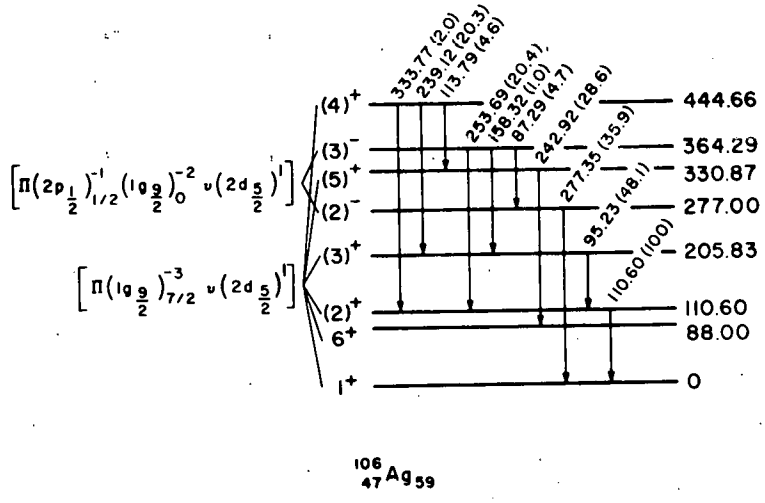

Fig. Al-a28. Level scheme and transitions for selected excited states of ^{106}Ag. The assignments and shell model configurations are discussed in the text. Relative gamma ray intensities as observed at 13.76 MeV are shown in parentheses.

Given the simple multiplet configurations suggested in fig. Al-a28, it is possible to compute this part of the spectrum of ^{106}Ag from the matrix elements taken from the spectra of ^{92}Nb.[1] The levels predicted for the even parity states have the correct order and relative spacing, but the absolute energy spacings are about three times that observed. The order of the odd parity multiplet states is again predicted correctly, but the predicted splitting is twice that observed. The correct ordering strengthens the validity of the configurations in fig. Al-a28, although substantial configuration mixing is also indicated.

[1] J. P. Schiffer, The Two-Body Force in Nuclei, edited by S. M. Austin and G. M. Crawley, Plenum Press, New York, 1972, p. 205.

[2] N. B. Gove and A. H. Wapstra, Nucl. Data Tables 11 (1972) 127 and private communication; A. H. Wapstra and N. B. Gove, Nucl. Data Tables 9 (1971) 267.

vi. ^{87,85}Rb(^{3}He,d)^{88,86}Sr - P. G. Brabeck, M. J. Schneider, and R. E. Anderson

In the region around mass 90 little attention has been paid to proton structure. This seems a worthwhile endeavor, however, since N=50 is a closed shell. We have studied the ^{85,87}Rb(^{3}He,d) reaction at 33.4 MeV bombarding energy, detecting deuterons in the energy loss spectrometer focal plane. Angular distributions from 2.5° to 45° were taken using natural metallic rubidium and isotopically enriched carbonate and chloride targets. The impurities (especially ^{36}Ar from the ^{35}Cl(^{3}He,d) reaction) helped in calibration of higher excited states. Fig. A1-a29 shows a spectrum at θ_{lab}=2.5°. All known ^{86}Sr

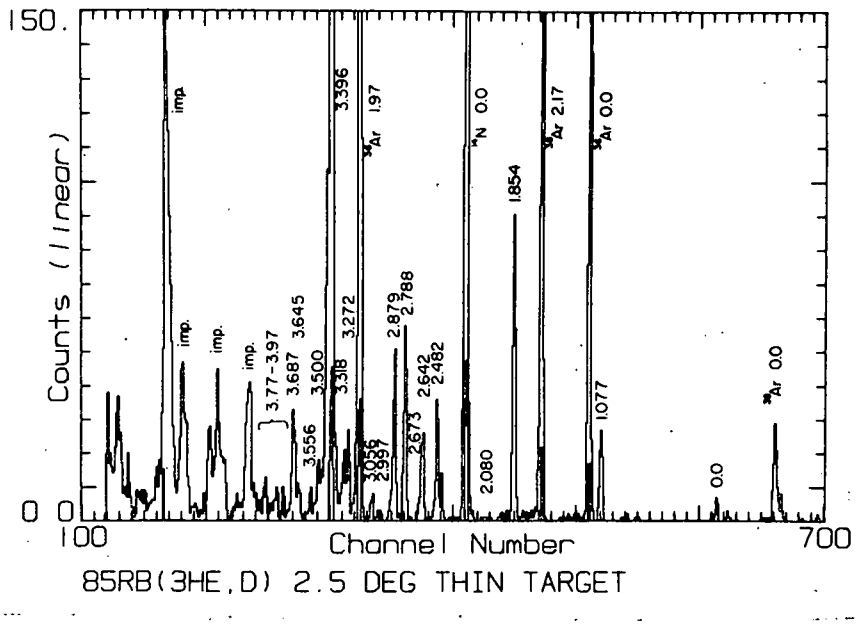

Fig. A1-a29. ^{85}Rb(^{3}He,d) spectrum at θ_{lab}=2.5°. Peaks labeled only with excitation energy are states of ^{86}Sr. Net resolution is ~25 keV.

levels below 3.7 MeV, plus a new one at 3.396 MeV (the strongest in the spectrum), were analyzed.

Fig. A1-a30 shows angular distributions for all levels assigned ℓ=1, along with DWBA calculations using optical parameters of Harrison

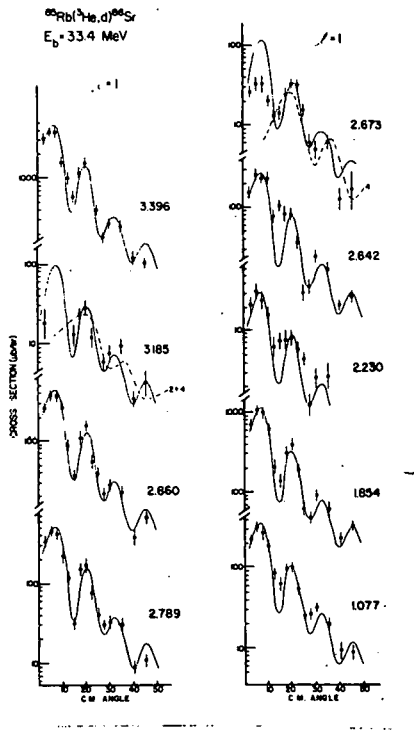

Fig. A1-a30. $^{85}Rb(^3He,d)^{86}Sr$ angular distributions assigned $\ell=1$.

and Hiebert.[1] Several anomalies appear when comparing these results to previous information on ^{86}Sr: the level at 2.673 MeV has been assigned 5^- by Ball in a (p,t) experiment, but an $\ell=1$ transfer on a $5/2^-$ target nucleus cannot lead to spin greater than 4^+. Our experimental angular distribution does indeed have too little forward strength for $\ell=1$, but too <u>much</u> forward strength for $\ell=4$. Adding some $\ell=2$ to the $\ell=4$ doesn't help very much because it raises back angle strength too much.

The level at 3.185 MeV has been assigned $3,4^-$, but $\ell=1$ means positive parity. The forward angles in our experiment were obscured by impurities, but the fit to $\ell=1$ is still a bit better than $\ell=4$. Note that both have similar slopes at about 25°.

Our angular distribution to the 2.860 MeV level is indisputably $\ell=1$, but this assignment just adds to the controversy in this region where the <u>higher</u> level of an apparent doublet has $J^\pi \leq 4^+$ and the 2.860 MeV level is 6^+. A careful calibration of our spectra shows that we see <u>mostly</u> the 2.860 MeV level, but any contribution from the 2.879 is too close to be separated out.

Fig. A1-a31 shows other angular distributions. The 2.997 has been assigned 3^- but that means ℓ should be even. However, $\ell=3+1$ fits better than 2+4. The level at 2.480 has some definite $\ell=0$ component, which is the first sign of filling of the 3s orbit. This level appeared broad in our spectra and could possibly be a doublet.

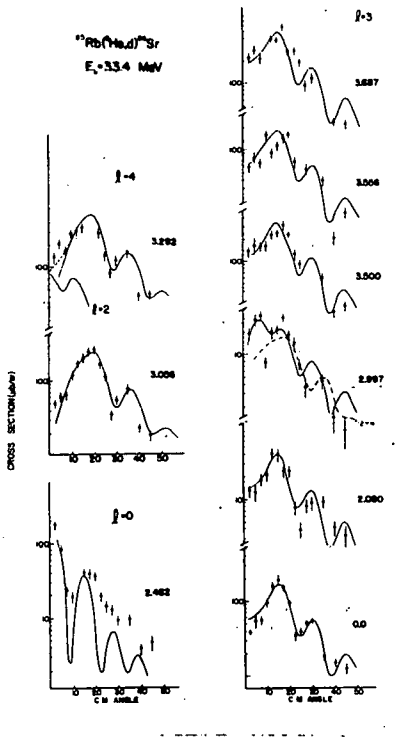

Fig. A1-a31. $^{85}Rb(^{3}He,d)^{86}Sr$ angular distributions assigned other ℓ values.

The $^{87}Rb(^{3}He,d)^{88}Sr$ experiment was analyzed for comparison with the results of Shreve[2] who studied this reaction at 21 MeV at Rochester. Our ℓ-values all agree with those of Shreve, but when we calculated spectroscopic factors, we found some large disagreements. Our ground state spectroscopic factor is about 50% larger than Shreve's, but our spectroscopic factor for the 3.49 level is about 3½ times smaller. Our ℓ=4 spectroscopic factors are smaller than those of Shreve by factors of 2/3 to 1/3. This could partly be explained by different DWBA calculations. It seems fairly unlikely that multi-step or compound processes are responsible for the differences, and we have no other explanation for them.

The important thing we learn from this experiment is that this nucleus needs closer study. In view of our good fits to pure ℓ values, it seems likely that the best fit combination ℓ values are correct and hence either this nucleus has several close doublets or some previous assignments are incorrect.

---

1. J. F. Harrison and J. C. Hiebert, Nucl. Phys. A185 (1972) 385.
2. D. C. Shreve, University of Rochester, report UR-NSRL-73 (1970).

vii. Weak Absorption Effects in the $^{48}Ca(^{16}O, ^{15}N)^{49}Sc$ Reaction - M. J. Schneider; J. V. Maher, T. J. Lewis, J. C. Peng, C. M. Cheng, H. S. Song (U. of Pittsburgh)

Analysis of the $^{48}Ca(^{16}O, ^{15}N)^{49}Sc$ experiment, performed initially at Pittsburgh as a BNL-Pittsburgh collaboration, has been completed at the University of Colorado. The experiment was motivated by the discovery of strongly oscillatory and apparently L- (transferred orbital angular momentum) dependent angular distributions in the analogous $^{48}Ca(^{14}N, ^{13}C)^{49}Sc$ reaction.[1] Analysis of the present experiment used the heavy ion DWBA code FRC, which was brought to the Colorado computer facility from Brookhaven National Laboratory.

As with the $(^{14}N, ^{13}C)$ reaction, the $(^{16}O, ^{15}N)$ data could be best reproduced with "weak" absorption in the optical parameters (fig. A1-32), that is W reduced to 10 MeV from the more typical value ~30 MeV. Other optical parameters were V=80 MeV, r_o=1.22 fm, and a=.5 fm, .6 fm for ^{16}O and ^{15}N channels respectively. The argument for L dependence is weak in the present experiment because when L values are reversed in the calculation (fig. A1-a33), the fits are not much poorer than when

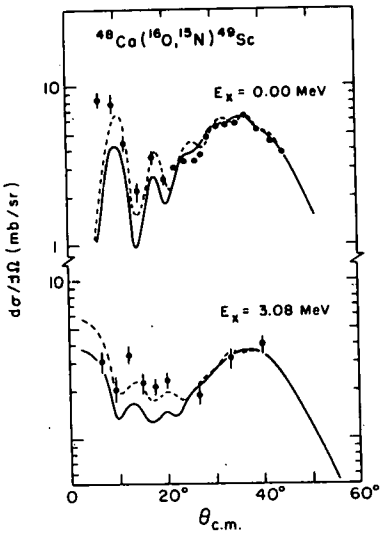

Fig. A1-a32. Comparison of weakly absorbing and strong absorbing optical parameter calculations using no-recoil code. Weakly absorbing calculation is shown by solid lines.

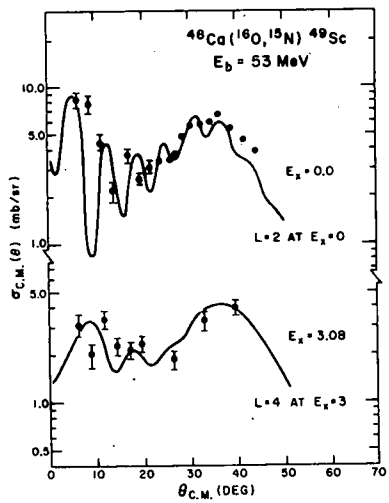

Fig. A1-a33. Reaction calculation with L values reversed to test L dependence hypothesis. Compare L=2 calculation with fig. A1-a32 to see effects of different Q values.

correct L values are used. Use of several other sets of optical parameters which fit the elastic scattering of ^{16}O on ^{48}Ca did not improve the fits for correct L values. The present calculation was successful, however, in reproducing $^{48}Ca(^{3}He,d)$ spectroscopic factors without an arbitrary normalization factor usually needed when strongly absorbing optical parameters are used.

54, 455

---

[1] M. J. Schneider, C. Chasman, E. H. Auerbach, A. J. Baltz, and S. Kahana, Phys. Rev. Letters 31 (1973) 320.

viii. $^{197}Au(^{3}He,d)^{198}Hg$ Reaction at 38 MeV - M. L. Munger

This reaction was studied with the energy-loss spectrometer from 0°-60° angular range. Fig. A1-a34 is our best spectrum with 30 keV resolution (50 keV typical) mostly due to a target thickness of .1 mg/cm^2. The energy was calibrated by bootstrapping from well resolved lower energy known peaks[1] of ^{198}Hg using program REGRES.[2]

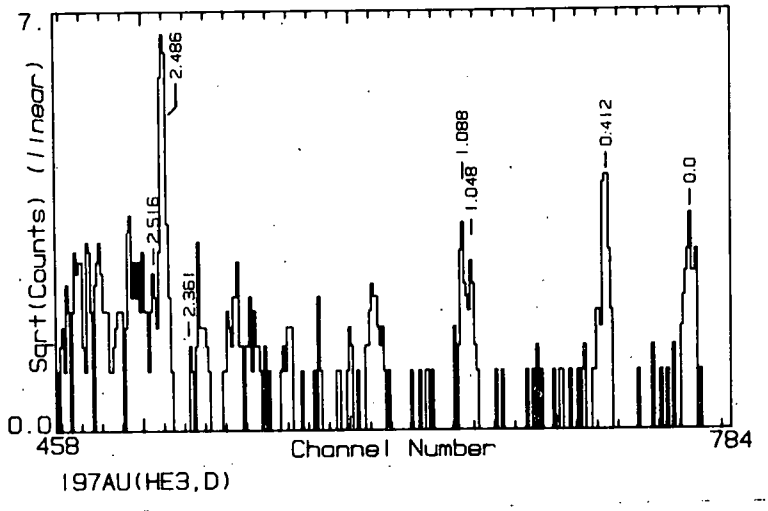

Fig. A1-a34. Spectrum taken with magnetic spectrograph of ^{198}Hg, at 30°, in the lab, with energies of excited states in MeV.

We can see that a lot of strength goes into the 2.486 MeV excitation of the residual nucleus. The cross-sections of fig. A1-a35 give a comparison of this state to the known 2^+ state at .412 MeV and the 0^+ ground state. A DWBA calculation using computer code DWUCK was performed using the parameters due to Wildenthal[3] for ^{3}He and Hinterberger[4] for deuterons. The 2.486 MeV cross-section follows the 2^+ .412 MeV state closely and is in disagreement at low angles with the ground state. It is "in phase" with the DWBA calculation but since the solid angle for the spectrometer is not well known, a spectroscopic factor cannot be

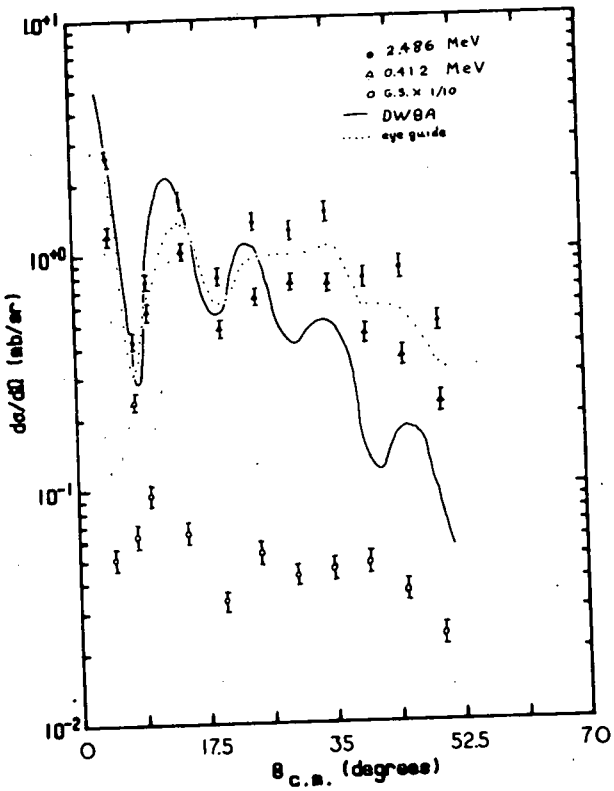

Fig. A1-a35. Angular distributions of three excited states of ^{198}Hg, and the DWBA fit to the 2.486 MeV excitation.

reported. The tentative assignment[1] of 2^+ to the 2.486 MeV excitation is not in disagreement with our findings.

---

1 Nuclear Data Sheets, B6 no. 4 (1971) 335.
2 Described elsewhere in this report.
3 B. H. Wildenthal et al., Phys. Rev. Lett. 19 (1967) 960.
4 Hinterberger, Nucl. Phys. A11 (1968) 287.

b. Two or More Nucleon Transfer Reactions

i. Search for Two-Step Processes in the (p,t) Reaction - J D. Burch, S. R. Chinn, J. J. Kraushaar, P. D. Kunz, B. W. Ridley, and M. J. Schneider

The search for two-step components in nuclear reactions usually analyzed as purely one-step has been extended to (p,t) reactions. Evidence for two-step processes in (p,t) has been noted by others,[1] but we are extending the search to the f-p shell using the advantages of the CU facility: the high flux of high energy protons on target and the energy-loss spectrometer. We are attempting to observe (p,t) at or near 0° where the nature of the two-step process can be determined.[2]

However, the spectrometer measurements present considerable experimental difficulties. The highly negative Q-values characteristic of (p,t) lead to unusual difficulties; a) zoom lens magnifications near the design limits of the spectrometer which necessitate careful interpretation of data; b) low outgoing triton energies requiring frequent resetting of focal plane detector gates; c) interference from elastic protons impinging on the detector. At low angles these elastic protons cannot be completely eliminated without the deflector plates originally fabricated for discrimination among heavier particles.

We have begun to investigate this reaction using ^{62}Ni and ^{54}Fe targets. To date, partial angular distributions have been obtained for both. Our initial interest is in the angular distribution for the 2.635 MeV 3^+ state in ^{60}Ni, which is forbidden in zero-range one-step theory. Its angular distribution will yield information on the two-step process in this moderately collective nucleus.

---

[1] R. J. Ascuitto, N. K. Glendenning, and B. Sorenson, Phys. Lett. 34B (1971) 17.

[2] T. Udagawa and D. K. Olsen, Phys. Lett. 46B (1973) 285.

ii. (^{3}He, ^{7}Be) Reaction Investigation in the Mass 120 Region - R. A. Emigh, C. D. Zafiratos, and C. S. Zaidins

A helical cathode proportional chamber (HCPC) detector has been developed for detecting ions heavier than ^{3}He and lower energies of lighter ejectiles. This HCPC has much thinner windows than the first HCPC built for the CU spectrograph (the carbon equivalent thickness of the second detector is of the order of 10 mg/cm^2 with 50 mm of Hg pressure in the chamber). Since Be ions are quite ionizing, no more than 50 mm of Hg gas pressure is needed for large anode signals. ^{7}Be ions with energies as low as 15 MeV can be detected in this HCPC to yield a barely usable scintillation signal.

Presently, another HCPC is being constructed with thinner windows. Thus, a more distinct scintillation signal will be obtained, helping to eliminate some of the background presently hindering the experiment.

We have made a preliminary study of the $^{120}Sn(^{3}He,^{7}Be)^{116}Cd$ reaction at $E(^{3}He)=41$ MeV. Data were obtained at laboratory angles of 5°, 10°, and 15°. Initial measurements (fig. A1-b1) indicate that the ground state differential cross sections for the angles measured are of the order of 0.1 μb/sterad. These cross sections are tentative as the spectrograph solid angle has not been fully determined.

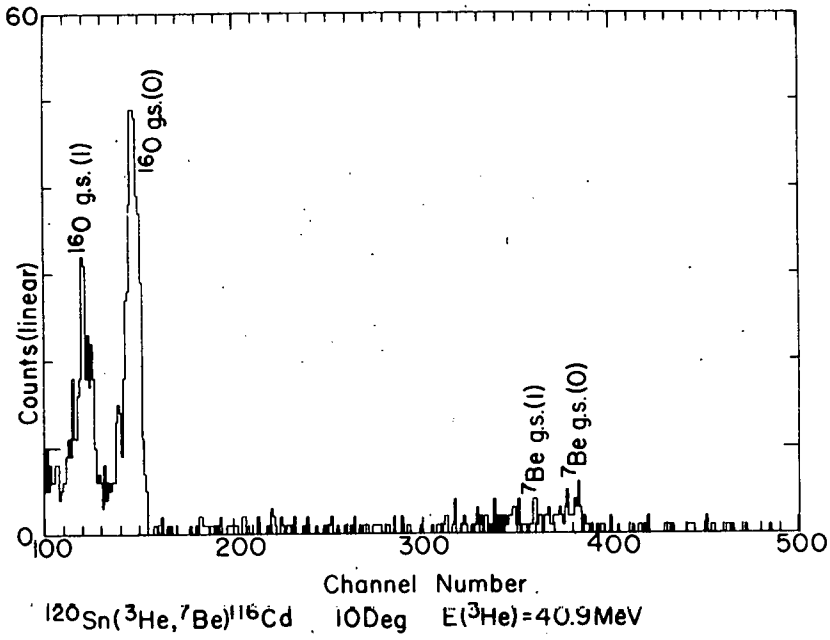

Fig. A1-b1. Energy spectra of ^{7}Be particles from a carbon backed ^{120}Sn target using 40.9 MeV $^{3}He^{++}$ ions. Since the ^{7}Be nucleus has two bound states, the ground state of ^{116}Cd appears as a doublet of peaks. Strong peaks at left are due to oxygen contaminant.

iii. $^{24}Mg(d,\alpha)^{22}Na$ - M. J. Schneider and J. W. Olness (Brookhaven National Laboratory)

As is well known, the two-nucleon transfer reaction shows strong coherence effects, and hence can be used as a stringent test of nuclear wave functions. It is also an intriguing problem to see how well the structure of clearly collective nuclei can be calculated with the shell model. Addressing both these possibilities, the $^{24}Mg(d,\alpha)^{22}Na$ experiment at 26 MeV bombarding energy was performed at Brookhaven National Laboratory using the multigap spectrograph, and is being analyzed at the University of Colorado.

The shell model wave functions being tested are those of Preedom and Wildenthal[1] for ^{22}Na, which has several well known rotational bands. Dr. Wildenthal has provided us with two-particle spectroscopic amplitudes for this purpose.

According to the "well-matching" prescription,[2] finite-range corrected (d,α) DWBA calculations become more reliable if the deuteron and alpha-particle optical wells are of similar geometry. Therefore, we have refitted published elastic scattering data for 25.9 MeV deuterons on Mg and for 28.5 MeV alphas on ^{24}Mg using the code OPTIM. Although we were not able to achieve perfect matching, r_o of the alpha well was reduced from 1.7 fm to 1.4 fm, and V increased from 54 MeV to 198 MeV, a more reasonable value for DWBA calculations. The resulting fits to (d,α) data are quite satisfactory (fig. A1-b2) and considerably better than those using the original published parameters.

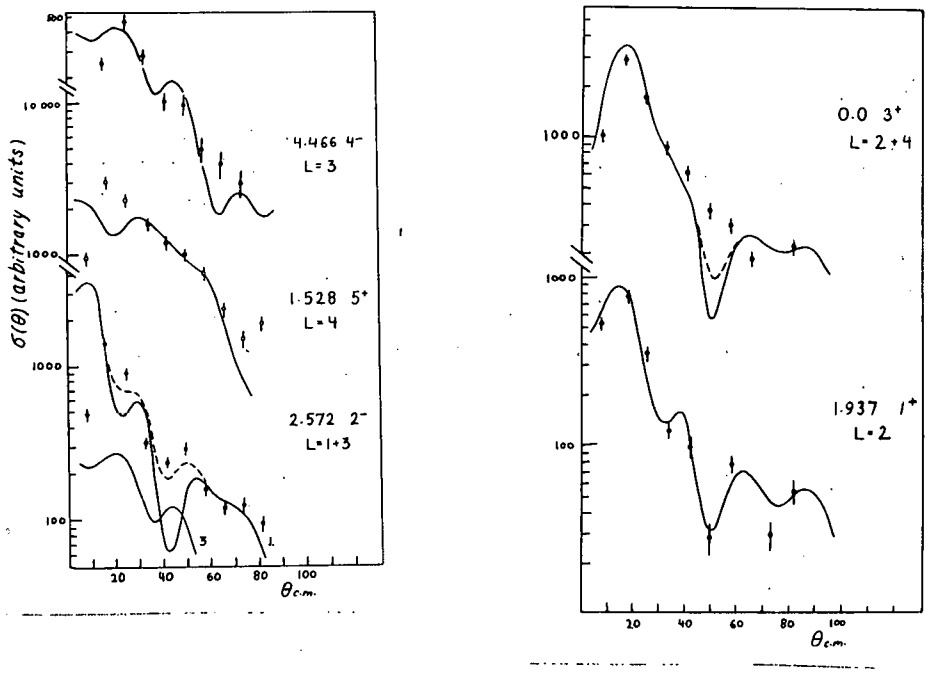

Fig. A1-b2. Angular distributions and microscopic DWBA calculations for five ^{22}Na levels populated in the ^{24}Mg(d,α) experiment. L admixtures, where present as indicated by dashed lines, have been chosen solely for best fit.

Substantial effort has gone into reconciling Wildenthal's spectroscopic amplitudes, which use the conventions of Yoshida, with code DWUCK2, which uses several opposite conventions of Towner and Hardy. At this writing we have good agreement between shell-model calculation and experiment for relative level strengths of six out of the eight levels for which this comparison is possible. The exceptions are the two lowest 1^+ states, and hence the possibility of calculational error is being looked into.

[1] B. M. Preedom and B. H. Wildenthal, Phys. Rev. C 6 (1972) 1633.
[2] M. J. Schneider and W. W. Daehnick, Phys. Rev. C 4 (1971) 1649.

iv. $^{40}Ca(d,\alpha)^{38}K$ at 16.3 MeV - E. W. Stoub

Conservation of isospin requires $\Delta T=0$ for a direct (d,α) reaction. Thus, the two low-lying isospin 1 states of ^{38}K should not be excited in a direct single step (d,α) reaction. These states may, however, be excited in a two-step reaction channel involving the processes $(d,t),(d,\alpha)$ or $(d,^3He),(^3He,\alpha)$. These two processes would still cancel to preserve the $\Delta T=0$ rule were it not for their differing Q values.

A study of the $^{40}Ca(d,\alpha)^{38}K$ reaction was undertaken with primary emphasis on the observation of the $\Delta T=1$ transitions. In addition, the strength of the zero range interaction, D_o, for $\Delta T=0$ transitions will be obtained from these data.

The reaction was studied using the C.U. magnetic spectrograph[1] and the HCPC[2] detector system. A practical limit to the (d,α) cross-section sensitivity was found to be about 0.5 μb/str with the copious neutron background characteristic of deuteron beams. (For these experiments, the spectrograph subtended a solid angle of only 0.15 mstr.) Data were taken in the angular range 7.5° to 67.5°. Natural calcium targets of thickness 100 $\mu g/cm^2$ were prepared by vacuum evaporation onto carbon foils. Deuteron elastic cross-sections were also measured using the spectrograph and using Si(Li) detectors in the cave scattering chamber.

The reaction cross-sections to the isospin 1 states of ^{38}K were nearly at the limit of sensitivity, so that accurate cross-sections could not be determined. For example, at 20°, the (J=0, T=1) state at $E_{xc}=2.405$ MeV is found to have a cross-section of about 9.5±1.0 μb/str. These data are illustrative of the limit of sensitivity and hence, the difficulty involved in accurate cross-section measurements for T=1 states under these circumstances. In spite of this, the large sensitivity of predicted cross-sections to configuration mixing should enable meaningful tests of various wavefunctions. The contributions of the (d,t), (t,α) and $(d,^3He)$, $(^3He,\alpha)$ processes were computed with the coupled channels code CHUCK. The shape and magnitude of these predicted cross-sections are in essential agreement with the data.

The data for T=0 states of ^{38}K will be used to test various wavefunctions as well as to examine the zero range strength, D_o, for the two-nucleon transfer in (d,α). The calculations are now being completed for the low-lying T=0 states using coherent sums of one- and two-step reaction amplitudes calculated by CHUCK.

[1] University of Colorado NPL Progress Report, 1973 and 1974.
[2] University of Colorado NPL Progress Report, 1973 and 1974.

c. Charge Exchange Reactions

i. Two-Step Processes in the (^{3}He,t) Reaction to the Analog and Anti-Analog States of ^{56}Co - L. D. Rickertsen, M. J. Schneider, H. Rudolph, J. J. Kraushaar, and W. R. Zimmerman

It is becoming more widely recognized that two-step processes can play an important role in certain direct nuclear reactions. For the (^{3}He,t) reaction, in particular, the coherent contributions of two-step processes, such as (^{3}He,α)(α,t) and (^{3}He,d)(d,t), and the direct charge exchange process have satisfactorily described many transitions in various nuclei.[1,2] The most striking effect, however, has been seen in the transitions to the 0^+ isobaric analog state (IAS) and the anti-analog state(AAS) in ^{40}K.[2,3] In that case the strength and anomalous shape of the AAS angular distribution could be explained in terms of the same parameters which described the IAS transition when the two-step mechanism was explicitly included.

Nonetheless, a number of open questions concerning these sequential nucleon transfer multistep processes still remain. The systematics of the two-step mechanism are not yet well-known, and the importance of these processes for other nuclei and configurations needs to be investigated. In an effort to resolve some of these questions, the ^{56}Fe(^{3}He,t)^{56}Co reaction was studied using the energy loss spectrometer, with an emphasis on small angle data where the calculations can most sensitively be tested.

A triton spectrum taken at 37.5° is shown in fig. A1-c1. The

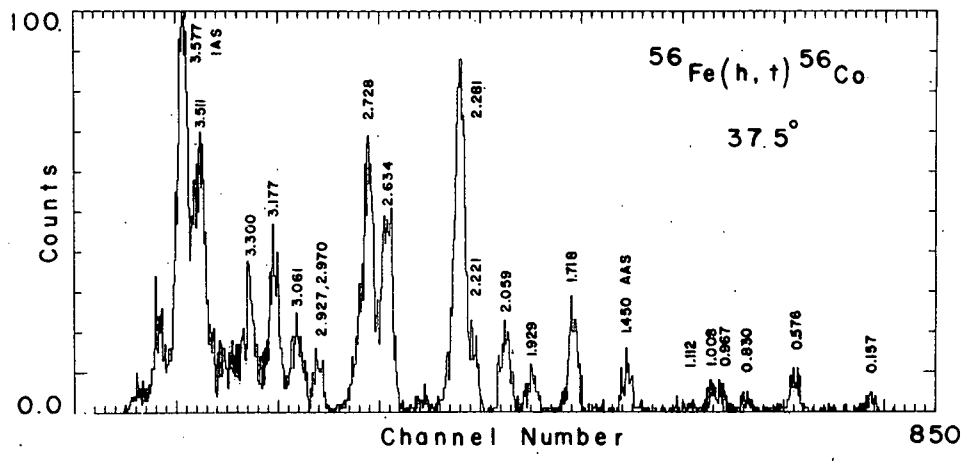

Fig. A1-c1. Spectrum of ^{56}Fe(^{3}He,t)^{56}Co at θ_{lab}=37.5°. IAS doublet and AAS are labeled explicitly.

experimental energy resolution of approximately 44 keV was sufficient to resolve all of the states of interest. The three important peaks for this study are the split IAS at 3511-3577 keV and the AAS at 1451 keV. In fig. A1-c2 are shown the experimental angular distributions for these three states. The angular distributions to the two IAS components are essentially identical except that the 3577 keV distribution has a somewhat sharper diffraction pattern.

To learn about the first step in the two-step process (^{3}He,α) angular distributions were also measured using the same target, bombarding energy, and procedures for analyzing the data as for the (^{3}He,t) reaction.

The simple direct mechanism predicts that the $\Delta L=0$ angular distributions to the IAS and AAS have the same shape and, moreover, that the AAS is much more weakly populated than the IAS, principally because a sum of transition amplitudes contributes to the IAS while it is the difference between these amplitudes which contributes to the AAS and produces strong cancellations.

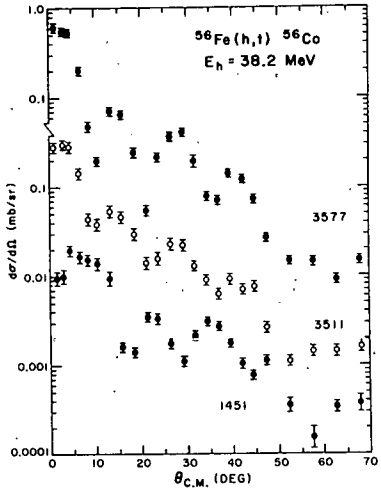

Fig. A1-c2. Angular distributions of two members of the IAS doublet and of the AAS.

The calculations for the IAS and AAS have been made using the method of coupled differential equations. The results of these calculations for the two-step (^{3}He,α)(α,t) reaction only are shown in fig. A1-c3. Here the two components for the IAS have been summed to provide the experimental angular distribution. The one-step contribution to the AAS is insignificant compared to the two-step, and the one-step contribution to the IAS decreases its magnitude slightly to bring the full calculation into better agreement with experiment. It is important to note that this excellent reproduction of the data is achieved without adjustment of any parameters. The sole uncertainty is the (^{3}He,α) spectroscopic factor.

In the ^{56}Fe(^{3}He,α) experiment only a little more than half the expected strength could be found. It is possible that the value of the zero range overlap, D_o, here taken to be -480 MeV fm$^{3/2}$, is

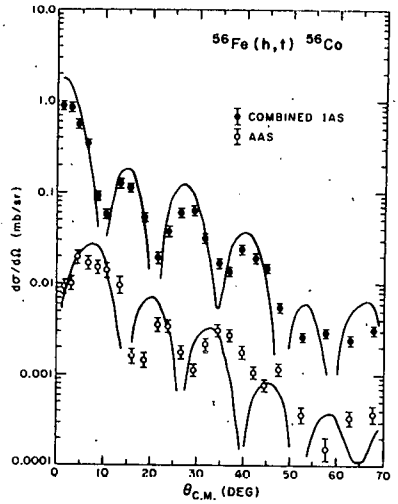

Fig. A1-c3. IAS (summed) angular distribution and AAS reproduced with two-step calculations. Inclusion of one-step improves agreement between data and theory for IAS. One-step contribution is negligible for AAS.

somewhat large,[4] implying that the expected strength is in better agreement with experiment. On the other hand, the assignments for the neutron pickup are not at all well predicted by the simple model and additional strength may lie at higher excitation. In fact an $f_{7/2}$ state in ^{55}Fe with appreciable pickup strength has been observed at 7.78 MeV excitation.[5] Therefore the two-step calculations used the theoretical spectroscopic factors of French and MacFarlane.[6]

A calculation of the two-step process involving a deuteron in the intermediate channels has also been made without non-orthogonality corrections.[7] The result for the IAS is very similar in shape and about 20% larger in magnitude for the $(^3He,\alpha)(\alpha,t)$ process. The cancellations expected for the AAS do not occur and this cross section is very close to that for the IAS, suggesting that the non-orthogonality corrections are expected to have a large effect. There are no non-orthogonality corrections necessary for the $(^3He,\alpha)(\alpha,t)$ process.[7] The deuteron intermediate channels were not included in the final calculation since arguments can be made for the inclusion of only those multistep processes which proceed through a single fragmentation of projectile and target masses (here ^{55}Fe + α) if a complete set of states is included in that fragmentation.[8]

In summary, the two-step process largely dominates the $(^3He,t)$ reaction for the transitions to the 0^+ IAS and AAS in ^{56}Co, providing an excellent fit to the angular distributions, particularly in the forward angles, and reproducing the magnitudes of the cross sections with little sensitivity to the parameters. Preliminary calculations for other states in ^{56}Co also show the importance of the two-step process and exhibit sensitivity to the orbitals which contribute to the transition. This suggests the possibility of obtaining detailed nuclear structure information for these states, which has not been

possible before because of the inaccuracy of the DWBA description of the reaction. Calculations in this direction are under way.

---

1 M. Toyama, Phys. Lett. 38B (1972) 147; N. B. DeTakacsy, Phys. Lett. 42B (1972) 1; W. R. Coker T. Udagawa, and H. H. Wolter, Phys. Lett. 46B (1973) 27; M. Toyama, Nucl. Phys. A211 (1973) 254.

2 W. R. Coker, T. Udagawa, and H. H. Wolter, Phys. Rev. C 7 (1973) 1154.

3 R. Schaeffer and G. F. Bertsch, Phys. Lett. 38B (1972) 159; W. R. Coker, T. Udagawa, and H. H. Wolter, Phys. Lett. 41B (1972) 237.

4 M. E. Edwards, J. J. Kraushaar, and B. W. Ridley, Nucl. Phys. A199 (1973) 463.

5 C. Glashausser and M. E. Rickey, Phys. Rev. 154 (1967) 1033.

6 J. B. French and M. H. MacFarlane, Nucl. Phys. 26 (1961) 168.

7 P. D. Kunz and E. Rost, Phys. Lett. 47B (1973) 136.

8 L. D. Rickertsen and P. D. Kunz, to be published.

ii. Study of the $^{60}Ni(^{3}He,t)^{60}Cu$ Reaction - W. R. Zimmerman, H. Rudolph, and M. J. Schneider

We have chosen the $^{60}Ni(^{3}He,t)^{60}Cu$ reaction for the second study in a projected series of $(^{3}He,t)$ two-step reaction mechanism investigations. We have observed this reaction and the $^{60}Ni(^{3}He,\alpha)^{59}Ni$ reaction at an incident energy of 38 MeV. The $(^{3}He,\alpha)$ data is needed in the two-step description of the $(^{3}He,t)$ reaction.

The experiment was carried out with the energy-loss spectrometer. It is hoped that we will be able to identify the AAS in ^{60}Cu. We will then investigate the importance of the two-step processes using second order DWBA calculations.

It is planned to compare these data to the data of Rudolph and McGrath[1] on the same reaction at 24 MeV incident energy. This should give us some insight into the energy dependence of multi-step reactions.

The data already in hand are currently being analyzed. A $(^{3}He,t)$ spectrum at 55° showing excitation energies ascertained so far is shown in fig. A1-c4.

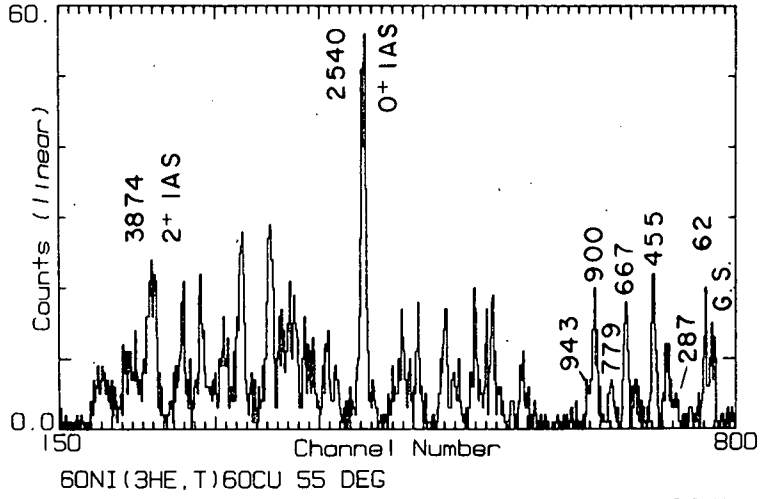

Fig. A1-c4. $^{60}Ni(^{3}He,t)$ spectrum at θ_{lab}=55 degrees.

[1] H. Rudolph and R. McGrath, Phys. Rev. C 8 (1973) 247.

iii. Charge-Exchange Analogs of the Giant M-1 Resonances in ^{24}Mg and ^{28}Si - R. J. Peterson, R. A. Ristinen, M. J. Fritts and N. Stein, E. R. Flynn, and J. Sherman (LASL)

For ^{24}Mg the shell-model isovector sum rule for electromagnetic M-1 transitions is exhausted by transitions to 1^+ T=1 states at 9.94 and 10.70 MeV.[1] The $\Delta T_z = -1$ charge exchange analogs in ^{24}Na of these states have been studied by the ^{24}Mg(t,h)^{24}Na reaction.[2] The $\Delta T_z = +1$ mode has been studied with the energy-loss spectrometer system by the ^{24}Mg(h,t)^{24}Al reaction at a beam energy of 38 MeV. A sample energy spectrum is shown in fig. A1-c5.

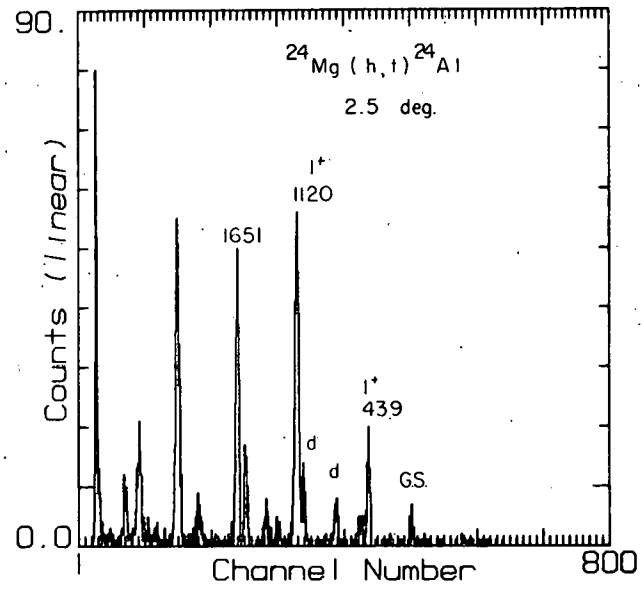

Fig. A1-c5. A spectrum from the ^{24}Mg(h,t)^{24}Al reaction. The 1^+ states are the analogues of the ΔT-1 giant M1 resonance in ^{24}Mg.

The spin assignments for ^{24}Al are not available except for the ground state (4+) and 0.441 MeV state (1+). This 1+ is the analog of the 9.94 MeV state in ^{24}Mg. By comparison to the mirror ^{24}Na, one expects the 0.514 MeV state to be 2+, and the 1.120 MeV state to be 1+. Angular distributions for the lowest 8 states have been taken from 2.5° to 50°. The low-spin states provide the data shown in fig. A1-c6. The identity of the shapes for the 0.441 and 1.120 MeV states confirms the 1+ assignment to the latter. The similarity of both to the 2+ data indicates that the $\Delta L=2$, $\Delta S=1$, $\Delta J=1$ reaction mode predominates. These transitions thus proceed by the highest

allowed L, while the photon experiments[1] measure only the $\Delta L=0$ mode. The expected $\Delta L=0$ and $\Delta L=2$ shapes were predicted by the DWBA code DWUCK and are included in fig. A1-c6. A collective model was used for these curves.

For ^{28}Si the photon experiments find five $\Delta T=1$, 1+ states.[3] Data have been taken for the $^{28}Si(h,t)^{28}P$ reaction, and show again a dominance by the $\Delta L=2$ mode. This analysis is not yet complete, and will be compared to the results of the $^{28}Si(t,h)^{28}Al$ reaction.[4]

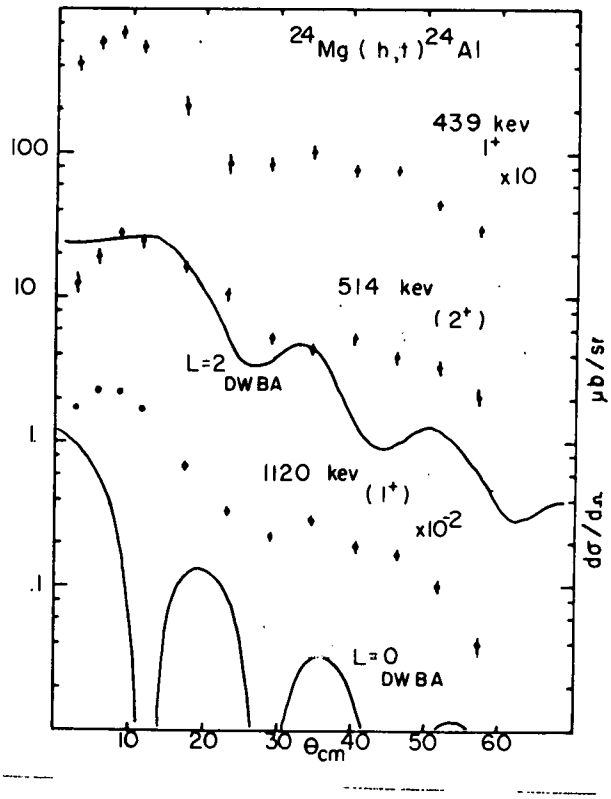

Fig. A1-c6. The angular distributions from the $^{24}Mg(h,t)^{24}Al$ reaction leading to the known 1+ state at .441 MeV and the .514 MeV state are seen to be nearly identical. The latter state is expected to be 2+ by comparison to ^{24}Na. The data for the 1.120 MeV state are also of this same shape. By analogy to ^{24}Na, this would be a 1+ state.

Rather than only demonstrating the isospin invariance of nuclear transitions by $\Delta T_z = \pm 1, 0$ reactions, the larger momentum transfer in the (h,t) or (t,h) reactions has allowed the next moment of the M1 transition to be studied.

These data will also be analyzed under the assumption of two-step reaction processes, through either the collective 2+ excitation or through one-nucleon transfer processes.

---

1 L. W. Fagg et al., Phys. Rev. C 1 (1970) 1137; H. W. Kuehne et al., Phys. Rev. 163 (1967) 1278.

2 E. R. Flynn, J. D. Garrett and N. Stein, in Proceedings of the International Conference on Nuclear Physics, Munich, 1973.

3 L. W. Fagg et al., Phys. Rev. 187 (1969) 1378; N. A. Jelley et al., Phys. Lett. 40B (1972) 200.

4 E. R. Flynn, J. Sherman, N. Stein, Phys. Rev. Letters, to be published.

54,459

iv. Study of Unbound Levels in ^{10}C via $^{10}B(^3He,t)$

M. J. Schneider, B. W. Ridley, M. E. Rickey, and J. J. Kraushaar

In conjunction with the $^{9}Be(d,p)^{10}Be$ experiment (see section II-A-1-a), the energy-loss spectrometer was used to study $^{10}B(^3He,t)$ leading to ^{10}C, which is the member of the T=1 isobaric triplet of mass 10 about which least is known. The rather low (~ 4 MeV) proton separation energy in ^{10}C increases the difficulty of any comparative investigation and only four levels (or groups of levels) have been located with certainty. In previous (^3He,t) and (p,t) experiments using solid state detectors the ground state, a narrow state at 3.35 MeV, and broad prominences at 5.28 and 6.60 MeV excitation were observed. The present experiment was designed to take advantage of the high resolution and low background of the energy-loss spectrometer to search for structure in the broad states, in particular, to try to determine how closely analogous are the ^{10}C 5.28 MeV region to the 6 MeV ^{10}Be quadruplet, and the ^{10}C 6.60 MeV region to the 7.5 MeV ^{10}Be doublet.

Eight spectra were taken, at lab angles from 2.5° to 30°, and in each spectrum the regions containing the broad peaks were decomposed using the Gaussian fitting code SPECTR on the PDP-9 computer. Fig. A1-c7 shows the spectrum at 2.5°. The perceptible asymmetry of the 5.28 MeV peak suggests that it is composed of more than one state. In each region fitted, the widths of the ^{11}C peaks from (^3He,t) on the ^{11}B impurity in the ^{10}B target were held fixed at the width of the ^{10}C 3.35 MeV state, and the widths, heights, and locations of the ^{10}C peak(s) present were allowed to vary, as was the magnitude of the linear background.

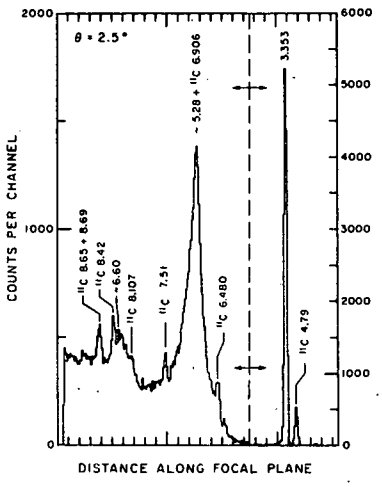

Fig. A1-c7. $^{10}B(^3He,t)^{10}C$ spectrum at θ_{lab}=2.5°. Peaks labeled ^{11}C are populated from ^{11}B impurity in target. Peaks in ^{10}C are labeled with excitation energies from earlier studies. Note separate scales for right and left sides of spectrum.

The 6.6 MeV region was well fit with three ^{11}C peaks (as indicated in fig. A1-c7) plus one ^{10}C peak of width 303±35 keV at E_x=6.590±.020 MeV. The decomposition of this region at 30° is shown in fig. A1-c8. In the 5.28 MeV excitation region, fits were attempted with one, two,

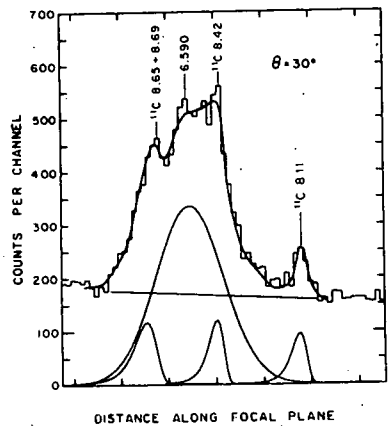

Fig. A1-c8. Decomposition of 6.60 MeV region of excitation in ^{10}C at $\theta_{lab}=30°$. In all spectra this region was well fit by three ^{11}C levels plus one ^{10}C level at the (average) excitation energy noted, plus variable linear background indicated by straight line.

three, or four ^{10}C peaks of variable width and location, plus the three ^{11}C peaks of fixed width. The fits with one ^{10}C peak were visibly deficient at all angles. Fits with four ^{10}C peaks failed to converge due to the high number of free parameters, or converged upon negative heights for one peak, suggesting that there are fewer than four ^{10}C peaks present. Fits with two or three ^{10}C peaks converged equally well and, on the basis of quality of fit, it is not possible to judge between these alternatives.

In the "two ^{10}C peak solution" the ^{10}C states are at 5.237±.011 MeV and 5.290±.070 MeV and have widths of 245±13 keV and 609±34 keV respectively. In the "three ^{10}C peak solution" the ^{10}C states are at 4.921±.025, 5.237±.011, and 5.473±.025 MeV. Their widths are 220±75, 275±30, and 488±68 keV respectively. Sample fits with the two- and three-peak solutions are shown in figs. A1-c9 and A1-c10.

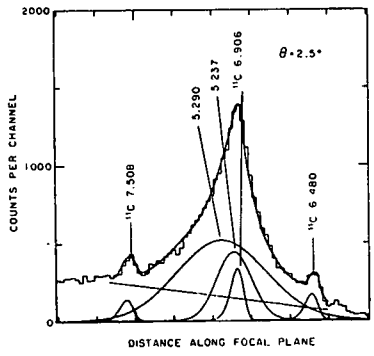

Fig. A1-c9. Decomposition of 5.28 MeV region of excitation in ^{10}C at $\theta_{lab}=2.5°$ into three ^{11}C peaks, linear background, and <u>three</u> ^{10}C peaks.

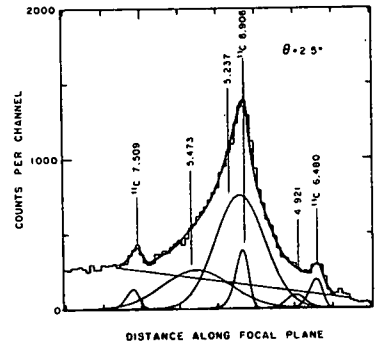

Fig. A1-c10. Same as fig. A1-c9 except that only <u>two</u> ^{10}C peaks are used.

Spectra were also taken using an enriched ^{11}B target, and it was hoped that angular distributions using this target could be used to differentiate between two- and three-peak solutions. However, both solutions yielded similar angular distributions which, furthermore, overlapped within experimental error the angular distributions from the ^{11}B target. Hence our hope was not fulfilled. The relative yields of ^{11}C states with both targets does suggest, however, that the linear background assumption is correct.

Our conclusion is that the onset of instability at excitation energies above the proton separation energy leads to level shifts and widths which preclude detailed comparative analysis between ^{10}C and ^{10}Be above the 3.353 MeV 2+ first excited state. It is unlikely that further studies of this type of the ^{10}C level structure will reveal much more detailed information.

d. Elastic and Inelastic Scattering

i. The (α,α') Reaction on Even Tin Isotopes - A. Rosenthal and R. J. Peterson

A series of experiments has begun to measure the interference between Coulomb and nuclear alpha-particle excitation of the first 2+ state of the even tin isotopes. Preliminary work showed that pure Coulomb excitation of these states could be observed with 12.2 MeV alphas. Typical Coulomb excitation cross-sections are of the order of several μb.

These experiments, which will continue this fall, are expected to result in a set of relative phase angles between Coulomb and nuclear scattering amplitudes as a function of neutron number in the tin isotopes.

ii. Scattering of 27-MeV Protons by Polarized ^{3}He - R. H. Ware and W. R. Smythe

54460

The results of the measurement of the spin analyzing power of 27-MeV protons on ^{3}He were reported in last year's Progress Report, and it was also reported that an attempt to obtain an absolute calibration of the ^{3}He target polarization was being made. The results of that effort are now available and will be reported here.

The target polarization calibration involves the observation of the scattering of alpha particles from the polarized ^{3}He target at and near an angle and energy where the analyzing power of ^{4}He is predicted to pass through unity by a theorem of Plattner and Bacher.[1] Such a calibration is very attractive because previous experimenters reporting on p-^{3}He scattering experiments using polarized ^{3}He targets have quoted a possible systematic error of 12% or more as a result of the uncertainty in the calibration of the optical measurement of the polarization.[2] In this work the optical method of polarization measurement was used before and after each run, and checked by doing the calibration experiment suggested by Plattner and Bacher. The result was that the uncertainty in the target polarization was reduced to approximately 5%.

See fig. A1-d1, on following page.

---

[1] G. R. Plattner and A. D. Bacher, Phys. Lett. 36B (1971) 211.
[2] S. D. Baker, D. H. McSherry, and D. D. Findley, Phys. Rev. 178 (1969) 1616.

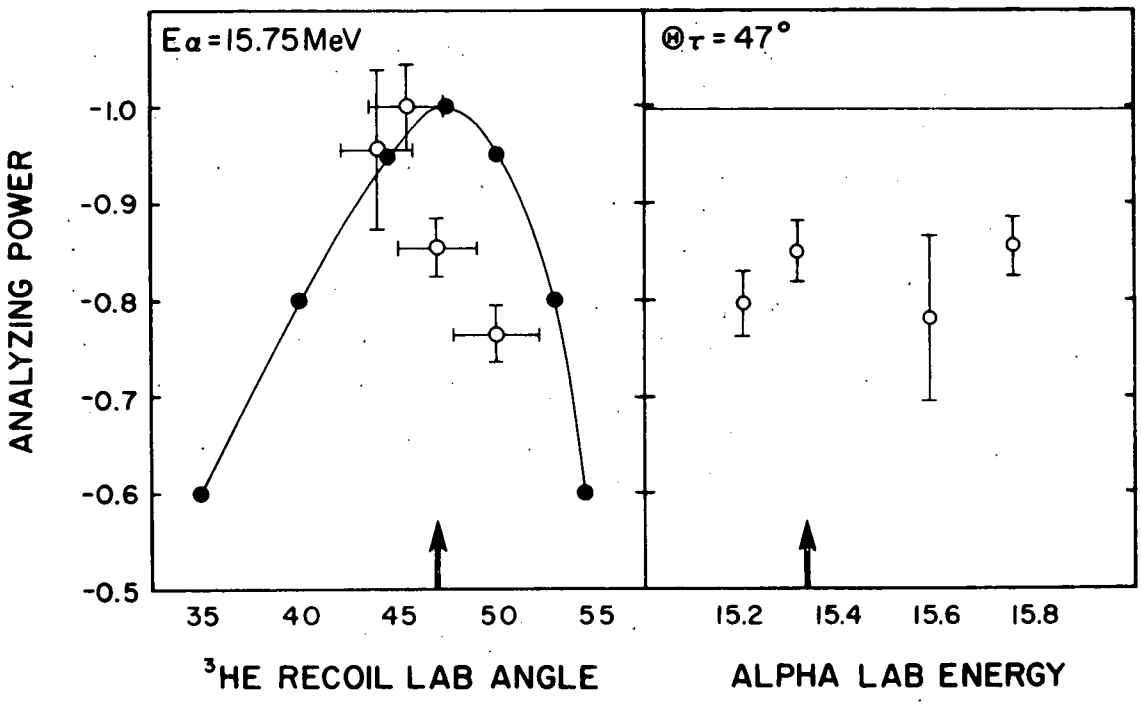

Fig. A1-d1. The search for the calibration point. The ^{3}He spin analyzing power of ^{4}He is shown in the vicinity of the point (indicated by arrows) near which it is predicted to pass through -1 by a theorem of Plattner and Bacher. The solid curves are drawn smoothly through points obtained from the contour map of Hardy et al.[3] The high point of 45.5° lab angle was taken to be the maximum and was set equal to -1.00. This agreed within 2% with the value determined from the optical measurement of the polarization, which had an uncertainty of 12%. Good data at smaller angles could not be obtained without the use of thin detectors for particle identification, which were not immediately available.

---

[3] D. M. Hardy, R. J. Spiger, S. D. Baker, Y. S. Chen, and T. A. Tombrello, Phys. Lett. 31B (1970) 355.

iii. Energy Dependence of the ^{3}He Optical Potential for ^{40}Ca and ^{58}Ni - H. H. Chang and B. W. Ridley

Earlier analyses at this laboratory[1] of the ^{3}He optical potentials from 21 to 83.5 MeV with a fixed set of geometrical parameters indicate the real central well depth changes abruptly with energy as the incident energy decrease below a certain value. This same phenomena is also observed by Marchese, Clark and Griffiths.[2]

Because of this behavior a more detailed examination of the energy dependence of the optical potential is desired.

The best fit parameters of the low energy data within the unique potential family that fit the 83.5 MeV data[1] were found by requiring a smooth variation of the optical parameters with energy. A fixed 2 MeV spin-orbit strength was used and the corresponding radius and diffuseness parameters were set equal to those of the real potential during the search. The final parameters and the volume integral J_R per pair of interacting particles are shown as a function of energy in fig. A1-d2.

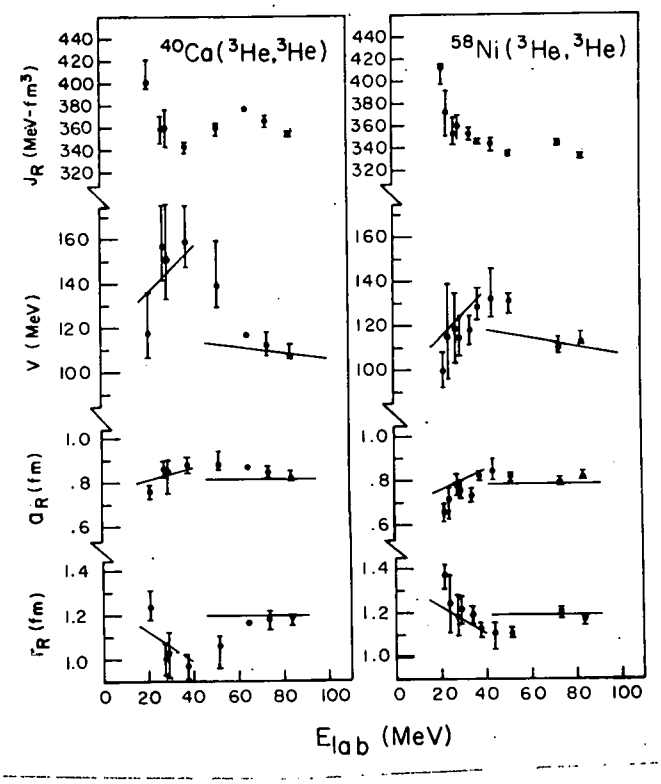

Fig. A1-d2. Best fit optical potential parameters were plotted as solid points against ^{3}He energies. The error bars associated with each point are explained in the text. The solid lines were obtained by fitting the elastic scattering data directly in four separate groups with either E_{lab} greater than 40 MeV or E_{lab} less than 40 MeV and on each target.

In order to evaluate the uncertainties in the parameters a fixed value was assigned to the real well depth at a small interval away from the best fit value and χ^2 again was minimized by varying the rest of the parameters. The end points of the error bars associated with each point in fig. A1-d2 correspond to a local minimum in χ^2, obtained as described above, with a value that is ten percent larger than the optimum one.

Two conclusions can be drawn from fig. A1-d2. First, the well-known continuous ambiguity in the model parameters becomes less pronounced as the energy increases. This is closely related to the effective band pass in angular momentum at each energy as described by Singh and Schwandt[3] for the elastic scattering of alpha particles. Secondly, a systematic variation of the real potential with energy was found, and a definite change in the shape of the real potential is observed for ^{3}He energies below 40 MeV.

The solid lines in fig. A1-d2 represent the results of global optical model searches on the two nuclei separately and in two groups with energies either greater or less than 40 MeV. The calculated cross-sections are shown as solid lines in figs. A1-d3a and A1-d3b. A special set of geometrical parameters was obtained by fitting the 33.5 MeV data of ^{40}Ca and ^{58}Ni simultaneously. The potential well depths of this particular set of geometrical parameters were found by assuming a linear dependence in energy and by fitting all the data from 21 to 33.5 MeV for each nucleus. The

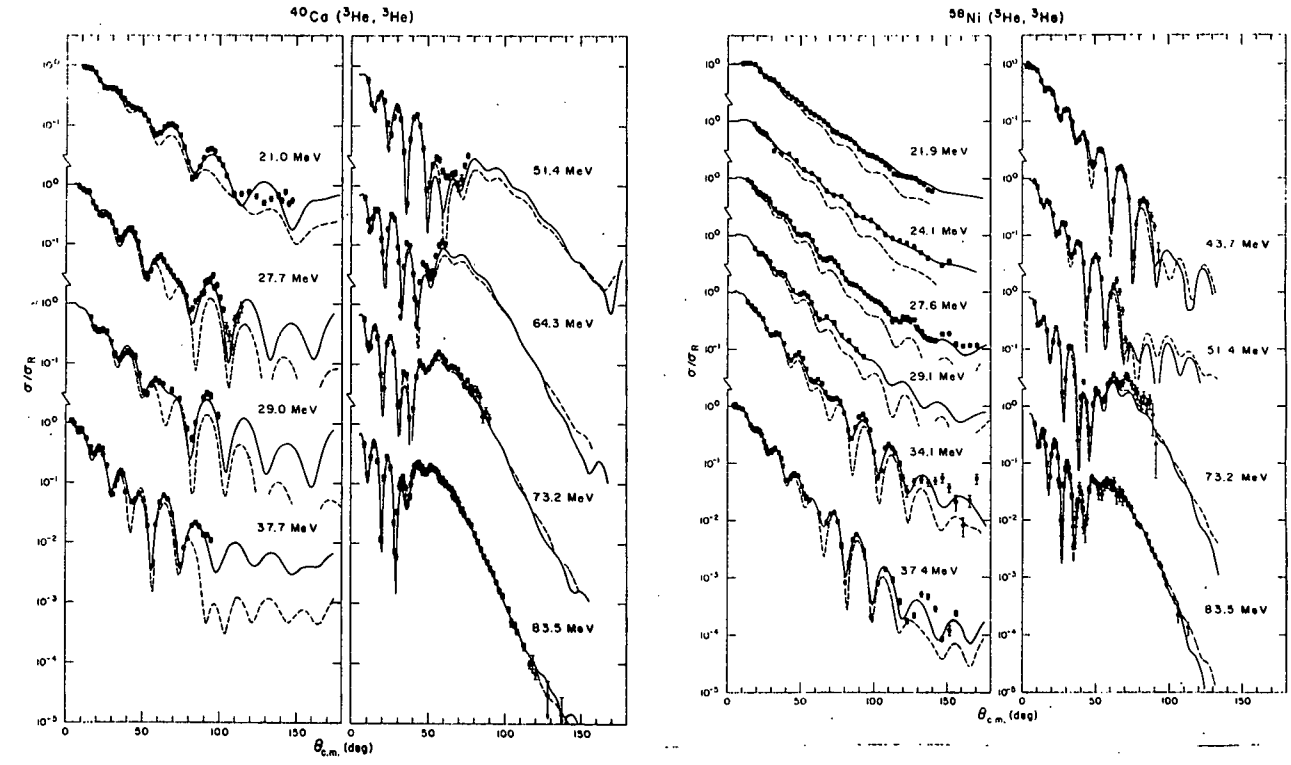

Fig. A1-d3a and A1-d3b. Angular distributions from the elastic ^{3}He scattering on ^{40}Ca and ^{58}Ni. The solid curves are calculated from four sets of global parameters (solid line in fig. A1-d2). The dashed lines are results of a fixed geometry analysis as explained in the text.

energy dependence found for ^{40}Ca was V=121.6-.17E MeV, W_d= 21.9-.043E MeV and for ^{58}Ni, V=118.2-.10E MeV, W_d=24.9-.069E MeV. The geometrical parameters are $r_R=r_{so}$=1.192 fm, $A_R=A_{so}$=.814 fm, R_I=1.239 fm and A_I=0.811 fm with a spin-orbit well depth of 2 MeV. The optical model predictions are shown as the dashed line in fig. A1-d3a and A1-d3b. The failure of these parameters to give the correct magnitude of the elastic cross-sections at low energies might also indicate a change in the shape of the potential is needed at low energies.

This work is complete and a detailed report will be shortly submitted for publication.

---

1 H. H. Chang, B. W. Ridley, N. S. P. King, E. F. Gibson, Univ. of Colorado Nuclear Physics Laboratory Progress Report, 1973, 14.

2 C. J. Marchese, N. M. Clarke, and R. J. Griffiths, Phys. Rev. Lett. 29 (1972) 660.

3 P. P. Singh and P. Schwandt, Phys. Lett. 42B (1972) 181.

iv. Energy Dependence of the α-Particle Optical Potential for ^{40}Ca and ^{58}Ni - H. H. Chang and B. W. Ridley

54,461

It has been shown that the discrete ambiguities in the real well depth of the optical potential for these two nuclei are resolved by taking data at sufficiently high energies and out to sufficiently large scattering angles.[1,2] In this analysis, emphasis has been placed on determining the energy dependence of this particular family (V ~ 125 MeV). In order to find the systematic trend of the model parameters with energy from 18 to 139 MeV considered here, the global search code OPTIM(M) was modified to include various energy dependent terms. It is worthwhile to point out that at each fixed energy the derivative of χ^2 against each parameter and its corresponding energy dependent term are essentially the same except for a fixed constant ratio between them. Based on this concept, we were able to include any number of energy dependent terms in the global search without significantly increasing the computing time.

The solid curves of figs. A1-d4 and A1-d5 represent the end results of the global searches done separately on ^{40}Ca and ^{58}Ni. A total of eight parameters (V, V_E, R_R, A_R, W_V, W_{VE}, R_I, A_I) were varied during the minimization of χ^2. The parameters thus obtained for ^{58}Ni are listed as the first row in table A1-VII.

The fits deteriorate very rapidly for both ^{58}Ni and ^{40}Ca as the incident energy falls below 50 MeV. The geometrical parameters are usually weighted more heavily by the high energy data. The failure to give the correct magnitude of the elastic scattering cross-section at low energies might indicate a change of the optical potential shape at low energy. Since the parameters obtained above

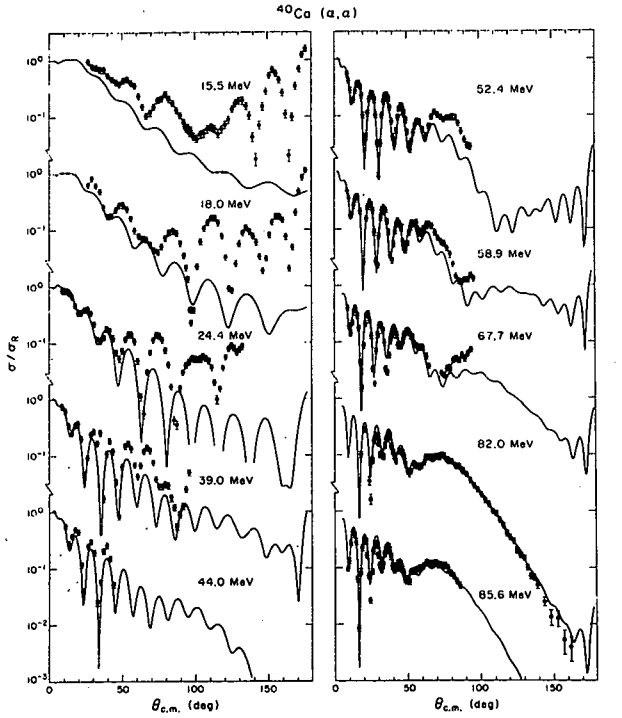

Fig. A1-d4. Angular distributions from the elastic α-scattering on ^{40}Ca. The points represent the experimental data. The solid curves are calculated from an averaged optical potential with linearly energy dependent terms in the well depths.

Fig. A1-d5. Angular distributions from the elastic α-scattering on ^{58}Ni. The points represent the experimental data. The solid curves are calculated from the first row of table A1-VII and the dashed line the last row of table A1-VII.

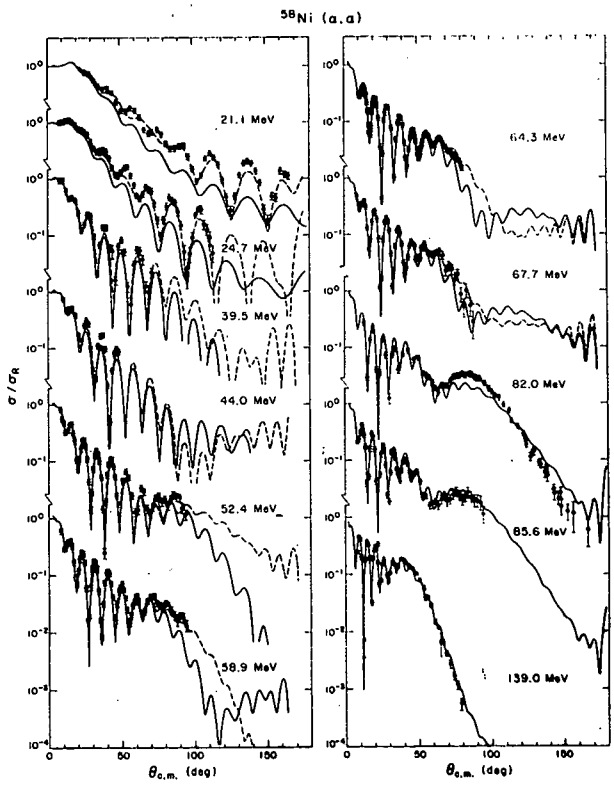

TABLE A1-VII. Energy dependent parameters for $^{58}Ni(\alpha,\alpha)$.

Energy Range (MeV)	V (MeV)	R_R (fm)	A_R (fm)	W_V (MeV)	R_I (fm)	A_I (fm)	χ^2N
21.1-139.0	127.87 -.142E	1.315	.724	14.94 +.0415E	1.645	.484	10.0
21.1-67.7	111.33	1.384	.649	19.83	1.605	.502	6.0
21.1-67.7	110.79 -.108E	1.428	.591	6.85 +.301E	1.476	.618	5.2
21.1-67.7	101.54 +.217E	1.504 -.00231E	.489 +.00297E	7.86 +.199E	1.585	.519	3.1

are weighted by all the data, we expect the actual change of potential shape should occur slightly higher than 50 MeV. These phenomena were also observed by L. W. Put, A. M. J. Paans[3] on ^{90}Zr and by D. Madland, P. Schwandt on nickel isotopes[4] in a slightly different way.

The last three rows of table A1-VII represent several attempts to fit the $^{58}Ni(\alpha,\alpha)$ data in the range from 21 to 67.7 MeV simultaneously using either energy independent or various linearly energy dependent terms. The optical model predictions from the last row of table A1-VII are shown as dashed lines in fig. A1-d5 from 21.1 to 67.7 MeV. Similar searches on $^{40}Ca(\alpha,\alpha)$ will be carried out in the near future.

[1] D. A. Goldberg, S. M. Smith, H. G. Pugh, P. G. Roos, and N. S. Wall, Phys. Rev. C 7 (1973) 1938.
[2] H. H. Chang, B. W. Ridley, N. S. P. King, E. F. Gibson, Univ. of Colorado NPL Technical Progress Report (1973) 17.
[3] L. W. Put and A. M. J. Paans, Phys. Lett. 49B (1974) 266.
[4] D. Madland and P. Schwandt, Bull. Am. Phys. Soc. 18 (1973) 604.

v. Inelastic Alpha Scattering to Unnatural Parity States - F. E. Cecil and R. J. Peterson

The importance of two-step processes in the excitation of unnatural parity states in two-nucleon processes has recently been reported.[1] Analogous arguments may be applied to inelastic alpha scattering to distinguish between double inelastic scattering and successive single-nucleon transfers leading to the final unnatural parity state. In order to test these arguments, we have measured the cross sections for the excitation in the inelastic scattering of 36 MeV alpha particles to the 12.71 1+ T=0 state in ^{12}C. Using the energy loss spectrometer and improved collimation at the exit to the scattering chamber, we were able to obtain good data at a laboratory scattering angle of 5°. Preliminary analysis of the data indicates that the cross section peaks at about 12° and drops

sharply inside of about 10°, suggesting that the reaction proceeds predominantly through a double inelastic scattering process.

---

[1] Takeshi Udagawa and David K. Olsen (to be published).

2. Gamma Ray Experiments and Beta Decay

a. (^{3}He,2n) Reaction Cross Sections on Several Light Nuclei - C. E. Moss and C. S. Zaidins

The analysis of the excitation functions taken in the reactions ^{9}Be(^{3}He,2n)^{10}C, ^{24}Mg(^{3}He,2n)^{25}Si, and ^{27}Al(^{3}He,2n)^{28}P was completed and a paper submitted to Nuclear Physics on this experiment. The ^{10}C and ^{28}P activities were detected by means of β-delayed gamma rays and the ^{25}Si activity was detected by counting β-delayed protons. A typical gamma spectrum for the ^{10}C is shown in fig. A2-2. The final cross sections from our excitation function are shown in fig. A2-1. The details on the analysis were given in last year's progress report. One further correction was necessary to modify the cross-sections presented last year. In the case of the ^{24}Mg(^{3}He,2n)^{25}Si reaction, the target had to be very thin to permit the β-delayed protons to be detected with sufficiently good resolution to be identified with a particular transition. As a result, a non-trivial fraction of the ^{25}Si nuclei were able to recoil out of the target. The correction factor necessary to compensate for this effect ranged from about five to ten depending on the ^{3}He energy. In all cases the Be and Al thickness allowed only a negligible fraction of the ^{10}C and ^{28}P to recoil from the target.

Statistical methods were used to try to fit the excitation functions. This technique has been successful in the region for A > 50 but did not fit our present data well. Although the shapes were generally correct, the predicted magnitude was about an order of magnitude too small. It is clear that a revised model is necessary to do a reasonable job of predicting cross sections for reactions on light nuclei, which involve the emission of two or more neutrons.

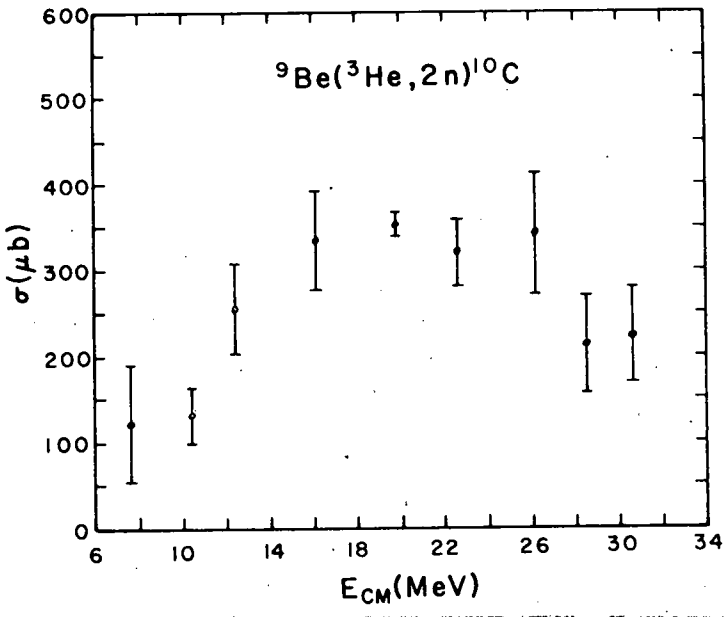

Fig. A2-1. Cross sections for the reactions I): ^{9}Be(^{3}He,2n)^{10}C

(Figure continued on next page.)

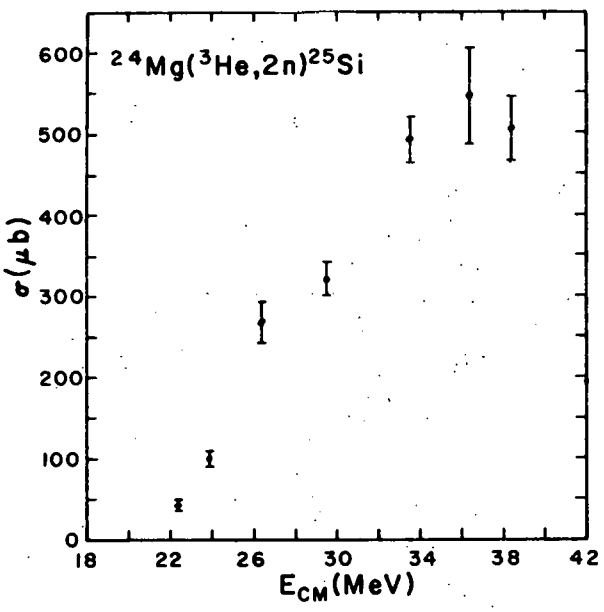

Fig. A2-1, continued.

Cross sections for the reactions II) $^{24}Mg(^{3}He,2n)^{25}Si$, and III) $^{27}Al(^{3}He,2n)^{28}P$.

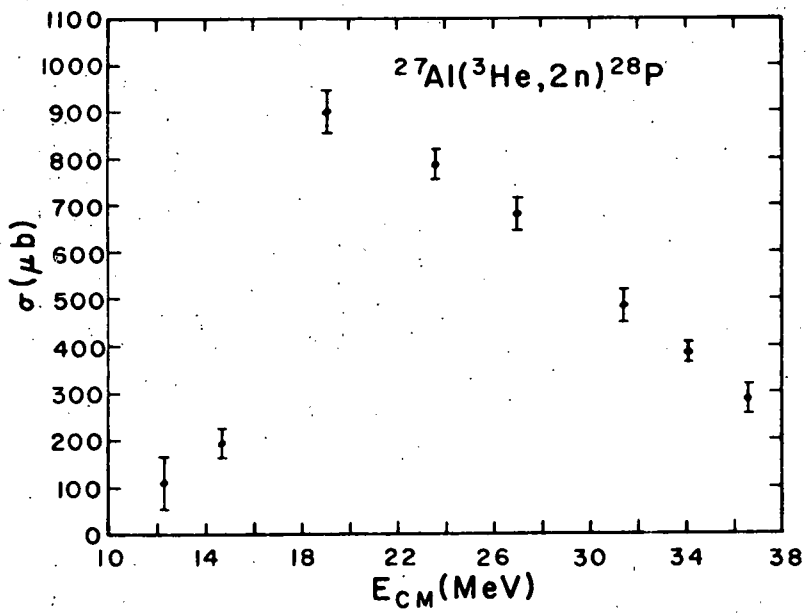

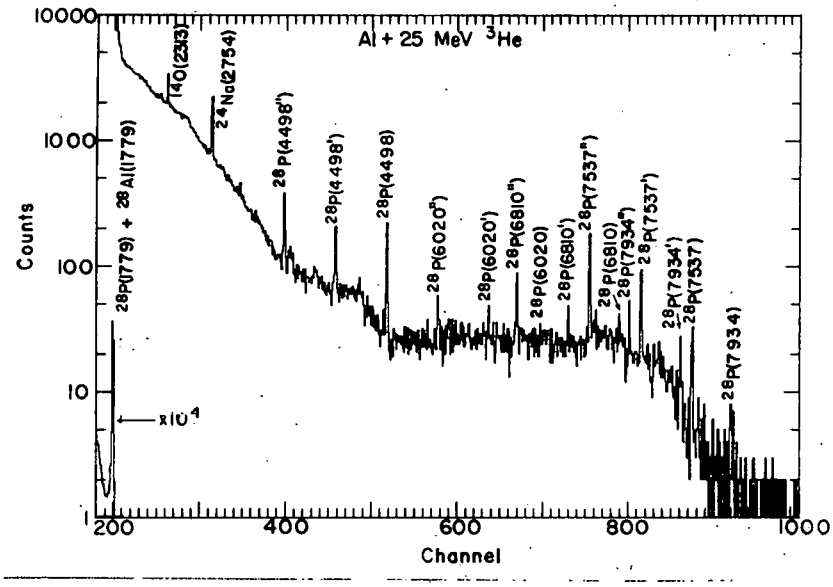

Fig. A2-2. A β-delayed γ-ray spectrum obtained in the first time bin for 21 MeV ^{3}He incident on an ^{27}Al target. The 4498 keV γ-ray was used to determine the ^{27}Al(^{3}He,2n)^{28}P cross section. The peaks are labeled with the parent nucleus and the γ-ray energy. One or two primes denote single or double escape peaks respectively.

b. The Decay of ^{36}K - M. J. Fritts

The investigation of the ^{36}K β^+ decay is nearly completed. Major problems in the analysis of the data had been the proper identification of contaminant peaks and the construction of an accurate relative efficiency curve extending up to 10 MeV. It was found that twenty nuclides were fairly strongly produced from reactions on the Havar foil window and brass mounts (see section II-C-3) in addition to the background lines due to ^{40}K, ^{124}Sb, and ^{122}Sb normally present in the switchyard. Competing reactions on the ^{36}Ar gas led to γ-rays from the decay of ^{33}Cl, ^{35}Ar, and possibly ^{37}K, while a small air contamination led to ^{14}O and ^{16}N activities. Although many of these lines hindered efforts to extract weak transitions in ^{36}Ar, they did at least provide excellent energy calibration points and copious consistency checks on the accuracy of the efficiency curve (see section II-C-4).

The spectrum of γ-rays produced following the decay of ^{36}K is shown in fig. A2-3. Their energies and intensities are listed in table A2-I, along with a comparison with previous work.[1] The agreement is good. The decay of those γ-rays which were followed in the sequential spectra are shown in fig. A2-4. Those weak γ-rays which could not be followed due to their merging with much larger neighboring peaks in the lower resolution (4 x 1024) spectra are so indicated

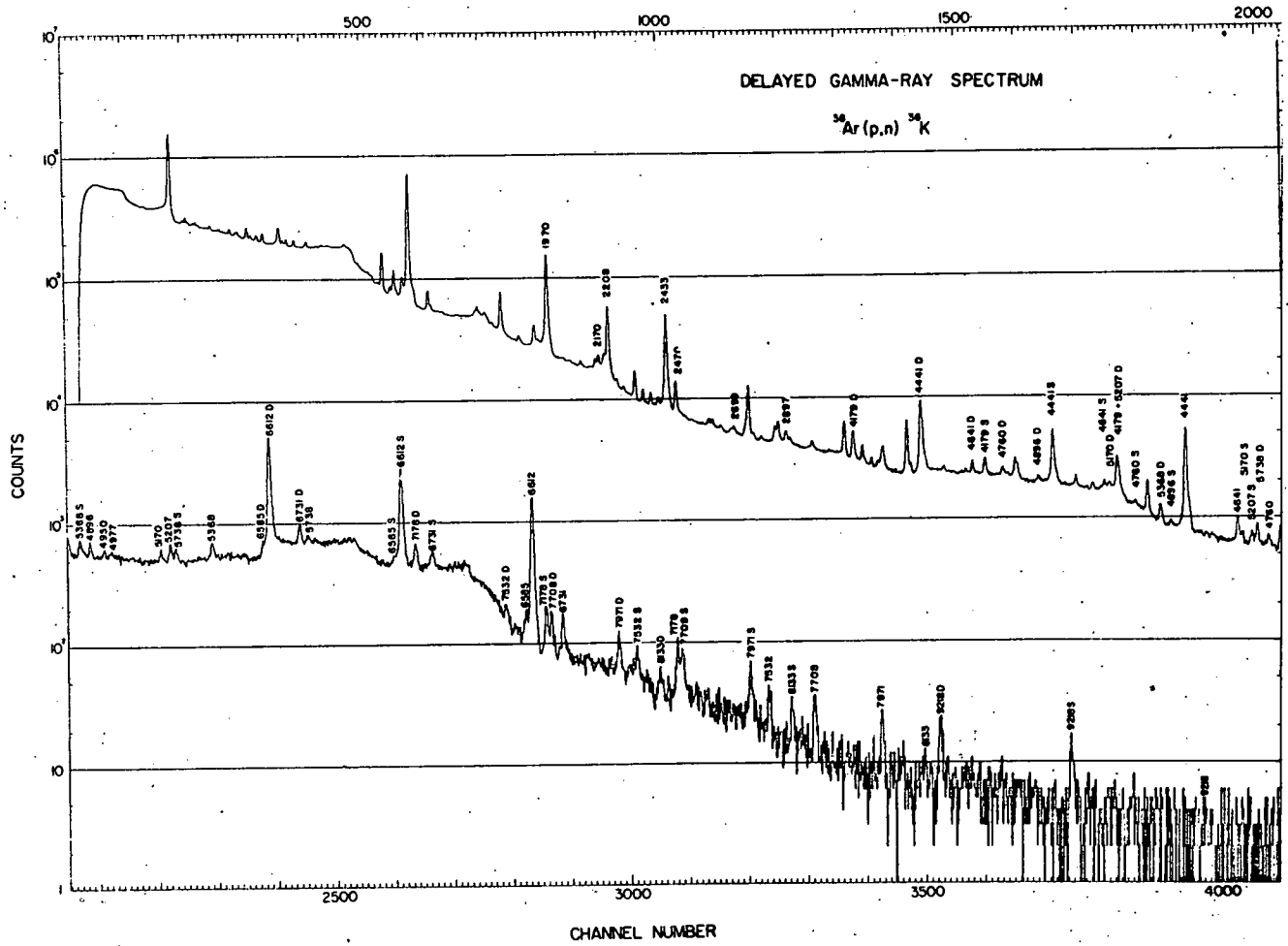

Fig. A2-3. The spectrum of γ-rays following the decay of ^{36}K. Full energy, single escape, and double escape peaks are all labeled. All other peaks are contaminants.

TABLE A2-I. Energies and intensities of γ-rays in ^{36}Ar following the decay of ^{36}K.

Present Experiment		Reference 1		
Energy (keV)	Relative Intensity	Energy (keV)	Relative Intensity	Transition
9218.35±1.18	60±15			gs.
8132.62±1.40	65±20			gs.
7970.53±0.69	155±25			9941→1970
7708.24±0.65	210±30			gs.
7531.57±1.04	155±30			9502→1970
7177.62±0.52	460±55			gs.
6730.53±0.50	550±70			gs.
6612.13±0.37	8140±590	6612.7±0.8	9250±1150	gs.
6585.05±0.49*	195±65			8555→1970
5738.24±0.55	440±70			7708→1970
5367.52±0.47	665±80			7338→1970
5206.53±0.42	385±90			7177→1970
5169.51±0.77	370±75			7140→1970
4977.15±1.05*	170±60			gs.
4950.04±0.91*	195±60			gs.
4896.27±1.09	420±75			6867→1970
4759.60±0.72	545±85			6730→1970
4640.96±0.50	875±95	4643.7±1.4	<1100	6612→1970
4440.79±0.34	9750±600	4441.7±0.6	11800±650	gs.
4178.53±0.41	2500±100	4180.4±1.0	3900±890	gs.
2896.97±0.34*	1210±85			7338→4441
2699.28±0.45*	470±35			7140→4441
2470.46±0.42	5830±230	2472.0±0.8	5570±890	4441→1970
2433.43±0.21	38800±1750	2433.7±0.4	41800±5100	6612→4179
2207.83±0.30	36500±1670	2208.3±0.4	36700±5100	4179→1970
2170.29±0.20*	3700±400	2171.5±0.9	2800±630	6612→4441
1970.44±0.46	100000±10300	1969.8±0.5	100000±10100	gs.

*Decay of γ-ray not followed.

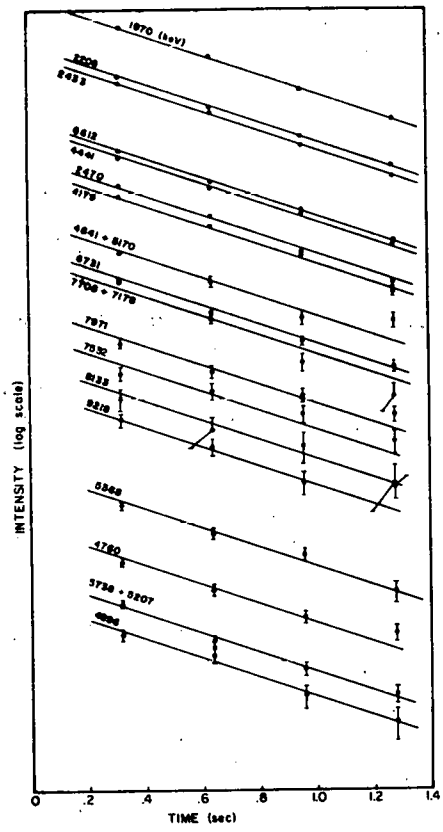

Fig. A2-4. The decay of γ-rays associated with transitions in ^{36}Ar.

in table A2-I. These lines are listed as arising from the ^{36}K decay since they have the appropriate energy for transitions between known ^{36}Ar levels[2,3] and they are at least due to reactions on either ^{36}Ar or air, since they are not present in background runs with a helium target. In addition, the branching ratios are either in good agreement with previous work or, if the other branches are not seen, these branches have ratios such that they should not be seen in the regions of the spectra in which they fall, i.e., there is no conflict with known branching ratios for these levels.

Table A2-II lists the excitation energies of levels in ^{36}Ar involved in the ^{36}K decay which were seen in this study, compared with the results of other investigations. The results are in good agreement for most levels, with values separated by more than one standard deviation for only very weak transitions. A similar comparison of branching ratios is shown in table A2-III. Again the agreement is good. As indicated in the table, for cases in which competing branches could not be seen, the values of ref. 3 were adopted.

This work will be submitted shortly to Physical Review for publication.

---

[1] D. W. Miller et al., Phys. Rev. C 6 (1972) 869.
[2] P. M. Endt and C. van der Leun, Nucl. Phys. A214 (1973) 1.
[3] P. M. Johnson et al., Nucl. Phys. A218 (1974) 333.

TABLE A2-II. Excitation energies of levels in ^{36}Ar seen in ^{36}K decay.

Present Experiment	Ref. 2	Ref. 3
1970.4±.5	1970.39±.05	1970.3±.2
4178.5±.5	4178.33±.11	4178.1±.7
4440.8±.5	4440.1± .2	4440.2±.5
4950.0±.9	4951.9± .5	4950.9±.5
4977.2±1.1	4974.05±.19	4974.1±.7
6611.8±.5	6610.8± .3	6611.4±.5
6730.5±.7	6729 ±9.0	6724 ±2.
6866.7±1.1	6868.5±1.0	6865.2±1.
7140.1±.9	7139.5± .4	7140.5±1.
7177.4±.6	7178.7± .9	7179.0±.5
7337.9±.7	7335.6± .7	7338.5±1.
7708.4±.8	7710.7±1.8	7711.1±1.5
8132.6±1.4	8136± 10.	8132 ±2.
8555.5±.6	8550± 30.	---
9218.4±1.2	9220	9220
9502.0±1.1	9501	9502
9941.0±.8	9941	9942

TABLE A2-III. Branching ratios of ^{36}Ar levels seen in ^{36}K decay.*

E_x (keV)	J^π	0 0^+	1970 2^+	4179 3^-	4441 2^+	Others E_x(%)
1970	2^+	100				
		100				
		100				
4179	3^-	7.7±0.6	92.3±0.6			
		5.9±0.6	94.1±0.6			
		6.0±0.6	94.0±0.6			
4441	2^+	64±2	36±2			
		65±3	35±3			
		62.5±2.5	37.5±2.5			
4950	2^+ a)	84±5	16±5	<2	---	---
		86±4	14±4	<2	---	---
		84	---	---	---	Unknown 16
4977	2^-	19±2	5±2	76±2	<0.3	---
		16±2	4.0±0.9	80±3		---
		19	---	---		Unknown 81
6612	2^+,T=1	22±3	<5	78±3	---	---
		15±3	<7	85±3	<6	---
		15.8±1.7	1.7±0.3	75.3±2.5	7.2±1.1	---
6730	$(1,2)^+$	70±10	---	---	---	Unknown 30
		---	---	---	---	---
		48±7	52±7	---	---	---
6867		25±5	75±5	---	---	---
		51±12	49±12	---	---	---
		<23	77	---	---	---
7140	3^+	<2	48±5	<3	52±5	---
		---	44±7	---	56±7	---
		---	44±7	---	56±7	---
7177	$(1,2)^+$	70±10	30±10	---	---	---
		63±13	37±13	---	---	---
		50±7	50±7	---	---	---
7338	3^+ a),T=1	<3	26±3	9±2	54±2	4415 (11±2)
		<6	31±5	17±4	52±5	---
		---	29±4	---	51±4	Unknown 20
7708	$(1-3)^-$	35±10	65±10	---	---	---
		39±7	---	---	---	Unknown 61±7
		32±8	68±8	---	---	---
8133		60±7	40±7	---	---	---
		---	---	---	---	---
		60	---	---	---	Unknown 40
8555	2^+,T=1	---	---	---	---	---
		---	---	---	---	---
		---	100	---	---	---
9218	$1^{(+)}$,T=1	34	50	<1	11	(4328(.4), 4950(0.8), 4977(3), 5836(0.8))
		---	---	---	---	---
		34	---	---	---	Unknown 66
9502	2,3,4	1	57	<1	14	4415(4), 6612(16), 7338(8)
		---	---	---	---	---
		---	57	---	---	Unknown 43
9941	2,3	1	55	1	3	4977(6), 5836(3), 6612(20), 6837(1), 7137(2), 7248(4), 7338(3)
		---	---	---	---	---
		---	55	---	---	Unknown 45

* Entries are in ref. 3, ref. 2, present experiment order.
a) All assignments are from ref. 2, unless indicated to show ref. 3.

c. An Attempt to Measure the Cross Section for Double Pair Production by Gamma Rays - R. A. Ristinen and R. J. Peterson

The basic nature of the electro-magnetic interaction is intriguing to most physicists. One second order process that could be studied is double pair production--the simultaneous creation of two electron-positron pairs by a single photon. The ratio to single pair production should be proportional to α^2, and hence weak. The experimental evidence is sketchy at best.[1]

The cyclotron rabbit facility was used to provide an intense source of 6.13 MeV gamma rays from the 7.1 second decay of ^{16}N produced by the $^{13}C(\alpha,p)^{16}N$ reaction. The gamma ray spectrum from the substantially monoenergetic source was then recorded in several time bins by a Ge(Li) detector through a 2 cm Pb plus 2 cm Lucite absorber. The very prominent full energy peak, single escape peak, and double escape peak were observed with excellent statistics and a search was made for triple and quadruple escape peaks which would result from double electron-positron pair production by a single 6.13 MeV gamma ray.

As a preliminary result, we have an upper limit for the intensity of the quadruple escape peak relative to the double escape peak which would correspond, when corrected for detector efficiency and geometry factors, to a ratio of $<1.4 \times 10^{-3}$ for double pair production processes relative to single pair production processes. This corresponds to $<30\ \alpha^2$. Of course double pair production could occur either through a single-step process or by a two-step process involving intermediate bremsstrahlung and these two types of contributions could be resolved by a series of measurements with different detectors and gamma ray energies, once the quadruple escape peak is found.

---

[1] W. Heitler, The Quantum Theory of Radiation, Third Edition, 1954, p. 338.

d. Addition to the Decay Scheme of ^{24}Al - R. J. Peterson and R. A. Ristinen

The first attempt to search for the quadruple escape peak for a photon incident upon a Ge(Li) counter was a study of the gamma spectrum from ^{24}Al decay, made by the (p,n) reaction on a natural magnesium target in the rabbit system. Excellent statistics were obtained, and a new peak was identified that fits into the earlier level scheme of ref. 1. This 5061 keV line corresponds to the decay from the 9298 keV (4^+) state of ^{24}Mg to the 4237 keV 2^+ state. Its strength is approximately equal to the strength of the 5177 keV transition from the 9298 keV state to the 4.23 keV 4^+ state. This observation changes the β branch to the 9298 keV state

from 2.4% to 3.4%.

---

[1] C. Détraz, Nucl. Phys. A188 (1972) 513.

e. Some Reactions Induced by ^{1}H, ^{2}H, ^{3}He, and ^{4}He Ions on Natural Targets of Mg, Al, and Si - C. S. Zaidins and C. Détraz in collaboration with D. J. Frantsvog, R. L. Wilson, and A. R. Kunselman (of the University of Wyoming)

The rabbit system was used to transport thin natural targets of Mg, Al, and Si between the irradiations in the target box to the gamma counter in a well shielded counting area. The irradiating was done with projectiles of ^{1}H, ^{2}H, ^{3}He, and ^{4}He and the gamma counting was done with a Ge(Li) detector. The data were accumulated with the ND 50/50 pulse height analyzer and were analyzed with the PDP-9 computer system.

A Faraday cup was used to measure the beam currents and comparison with other data, where possible, indicates consistent results. The beam current information was combined with the measured gamma activities to calculate the total cross sections for reactions which occurred. Half lives were also measured as an indication of the confidence one could have in the measurements. The analysis is essentially complete and articles describing the results are in preparation for publication in Nuclear Physics.

The results are excitation functions for various reactions on these s-d shell nuclei. The major usefulness of this information is in designing and optimizing experiments with nuclei in this mass-region.

f. Short-Lived Radioactivity Induced in Ge(Li) Gamma-Ray Detectors by Neutrons - R. L. Bunting and J. J. Kraushaar

54.462

When a Ge(Li) detector is used to measure the gamma-ray spectra that follow a reaction involving neutrons as outgoing particles, a number of spurious peaks can appear. Prominent peaks are seen, for example, in the gamma-ray spectra due to inelastic neutron excitation of the first excited states of the nuclei of several isotopes of the germanium atoms in the detector. These peaks result from the interaction of gamma-rays, internal conversion electrons or x-rays in the detector. Peaks at 690 keV (^{72}Ge) and 596 keV (^{74}Ge) are commonly seen in reaction studies such as (p,xnγ) or (α,xnγ).

In practice with the larger Ge(Li) detector now available, the main source of interference is excitation by inelastic neutron

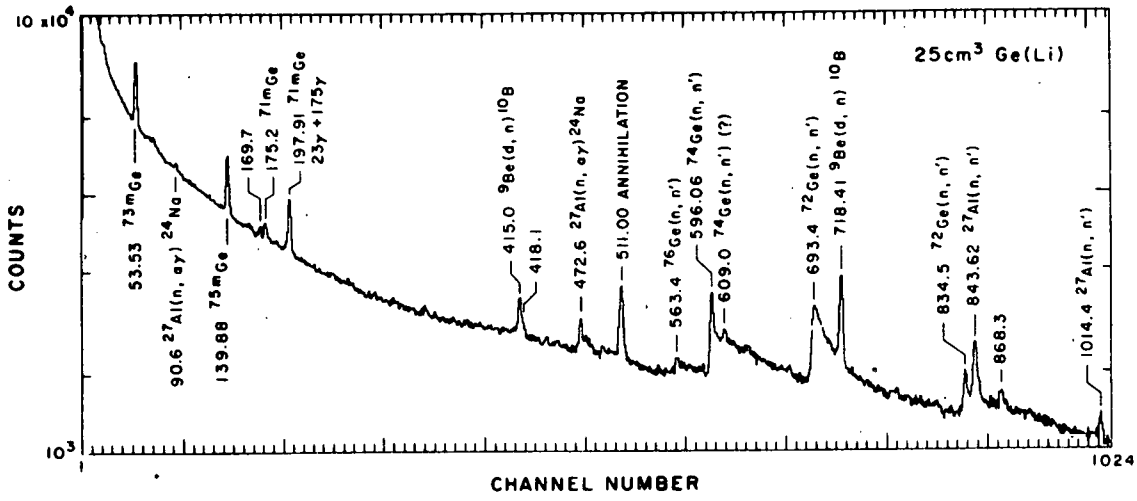

Fig. A2-5a.

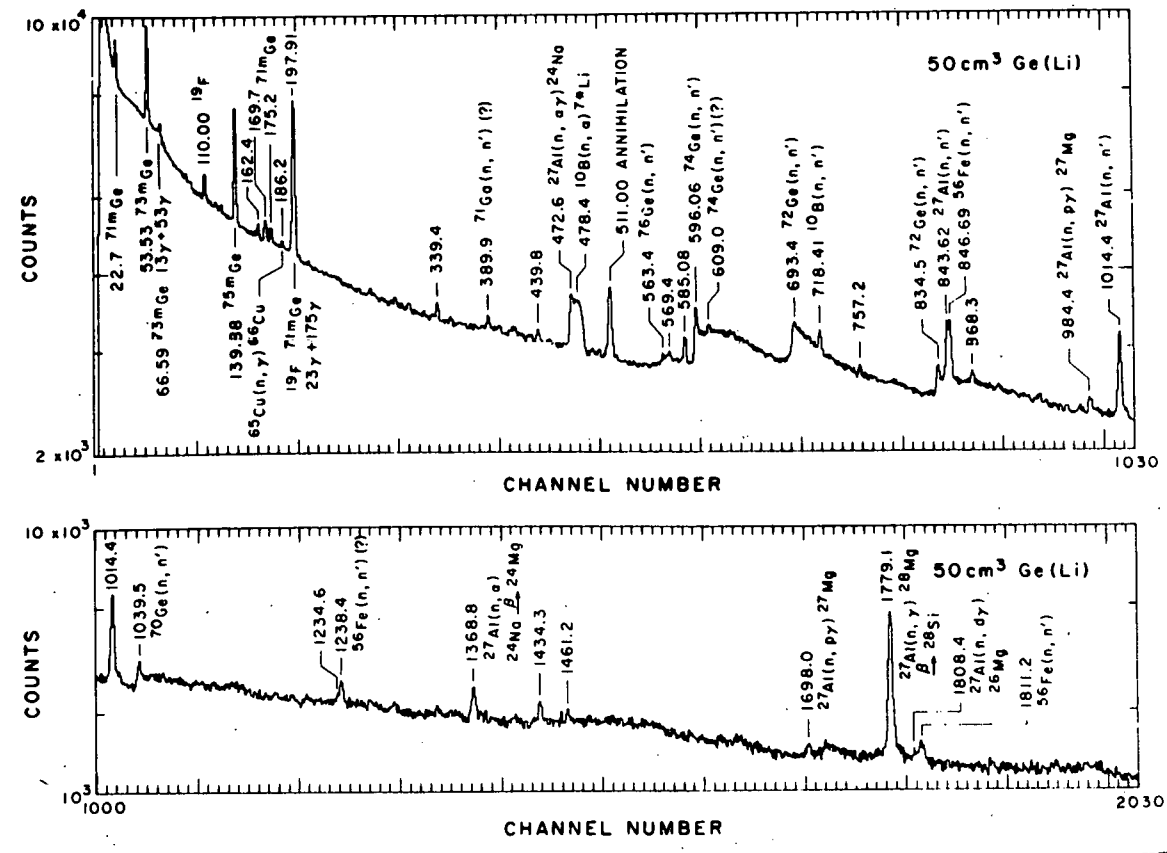

Fig. A2-5b.

Fig. A2-5. Prompt pulse height spectra produced by neutron irradiation of Ge(Li) detectors. In fig. A2-5a, a 25 cm^3 detector was used with neutrons produced by 17 MeV deuterons on thick Be target. In fig. A2-5b, a 50 cm^3 detector was used with neutrons from 17 MeV deuterons on a deuterium gas target.

scattering. There is little chance of misidentification of these peaks, however, as the peak shape is not that of a typical gamma-ray but is noticeably broadened. This occurs because a varying fraction of the nuclear recoil energy is converted into electron-hole pairs that add to the electron-hole pairs from associated nuclear de-excitation. These effects were also extensively investigated by Chasman et al.[1]

In the process of studying the $(\alpha,n\gamma)$ reaction on several isotopes we became aware of some additional spurious peaks generally in the region below 200 keV where data from Chasman et al. were not generally available. These peaks, in contrast to most of the higher energy lines, were not broadened but appeared with widths identical to those of gamma rays from the target and hence could be easily misidentified. To further complicate the problem, some of these transitions were observed in delays of the order of seconds after the irradiation ceased and hence had the potential for causing confusion when short-lived isomeric transitions were being observed.

To get a complete picture of the low energy peaks that result from energetic neutrons incident upon a Ge(Li) detector, two separate experiments were done. The experiments involved the observation of the pulse height spectra using two different Ge(Li) detectors with a beam of neutrons generated by 17 MeV deuterons on a thick beryllium and a deuterium gas target. Spectra were recorded both during the beam burst and in varying periods after the termination of the beam.

In fig. A2-5a is shown the spectrum obtained with the 25 cm^3 detector and neutrons from the Be target. The irradiation took about 20 minutes. Using the number of counts under the triangular shaped inelastic neutron peak around 690 keV it was determined that about 5×10^5 neutrons/cm^2 were incident on the detector during the exposure that produced the spectrum shown. The integrated flux was obtained by multiplying the total number of counts under the 690 keV peak by 20. The identification of the origin of the gamma-ray is shown above most of the peaks.

The spectrum obtained with the 50 cm^3 detector irradiated with neutrons from the deuterium target is shown in fig. A2-5b. The irradiation took about 20 minutes and about 6×10^5 neutrons/cm^2 were incident upon the detector during the run. The energy resolution for this detector is considerably better than the one previously used and the spectrum extends to 2 MeV. For these reasons, and because of the larger size of the detector, a number of additional lines are apparent although the main features of the spectrum are the same as shown in fig. A2-5a.

Five spectra are shown in fig. A2-6 that were taken sequentially for periods of 25.6 ms each. The decay of the 22.7, 175.2, and 197.91 keV transitions is quite apparent whereas the 53.53 and 139.88 keV lines are obviously from longer lived isomers. The half-life of the short-lived activity was determined to be 21.5±0.4 ms. This certainly is consistent with the activity being ^{71m}Ge that has a listed[2] half-life

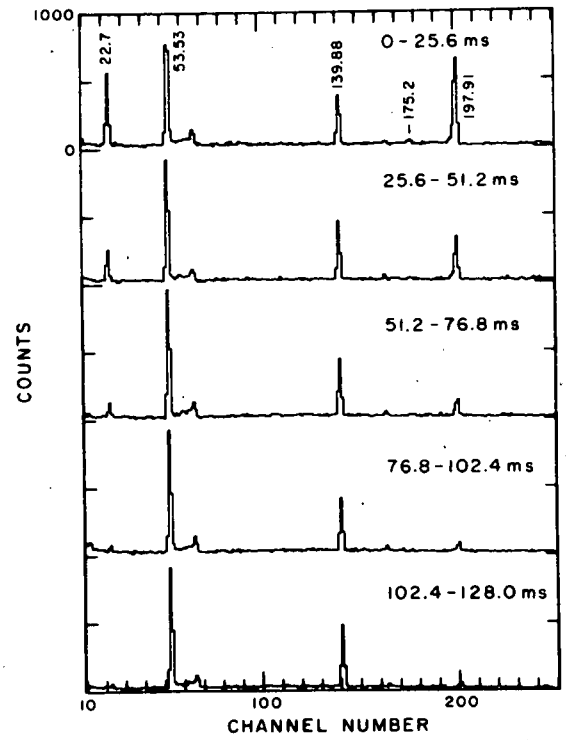

Fig. A2-6. Spectra taken sequentially for periods of 25.6 ms each after the irradiation. Lines at 22.7, 175.2 and 197.91 keV are associated with the decay of 21.5 ms ^{71m}Ge.

of 21.9±0.1 ms. This isomer decays by a 23 keV M2 transition that is highly converted followed by a 175 keV E2 transition to the ground state of ^{71}Ge. The spectra in fig. A2-6 show these transitions and the sum peak at 197.91 keV. Because the transitions appeared with so little background in fig. A2-6, reasonably precise energy determinations could be made (22.7±0.3, 175.2±0.1, and 197.91±0.07 keV). The weighted averages of the tabulated[2] values are 23.5±0.1 and 174.9±0.1 keV. The relatively low intensity of the 175 keV transition can be accounted for by the fact that if the pulse height analyzer is processing a pulse corresponding to the 23 keV transition, it will not be available to process a 175 keV pulse for about 13 μs. Since the half-life of the intermediate state is 70 ns, the 23-keV transition and 198-keV sum peak are more prominent.

Observed, but not shown in the spectra in fig. A2-6, is a weak line at 472.6 keV. This is quite consistent with identification of this line in fig. A2-5 as resulting from the ^{27}Al(n,α)^{24}Na reaction to the first excited state of ^{24}Na that has a half-life of 20 ms.

In fig. A2-7 are shown the delayed spectra with 256 ms counting time in each sub-group. The lines at 53.53 and 66.59 keV were found to decay with a half-life of 499±11 ms. This value represented a weighted average of values obtained with the 25 and 50 cc detector and is to be compared with the previous measurement of 530±30 ms.[3] The 0.5 s isomer of ^{73}Ge is known[4] to decay with the emission of a

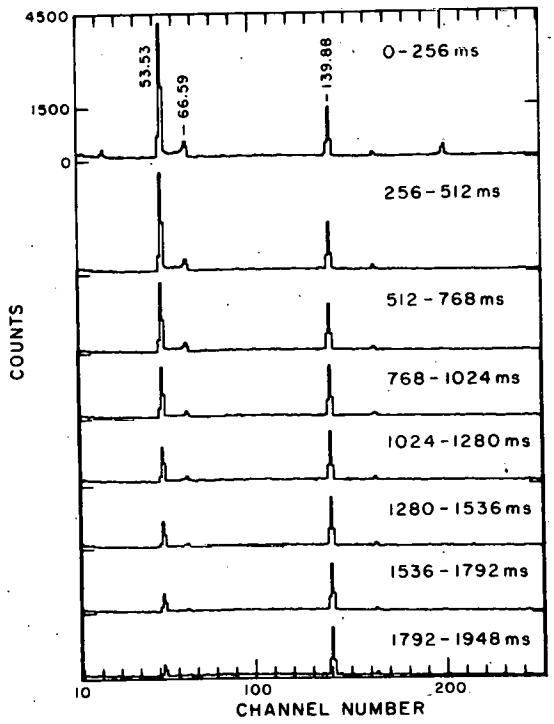

Fig. A2-7. Spectra taken sequentially for periods of 256 ms after the irradiation. Lines at 53.53 and 66.59 keV are associated with the decay of 499 ms ^{73m}Ge.

53.3 keV E2 or M2 transition followed by a 13.5 keV E2 or M2 transition with a half-life of 4.0 μs for the intermediate state. In fig. A2-7 the 53.53 and 66.59 keV sum peaks are clearly seen but the 13.06 keV transition is not observed for reasons already presented. There are known to be close lying states in ^{73}Ge, one of which is the isomeric level under discussion here and another level established by Coulomb excitation data with an energy of 67.03±0.01 keV.

The decay of the 139.88 keV transition of ^{75m}Ge is seen in fig. A2-8. The half-life was measured from the spectra shown and found to be 45.8±3.1 s. This is quite consistent with this activity, being the 46 s isomer in ^{75}Ge. It is known[4] that ^{75m}Ge decays with the emission of a 139 keV transition and this is just what is observed in the present data.

The need for caution on the part of the experimenter when using Ge(Li) gamma-ray detectors in a neutron environment should be evident from the results presented above. For in-beam gamma-ray spectroscopy studies, many of the peaks identified above will most likely be lost in the background of Compton events from target produced gamma-rays as previous experiments indicate. However, the most obvious signature of neutron interactions will be the presence of the 53.53, 139.88, 197.91, 1014.4 and 1779.1 keV peaks, as well as the 596.06, 693.4, and 1039.5 keV peaks from inelastic neutron scattering. The 717.4 keV transition should also be expected whenever boron nitride or borated paraffin is present in the cryostat or shielding.

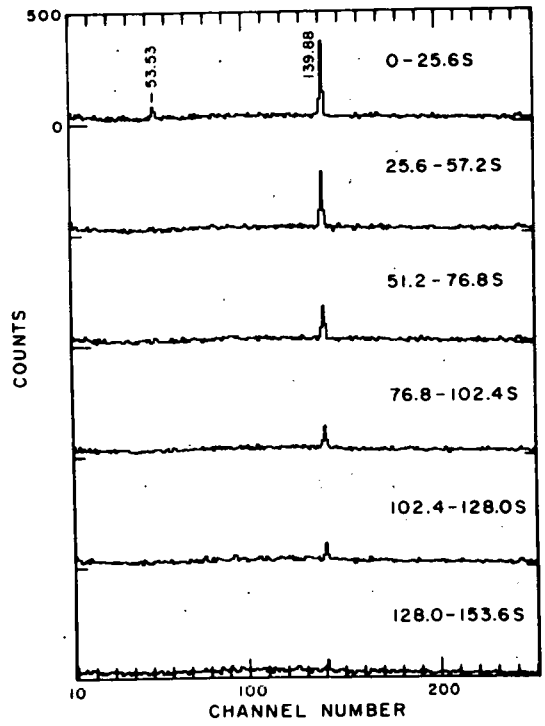

Fig. A2-8. Spectra taken sequentially for periods of 25.6 s after the irradiation. The line at 139.88 keV is associated with the decay of 46 s ^{75m}Ge.

---

1 C. Chasman, K. W. Jones and R. A. Ristinen, Nucl. Instr. and Meth. 37 (1965) 1.

2 K. R. Alvar, Nuclear Data Sheets 10 (1973) 225.

3 E. C. Campbell and F. Nelson, Phys. Rev. 107 (1957) 502.

4 W. B. Ewbank, M. J. Martin, S. C. Pancholi and K. Way, Nuclear Data B1 No. 6 (1966) 1.

3. Neutron Time-of-Flight Experiments

a. Studies of the (^{3}He,n) Reaction on Sn, Cd, Zn, and Sr Isotopes - H. W. Fielding, R. E. Anderson, D. A. Lind, C. D. Zafiratos, and W. P. Alford (University of Ontario)

We report here studies of the (^{3}He,n) reaction in the vicinity of the Z=50 major shell closure and the Z=40 sub-shell. The measurements were made at an incident energy of 25.4 MeV.

From systematics observed for the (t,p) reaction[1] one would expect that the (^{3}He,n) reaction on a closed proton shell target would give a strong ℓ=0 transition to the ground state with little other low-lying ℓ=0 strength. The reaction on a Z-2 target, where Z is a magic number, should excite a strong low-lying ℓ=0 transition in addition to the ground state. The cross-section for this excited state transition should equal that for the ground state transition on the closed shell (Z) target. The excitation energy of the excited ℓ=0 state for the Z-2 target should equal the Q-value difference for the (^{3}He,n) reaction on the Z and Z-2 targets.

For the specific case of the tin region (Z=50) one expects a strongly excited ℓ=0 transition at 5 MeV excitation in the residual tin nucleus when the (^{3}He,n) reaction occurs on Cd targets. In fig. A3-a1 we see time-of-flight spectra for ^{112}Cd and ^{114}Cd targets. In both cases the level near 2 MeV excitation

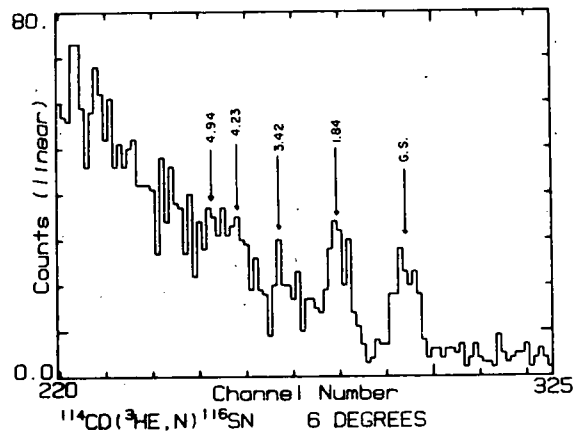

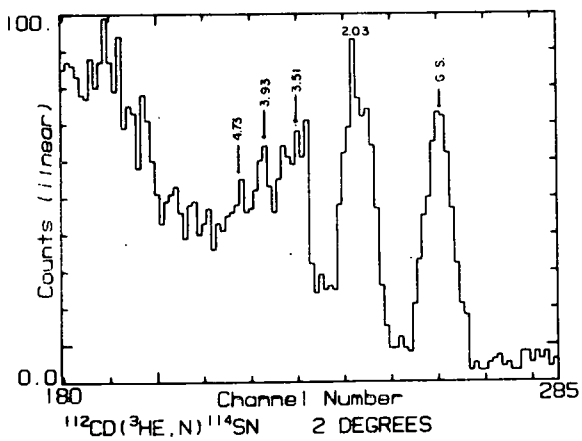

Fig. A3-a1. Time-of-flight spectra. In both cases the state near 2 MeV excitation is excited as strongly as the ground state with an ℓ=0 angular distribution.

has an ℓ=0 angular distribution (see figs. A3-a2 and a3) which has nearly the same strength as the ground state transition. This excitation energy is less than half that expected for the pairing vibrational state.

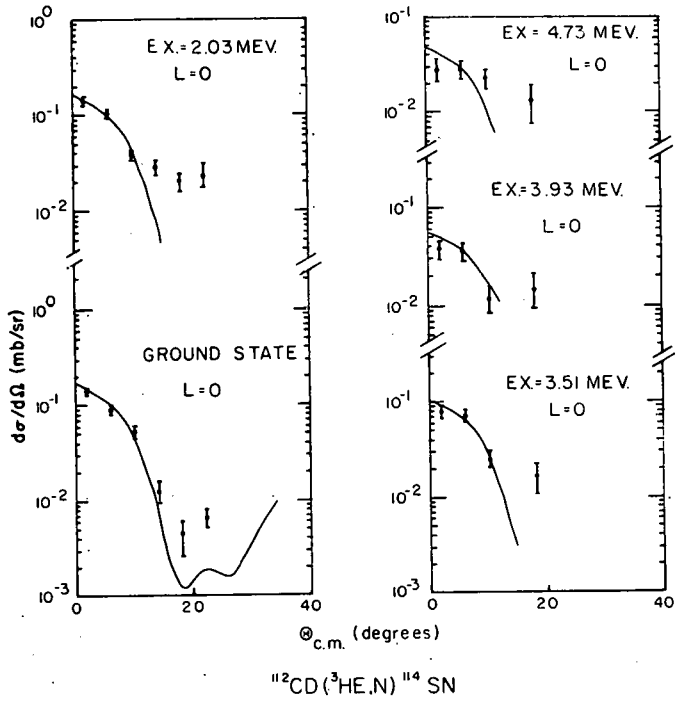

Fig. A3-a2. Angular distribution for states in ^{114}Sn. The solid curves are DWBA calculations.

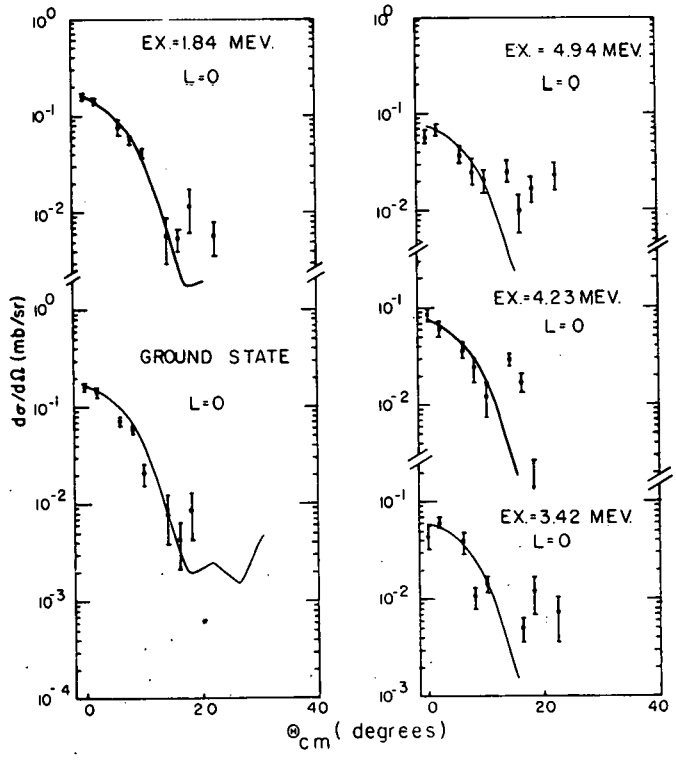

Fig. A3-a3. Angular distributions for ^{116}Sn. The solid curves are DWBA calculations.

This strong 0^+ state is at twice the 2^+ one-phonon excitation at about 1 MeV, and would thus coincide with the 0^+ member of a 0^+ 2^+ 4^+ vibrational triplet. Sorensen[2] discusses a number of possibilities for explanation of the strength of this transition but it is not clear which one applies here.

Additional ℓ=0 strength is found in states near 4 MeV excitation in the Cd(^{3}He,n)Sn data. These transitions are summarized in fig. A3-a4. Also shown in fig. A3-a4 are strengths[3] for the analogous (t,p) transitions near N=50. In both cases the strength of the pairing vibrational state seems to be spread over a few levels with a center-of-gravity slightly lower than expected.

The (^{3}He,n) reaction on tin targets leading to tellurium should not produce low-lying ℓ=0 strength (other than the ground state) but the spectra of A3-a5 and angular distributions of fig. A3-a6 show some excited ℓ=0 states. These transitions are indicated in fig. A3-a7.

Spectra for nuclei near Z=40 are shown in fig. A3-a8. The ground state ℓ=0 transition dominates the forward angle spectra as usual. In the ^{90}Zr(^{3}He,n)^{92}Mo spectrum the 1.49 MeV 2^+ state is excited as would be expected for a closed shell target nucleus. However, this same behavior is not seen for the other Zr isotopes. The relevant angular distributions are shown in figs. A3-a9 and A3-a10.

---

1 Ricardo A. Broglia, Ole Hansen, and Claus Riedel, Advances in Nuclear Physics, edited by Michel Baranger and Erich Vogt, page 287, Plenum Press, New York-London (1973).

2 Bent Sorensen, Nucl. Phys. A134 (1969) 1.

3 R. Ragaini, J. Knight, and W. Leland, Phys. Rev. C 2 (1970) 1020.

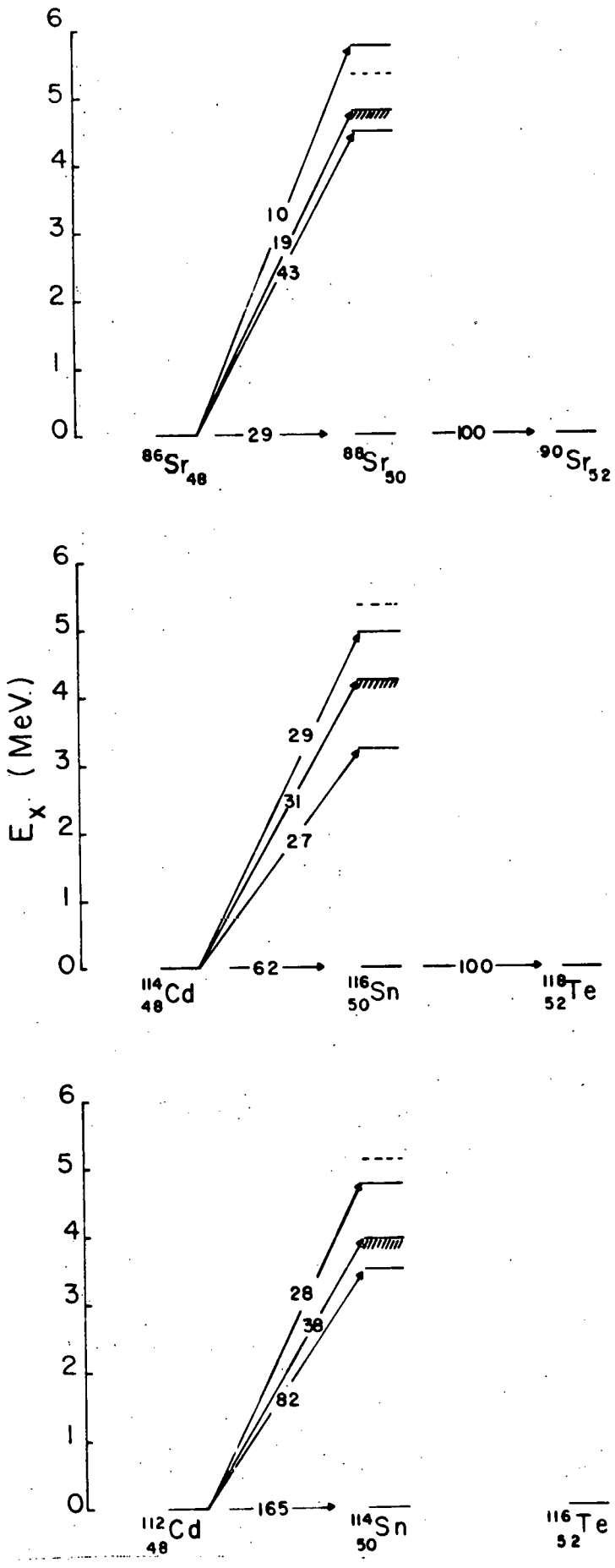

Fig. A3-a4. Strengths of $\ell=0$ transitions for $^{112}Cd(^{3}He,n)^{114}Sn$, $^{114}Cd(^{3}He,n)^{116}Sn$ and the analogous $^{86}Sr(t,p)^{88}Sr$ reaction.[3]

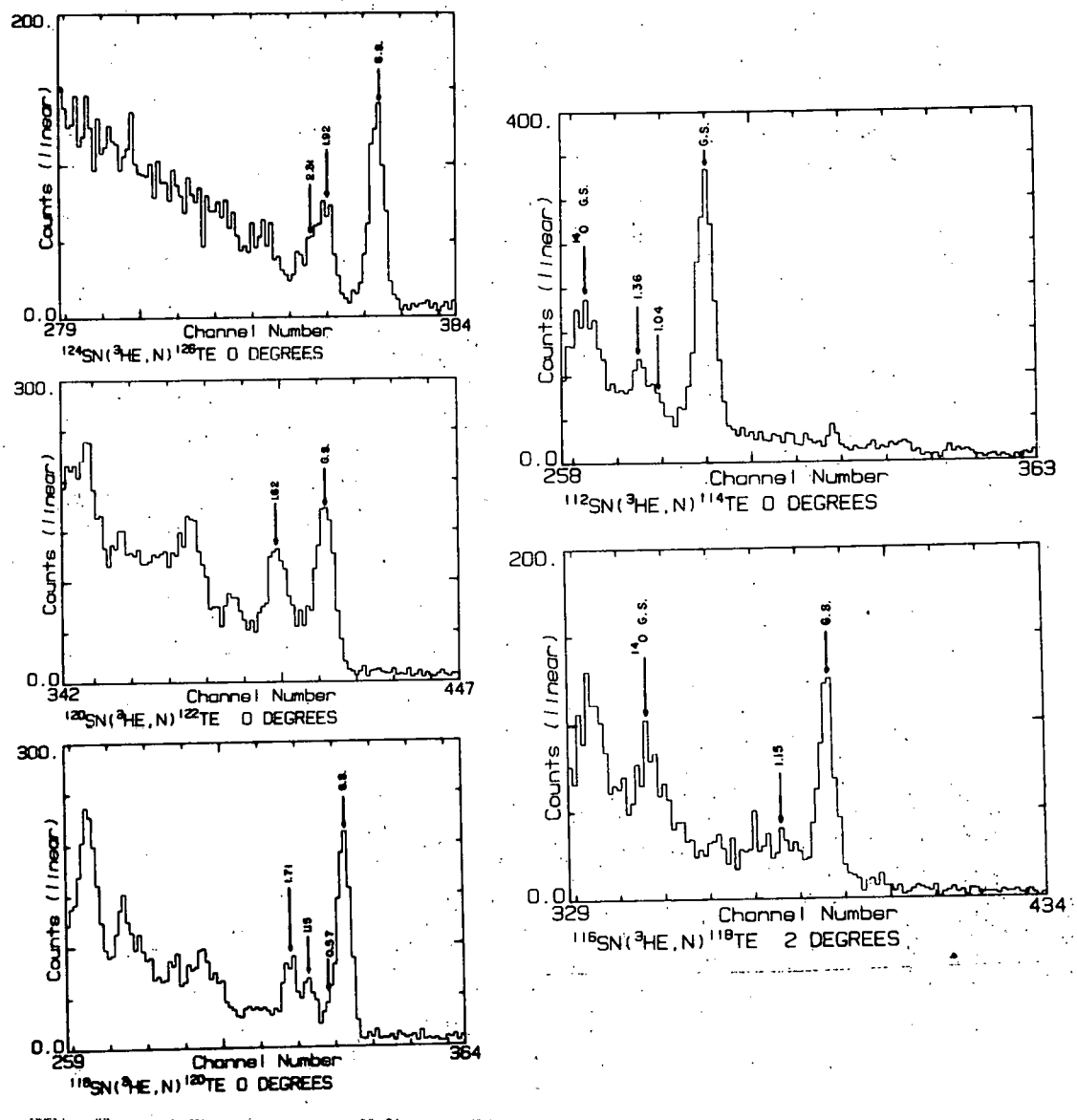

Fig. A3-a5. Time-of-flight spectra for the Sn isotopes studied.

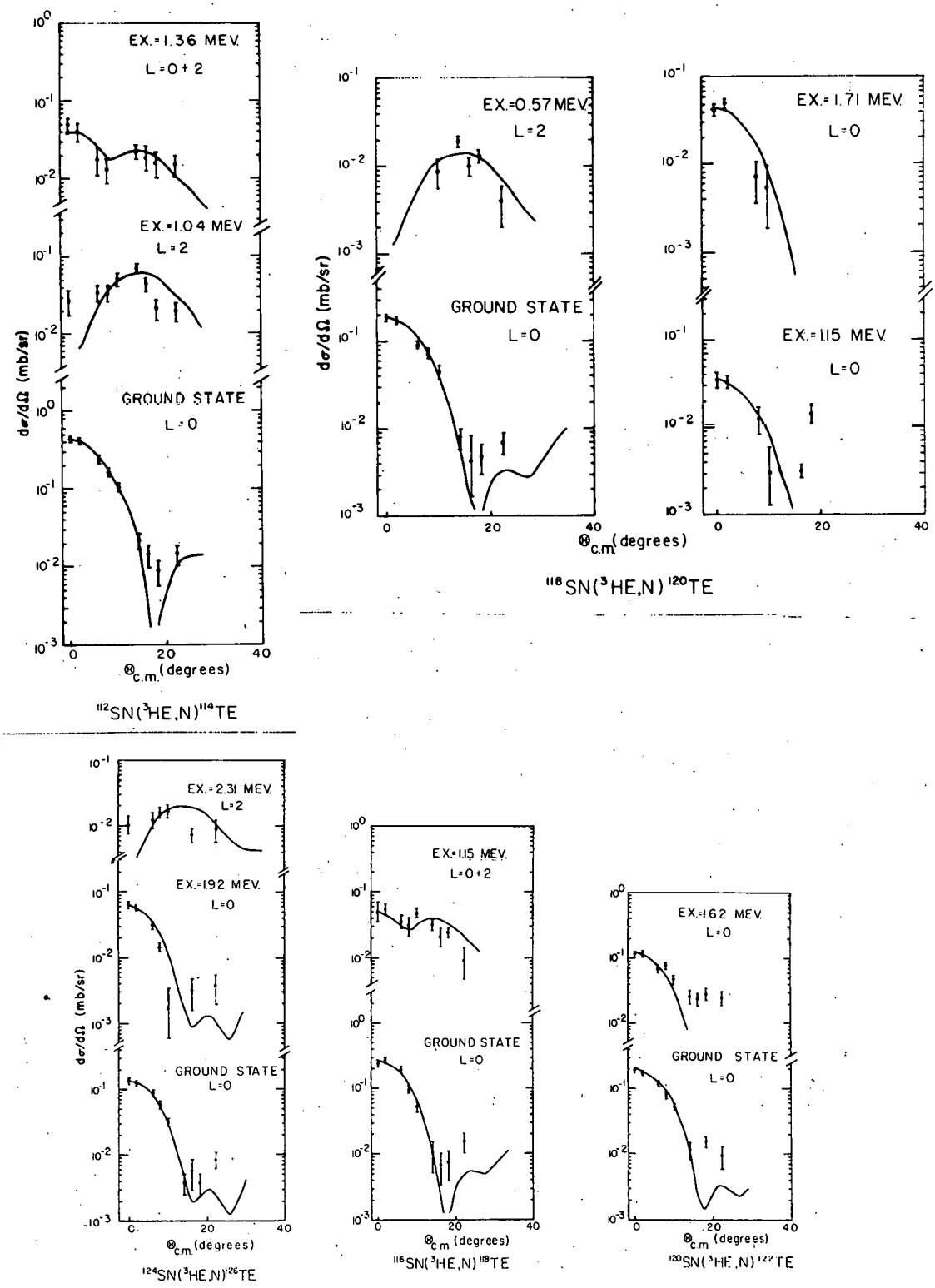

Fig. A3-a6. Angular distributions and DWBA calculations for the Sn isotopes.

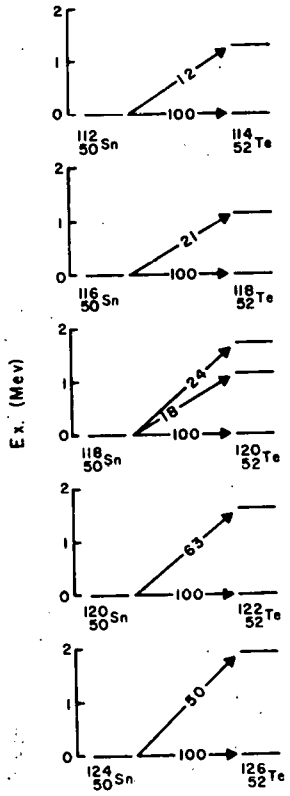

Fig. A3-a7. Strengths for ℓ=0 transitions on Sn targets.

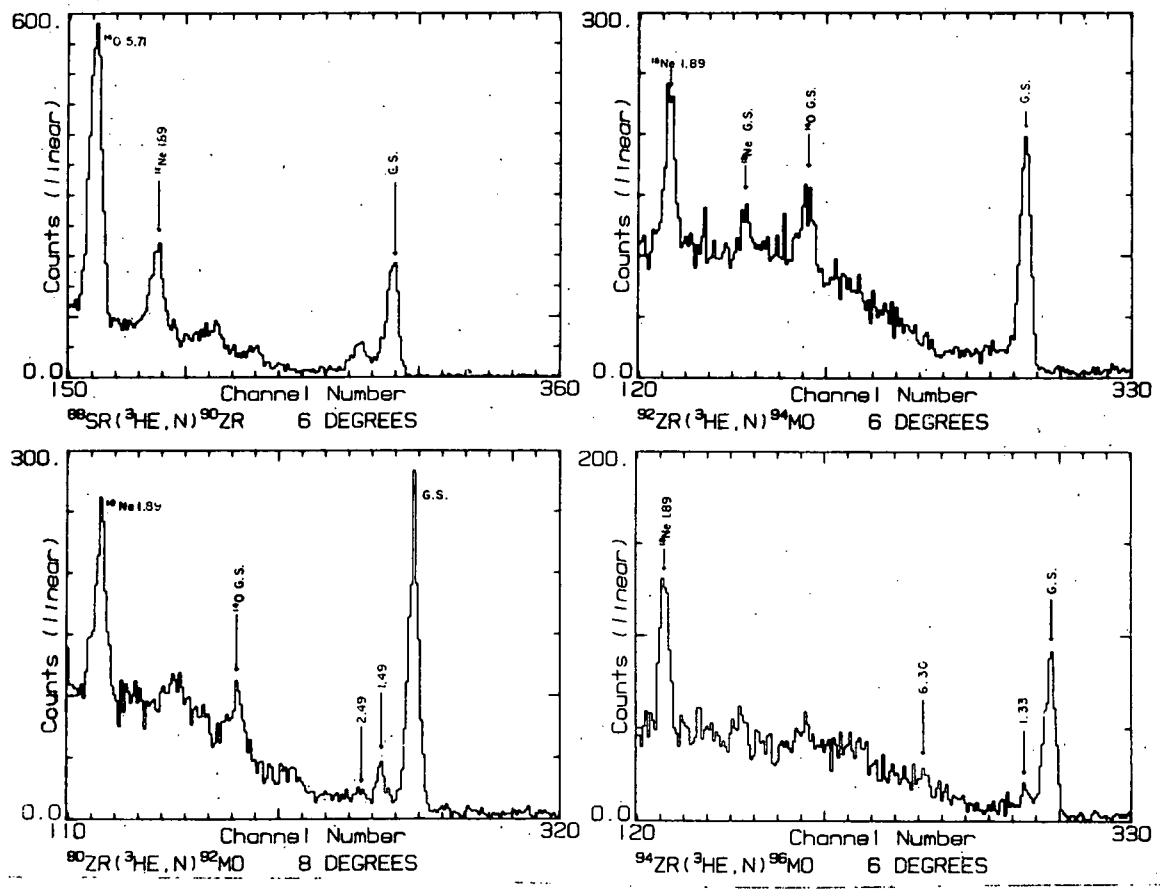

Fig. A3-a8. Time-of-flight spectra for targets with Z=38 and 40. The Sr target was natural so that no information could be extracted for excited state transitions.

Fig. A3-a9. The solid curve is a DWBA calculation.

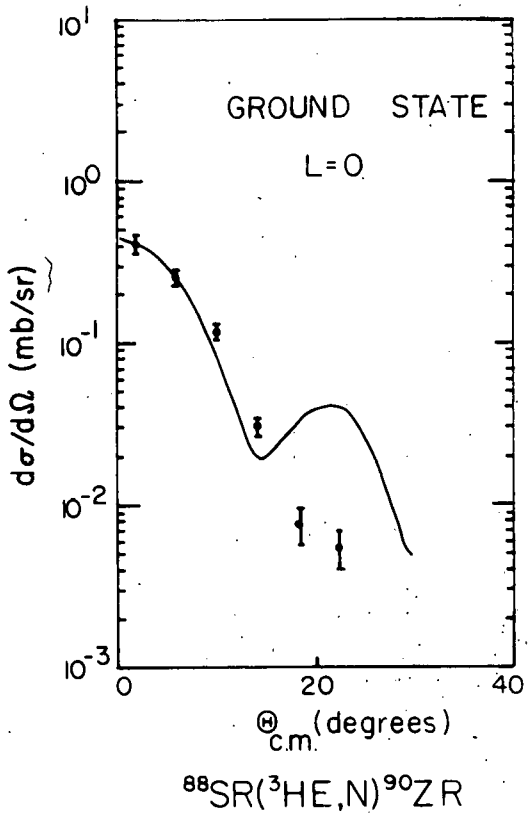

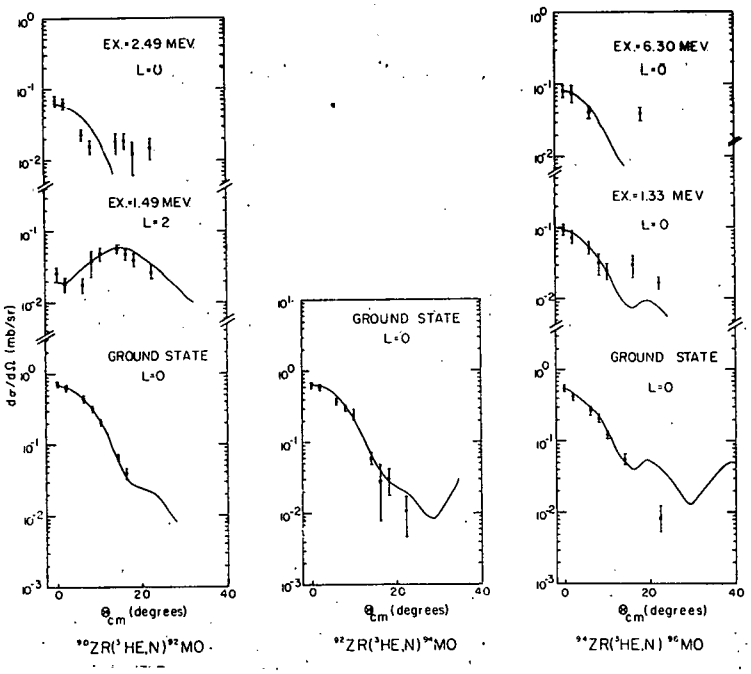

Fig. A3-a10. Angular distributions for data obtained with the three Zr targets.

b. Studies on Even Nuclei in the f,p Shell - H. W. Fielding, R. E. Anderson, F. M. Edwards, D. A. Lind, and C. D. Zafiratos

The (^{3}He,n) reaction has been investigated for the following targets: ^{46,48}Ti, ^{56}Fe, ^{60}Ni, ^{64,68}Zn, and ^{70,72}Ge. The experiment was performed at a bombarding energy of 25.4 MeV using the 9-meter flight path facility of the time-of-flight spectrometer.[1] The time resolution was 0.9 ns, which was sufficient to resolve the ground state and low-lying excited states. Typical spectra obtained are shown in figs. A3-b1, a through e. The angular distributions were obtained between 0 and 90 degrees.

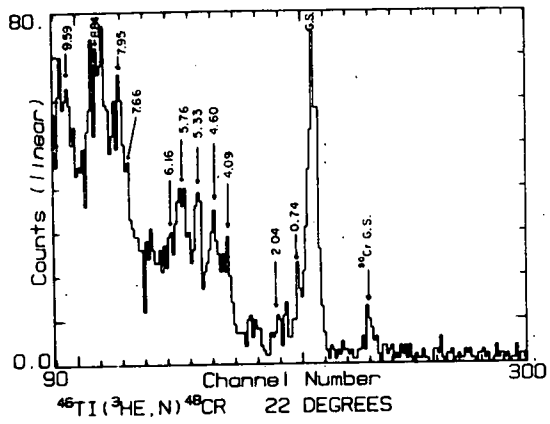

Fig. A3-b1-a.

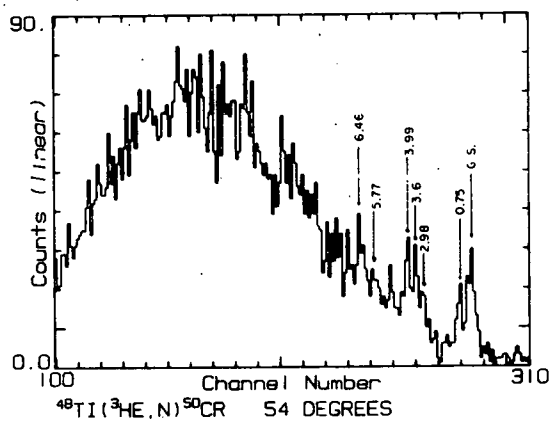

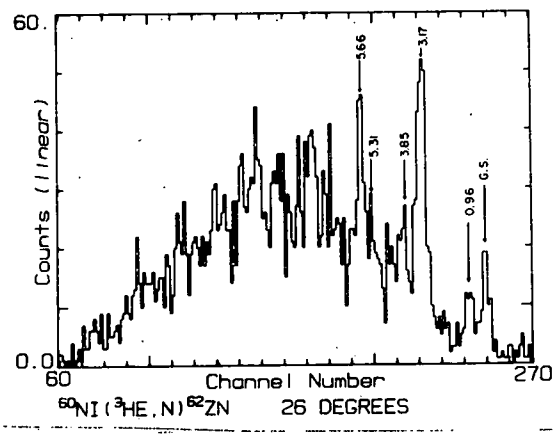

Fig. A3-b1-c.

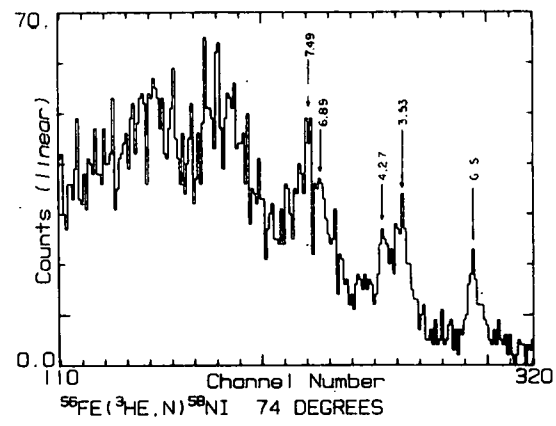

Fig. A3-b1-b.

Typical neutron time-of-flight spectra for the (^{3}He,n) reaction at 25.6 MeV on f,p shell nuclei. The time scale is 0.18 ns/channel and the flight path is 9 meters.

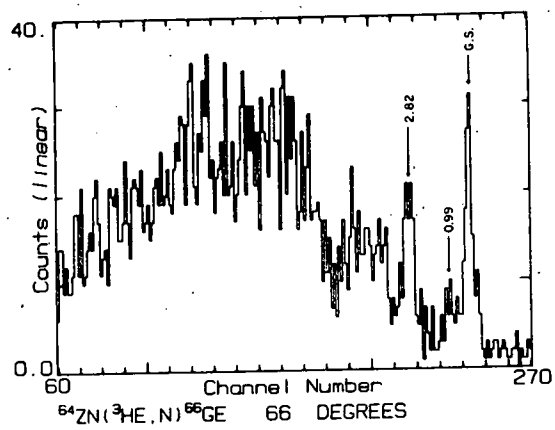

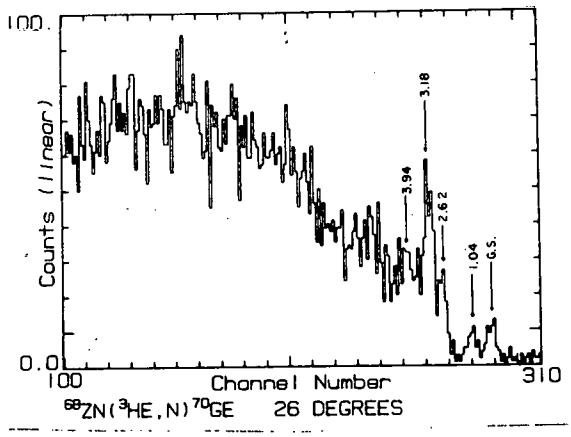

Fig. A3-b1-d.

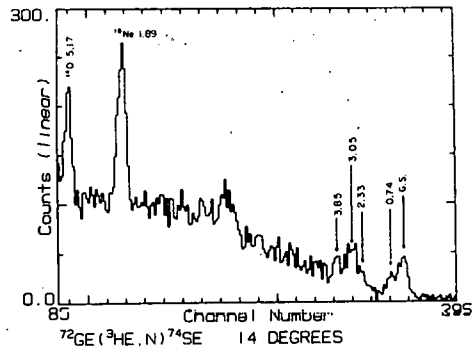

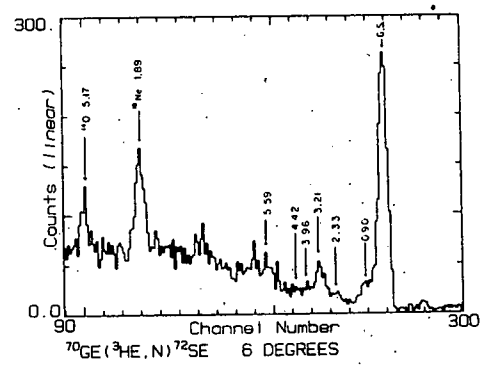

Fig. A3-b1-3.

Typical neutron time-of-flight spectra for the (^{3}He,n) reaction at 25.6 MeV on f,p shell nuclei. The time scale is 0.18 ns/channel and the flight path is 9 meters.

Two-step processes proceeding through an intermediate channel of different fragmentation than either the initial or final fragmentation are known to be important for two-neutron transfer reactions (p,t) and (t,p).[2] Thus it was considered worthwhile to investigate the simple DWBA one-step predictions for the two-proton transfer reaction (^{3}He,n) in order to ascertain whether it is necessary to invoke two-step reaction mechanisms.

The DWBA calculations were performed for numerous different optical potential parameter sets for both the neutrons and helions. Fig. A3-b2 shows the predictions for the ^{60}Ni(^{3}He,n)^{62}Zn (ground state) transition using the ^{3}He optical parameter sets of Cage et al.,[3] Luetzelschwab,[4] and Becchetti and Greenlees.[5] It was

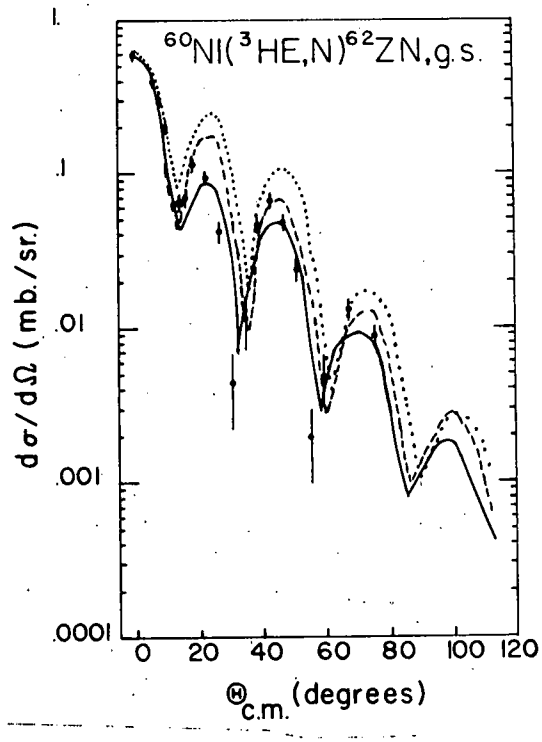

Fig. A3-b2. Results of DWBA calculations for the ^{60}Ni(^{3}He,n)^{62}Zn (g.s.) transitions for different ^{3}He optical potential parameters. The dotted line used the ^{3}He parameters of Cage et al.,[3] the dashed line those of Luetzelschwab,[4] the solid line those of Becchetti and Greenlees.[5]

found that the global set of ^{3}He optical parameters of Becchetti and Greenlees were preferred. Neutron parameters of Rosen, Perey, and Becchetti and Greenlees were tried. The neutron parameters of Becchetti and Greenlees[6] were found to provide the better predictions. The result of ground state transitions for the nuclei investigated here using the optical potential parameter sets of Becchetti and Greenlees for both neutrons and helions is shown in fig. A3-b3. The overall quality of the "fit" varies from quite good for the lighter f,p shell nuclei to poor for the Ge and Se nuclei. The DWBA fails to predict the observed trend of the first minima becoming less and less pronounced as A increases. The predictions for the low-lying 2^+ states are shown in fig. A3-b4. Generally, the agreement is quite good. It

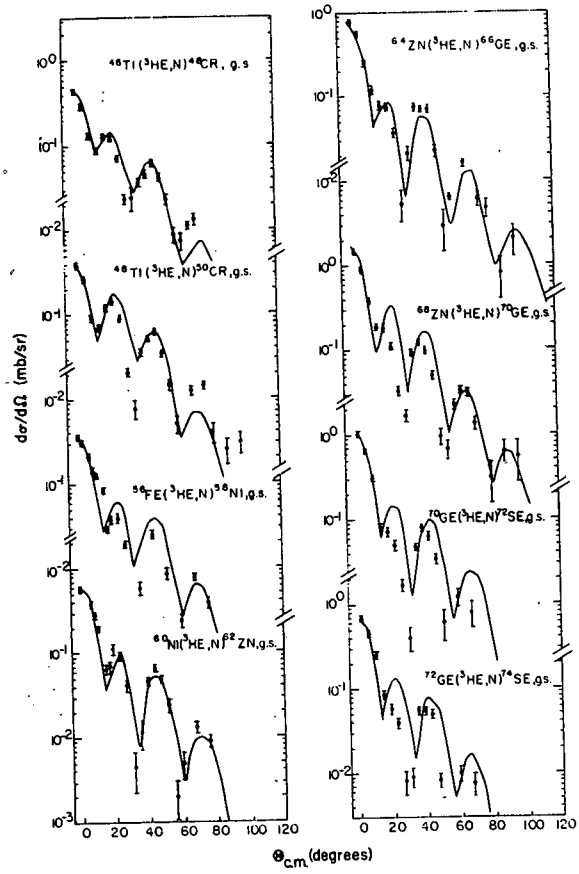

Fig. A3-b3. Results of DWBA calculations for the ground state transitions investigated. The ^{3}He parameters are those of Becchetti and Greenlees.[5] The neutron parameters are those of Becchetti and Greenlees.[6]

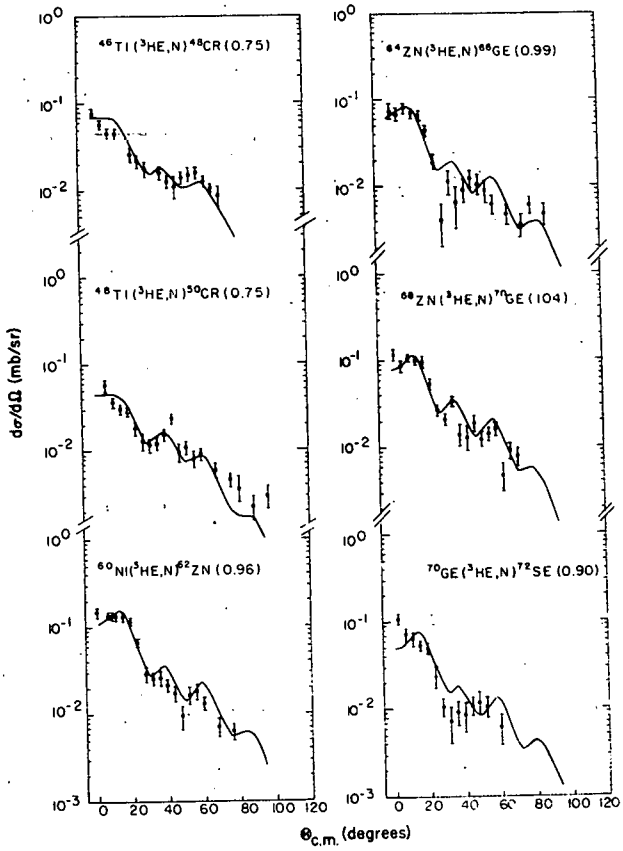

Fig. A3-b4. Results of DWBA calculations for the low-lying 2^+ transitions. The optical parameters are the same as in fig. A3-b3.

might eventually be necessary to include two-step processes in order to obtain good agreement for the wide variety of data we have obtained.

The (^{3}He,n) reaction transfers a pair of protons in an L=0, S=0, and T=1 state and is hence a specific probe of pairing correlations. For medium A nuclei, predictions concerning the two-nucleon transfer reaction using a pairing model with isospin have been made by Bayman et al.[7] Comparisons of the predictions of the pairing model description of 0^+ states in the f,p shell have been performed for (t,p) by Casten et al.[8] and for (^{3}He,n) by Evers et al.[9] Comparison of theory and experiment for our measurements is shown in table A3-I. The agreement is quite good around the closed shell ^{56}Ni. Deviations can be seen to occur away from the closed shell.

TABLE A3-I. Comparison of pairing theory with experiment for the (^{3}He,n) reaction on the f,p shell nuclei.

Final Nucleus	E_x MeV	Final Config. $(N'_rT'_rN'_aT'_a/T'T'_z)$	Expt. mb/sr	P.V. mb/sr	Experiment / P.V.
^{48}Cr	0.0	(40,00/00)	.485	1.93	.25
	5.33	(51,11/00)	.099	.033	3.00
	8.84	(42,00/20)	.36	.183	1.97
^{50}Cr	0.0	(31,00/11)	.44	1.37	.32
	5.77	(42,11/11)	.10	.42	.24
^{56}Ni	0.0	(00,00/00)	.487	.487	1
^{58}Ni	0.0	(00,11/11)	.52	.45	1.16
	3.55	(11,20/11)	.46	.46	1
^{60}Zn	0.0	(00,20/00)	.52	.52	1.0
^{62}Zn	0.0	(00,31/11)	.59	.49	1.2
^{64}Zn	0.0	(00,42/22)	.48	.40	1.2
^{66}Ge	0.0	(00,51/11)	.88	.931	0.95
^{70}Ge	0.0	(00,73/33)	1.7	.61	2.79
^{72}Se	0.0	(00,82/22)	1.12	1.04	1.08
^{74}Se	0.0	(00,93/33)	.71	.73	.97

1 University of Colorado NPL Progress Report, 1973.
2 N. B. de Takacsy, to be published.
W. R. Coker, T. Udagawa, and J. R. Comfort, to be published.
3 M. E. Cage et al., Nucl. Phys. A183 (1972) 449.
4 J. W. Luetzelschwab et al., Phys. Rev. 180 (1969) 1023.
5 F. D. Becchetti et al., Nucl. Phys. A190 (1972) 437.

[6] F. D. Becchetti et al., Phys. Rev. 182 (1969) 1190.
[7] B. F. Bayman et al., Phys. Rev. Lett. 23 (1969) 1299.
[8] R. F. Casten et al., Phys. Rev. C 4 (1971) 130.
[9] D. Evers et al., Nucl. Phys. A198 (1972) 268.

c. The (^{3}He,n) Reaction on Selected Odd-A Nuclei -

R. E. Anderson, H. W. Fielding, F. M. Edwards, D. A. Lind, and C. D. Zafiratos

In conjunction with the (^{3}He,n) reaction studies for even-even targets ranging from Ti to Sn discussed in the preceding sections, neighboring odd-A nuclei were also studied. Those odd-A target nuclei studied thus far include ^{45}Sc, ^{51}V, ^{55}Mn, ^{57}Fe, ^{59}Co, ^{61}Ni, and ^{115}In. We can thus examine the validity of weak coupling for both proton and neutron particles and holes coupled to a given core. For example, a comparison of the ^{60}Ni(^{3}He,n)^{62}Zn and ^{61}Ni(^{3}He,n)^{63}Zn reactions provides information on the neutron-core coupling while a comparison of the ^{115}In(^{3}He,n)^{117}Sb and ^{116}Sn(^{3}He,n)^{118}Te reactions studies the coupling of a proton hole to the core.

Typical spectra seen in these reactions are seen in figs. A3-c1 through c7. Note that in most cases the ground state to ground state transitions are either absent or only weakly excited. In all cases but one the strong lowest lying transition in each residual nucleus is presumed to be a pure L=0 transition to a state in the residual nucleus which has the same J^π as the ground state of the target. The exception to this rule is the ^{115}In(^{3}He,n) reaction. The ^{115}In ground state has been assigned as a $9/2^+$ state while there are no known 9/2+ states in ^{117}Sb. In addition, this reaction is also anomalous for a second reason. Conceptually one might think of ^{115}In as either a single proton coupled to ^{114}Cd or as a single proton hole coupled to ^{116}Sn. However, since the 50th proton closes a major shell at Z=50, the L=0 transitions observed in the ^{115}In(^{3}He,n) reaction should be compared to those seen in the ^{116}Sn(^{3}He,n) reaction rather than the ^{114}Cd(^{3}He,n) reaction. However, the strongly excited 1.72 MeV state in ^{117}Sb appears to have an ℓ=0 angular distribution. This behavior is reminiscent of the behavior of ^{114}Cd(^{3}He,n)^{116}Sn, as described in a preceding section.

DWBA analysis for the various reactions is now in progress, having been completed only for the ^{57}Fe(^{3}He,n)^{59}Ni reaction. In this case the analysis was carried out using the global ^{3}He parameters of Becchetti and Greenlees. The neutron parameters used were also the Becchetti and Greenlees global fits. Fits to the L=0 transitions at 0.47, 1.30, and 3.53 MeV, as well as the L=2 transition at 6.99 MeV, were obtained with results comparable to the analogous transitions seen in the ^{56}Fe(^{3}He,n)^{58}Ni reaction.

The transfer of two identical nucleons has been the subject of much study because of the highly correlated nature of nuclear wavefunctions. This property has long been recognized in G.S. → G.S.

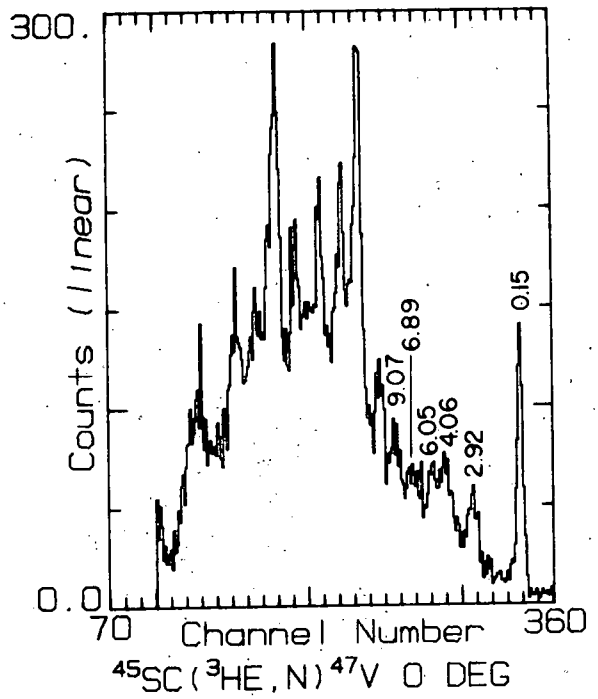

Fig. A3-c1. A spectrum taken for the $^{45}Sc(^{3}He,n)^{47}V$ reaction.

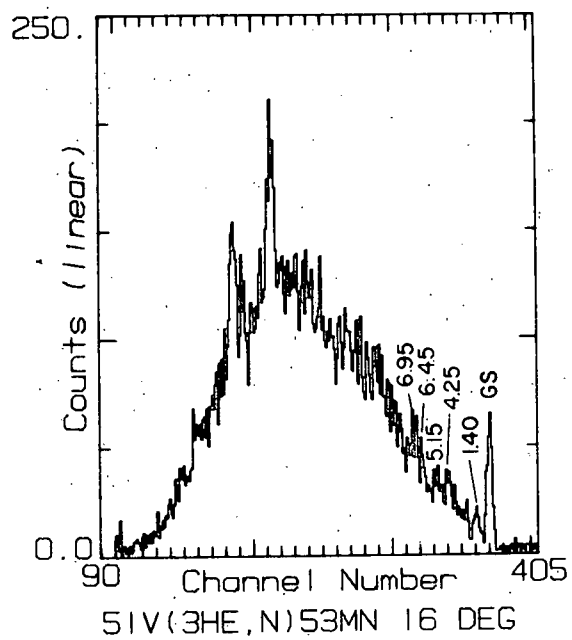

Fig. A3-c2. A spectrum taken for the $^{51}V(^{3}He,n)^{53}Mn$ reaction.

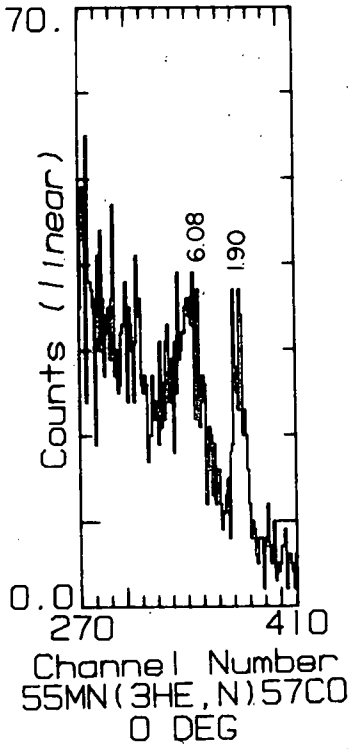

Fig. A3-c3. A spectrum taken for the $^{55}Mn(^{3}He,n)^{57}Co$ reaction.

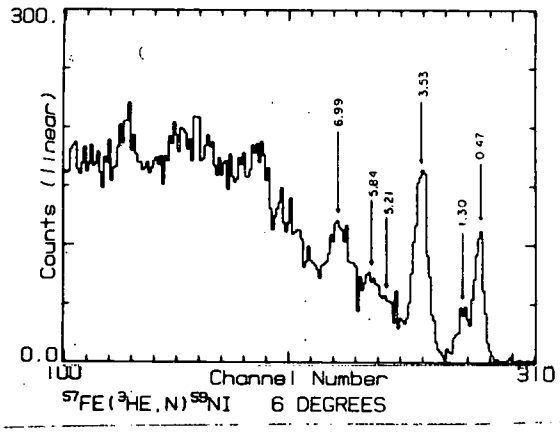

Fig. A3-c4. A spectrum taken for the $^{57}Fe(^{3}He,n)^{59}Ni$ reaction.

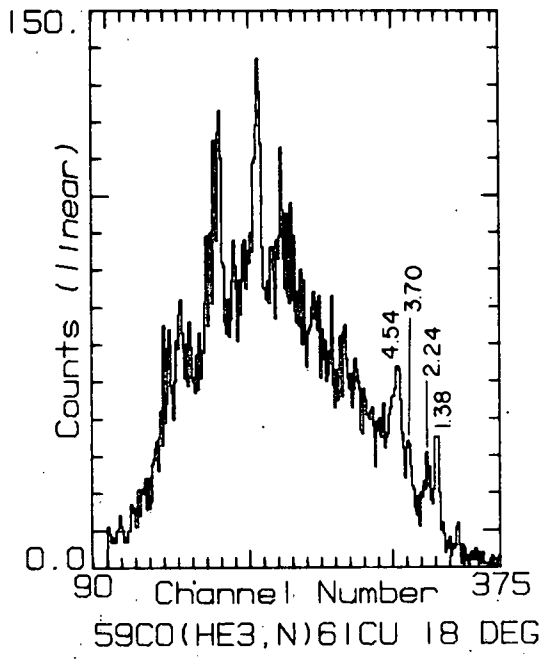

Fig. A3-c5. A spectrum taken for the $^{59}Co(^{3}He,n)^{61}Cu$ reaction.

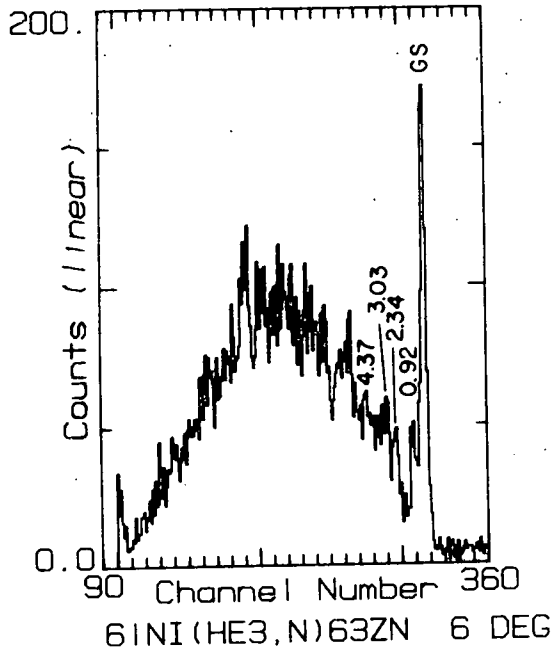

Fig. A3-c6. A spectrum taken for the $^{61}Ni(^{3}He,n)^{63}Zn$ reaction.

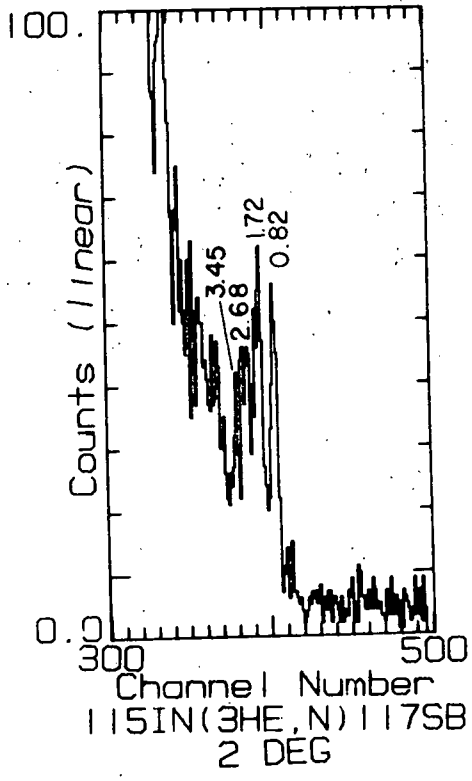

Fig. A3-c7. A spectrum taken for the $^{115}In(^{3}He,n)^{117}Sb$ reaction.

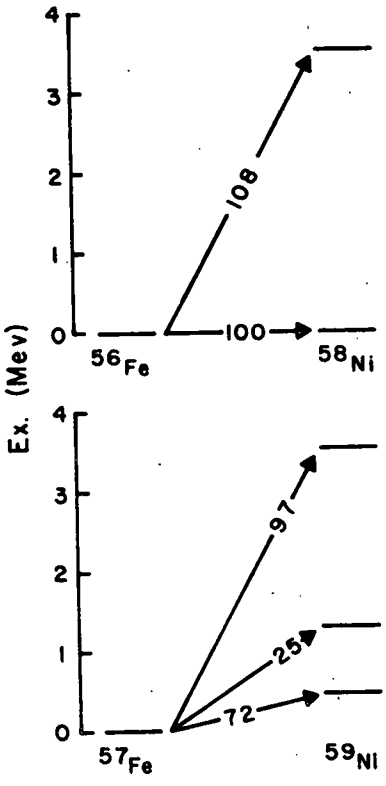

Fig. A3-c8. A comparison of the L=0 transition strengths for the $^{56,57}Fe(^{3}He,n)^{58,59}Ni$ reactions.

transitions. However, this highly correlated nature can also be seen when cross-sections involving excited state L=0 transitions are compared. The cross-sections for the G.S. → G.S. L=0 transitions and the G.S.→ excited state L=0 transitions are compared in fig. A3-c8 for the $^{56}Fe(^{3}He,n)^{58}Ni$ and $^{57}Fe(^{3}He,n)^{59}Ni$ reactions. In the case of ^{59}Ni the nearby presence of a second 1/2- state results in the mixing of the wavefunctions for those two states, but the sum of the transition strengths is equal to the strength seen in the ^{56}Fe(G.S.) → ^{58}Ni(G.S.) transfer. The interesting thing, however, is that the coherence seen in the ^{56}Fe(G.S.) → ^{58}Ni(3.55 MeV) transition is preserved in the ^{57}Fe(G.S.) → ^{59}Ni(3.53 MeV) transition. That is, the 3.53 MeV state in ^{59}Ni may be viewed as the 3.55 MeV state in ^{58}Ni with a neutron weakly coupled to it just as the ^{57}Fe(0.47) is viewed as the ^{56}Fe(G.S.) plus a weakly coupled neutron. It will be interesting to see if this effect persists in other odd nuclei when the valence particle is a proton (or proton hole, etc.).

d. Comparison of the $^{24}Mg(^{3}He,n)^{26}Si$ and $^{24}Mg(^{3}He,p)^{26}Al$ Reactions at 25.5 MeV -
R. E. Anderson, H. W. Fielding, F. M. Edwards, D. A. Lind, and C. D. Zafiratos

Since theoretical wavefunctions for s-d shell nuclei have become available in the last few years, the possibility emerges of studying the effects of an isospin dependent interaction potential in the typical DWBA analysis of two-nucleon transfer reactions. For example, these effects may be studied in a comparative fashion by observing the transfer of two neutrons, two protons, and a neutron and a proton for the same target nucleus. The experiment which is now in progress here at the University of Colorado will compare the results of the $^{24}Mg(^{3}He,n)^{26}Si$ and $^{24}Mg(^{3}He,p)^{26}Al$ reactions at a bombarding energy of 25.5 MeV.

Data has already been accumulated for the $^{24}Mg(^{3}He,n)^{26}Si$ reaction over an angular range of 0° to 74° and a typical spectrum is shown in fig. A3-d1. The excitation energies shown are those determined in the present experiment. No data has been taken as yet for the $^{24}Mg(^{3}He,p)^{26}Al$ reaction. The impurity peaks result from the $^{12}C(^{3}He,n)^{14}O$ and $^{16}O(^{3}He,n)^{18}Ne$ reactions. Both ^{16}O and ^{12}C are present on the Faraday cup surface (which is seen by the detectors at angles <8°) and ^{16}O is present in the target as well. The DWBA calculations have not been completed as yet for this reaction.

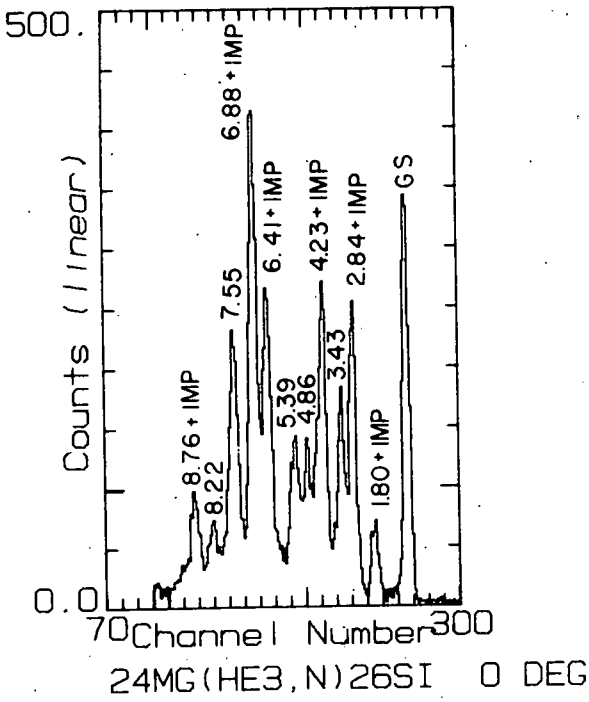

Fig. A3-d1. Time-of-flight spectrum for $^{24}Mg(^{3}He,n)^{26}Si$. The peaks labeled IMP contain events due to neutrons from the $^{12}C(^{3}He,n)$ and $^{16}O(^{3}He,n)$ reactions.

e. Precision Comparison of (p,n) Quasi-Elastic Scattering for Tin Isotopes - S. D. Schery, P. G. Brabeck, S. T. Durrance, D. A. Lind, A. Wilmeth, and J. Comfort (Ohio University)

The (p,n) reaction to isobaric analog states (IAS) is successfully described by a macroscopic model in which the isospin-dependent portion of the nucleon-nucleus optical model is the interaction causing the (p,n) reaction. The isospin-dependence of the optical model reflects the effects of anti-symmetry between the projectile nucleon and target nucleon and hence varies with the target neutron excess. Thus, a simple macroscopic model of the (p,n) reaction to IAS views the interaction as proportional to the difference in densities of neutrons and protons in the target nucleus, i.e. to the target isospin density. Since this quantity may vary with radius, the target isospin density becomes a form factor in a DWBA calculation of quasi-elastic scattering. The (p,n) angular distribution strongly depends upon this form factor.

It would thus appear that the (p,n) IAS reaction would be sensitive to the variations of neutron radial distributions that occur along a series of isotopes. In the work reported here we chose to study three isotopes spanning the range of stable Sn isotopes: $^{112,116,124}Sn$. The studies were made with a 9-meter flight path with E_p=23 MeV.

In order to reduce relative errors caused by target thickness uncertainties, mixed isotope targets were prepared. Accurately measured quantities of the isotopically enriched oxides were mixed, then the composite oxide mixture was reduced to the metal in a hydrogen atmosphere. Targets containing ^{124}Sn with ^{116}Sn and ^{124}Sn with ^{112}Sn were rolled from mixed isotope metal samples prepared in this way.

The slight shift in Q-value for the IAS transition in differing tin isotopes was sufficient to resolve the analog state peaks of ^{116}Sn and ^{124}Sn in a mixed target. Separate ^{112}Sn, ^{116}Sn, and ^{124}Sn targets were studied as well. At this writing we have not yet measured the quasi-elastic cross-sections for the mixed ^{112}Sn - ^{124}Sn target.

Preliminary analysis indicates that the magnitude of the IAS cross-section increases in a reasonable way from ^{112}Sn to ^{124}Sn and that the angular distribution minima became sharper with increasing N. Preliminary DWBA analysis indicates a neutron distribution which is progressively further outside the proton distribution as N increases.

4. Other Activities

54,465

a. Thick Target Measurement of Stellar and Thermonuclear Reaction Rates - N. A. Roughton, M. J. Fritts, R. J. Peterson, C. J. Hansen (JILA), and C. S. Zaidins

We have continued our program of measuring thick target yields from which average cross sections and thermonuclear reaction rates can be determined. We have completed the analysis of the reactor rates shown in Table A4-I, and have used the standard form for the temperature dependence of these rates,

$$N_A\langle \sigma v \rangle = \exp\left(A \rightarrow BT_9^{-1/3} + CT_9^{-1}\right)/T_9^{3/2}.$$

The table lists the coefficients A, B, and C and range of values of T_9 over which the rates are expected to be valid. In addition, we have measured the rates for the reactions $^{10}B(p,\alpha)^{7}Be$ and $^{10}B(p,\gamma)^{11}C$ by the same techniques, and these are discussed in section II-A-4-d of this report. Work in progress includes the reactions which involve the proton bombardment of targets of Mg, S, Ca, Zr, Cd, Sn, Nd, and Pd. As we proceed through the periodic chart we study the reactions that are expected to be important in both explosive nucleosynthesis and the p-process, and we are progressing towards our goal of establishing benchmark data to test models of proton induced reactions.

The short distance target transfer mechanism, called the Ram, (see also section II-C-2 in this report), has proved to be a valuable tool in measuring the yields of short half-life products. Besides its use in Si, Mg, and S bombardments, it achieved the transit time necessary to measure the $T_{1/2}$=182 ms ^{41}Sc yield in the $^{40}Ca(p,\gamma)^{41}Sc$ reaction. It is an important addition to the existing facilities in the lab and has been used by other groups in the past year.

The data analysis has been speeded up considerably by the addition of a number of programs which can be run on the PDP-9. The use of the CDC-6400 is no longer required, greatly reducing the cost and time involved in calculation of the reaction rates. The program YIELD converts the raw data into the yield points which are the radioactive nuclei produced per incident proton. The program ASTRO uses these yields as input data and determines the parameters a, b, c, and d used in the parametrization of the cross section with the form

$$\sigma(E) = \exp\left(a+bE^{-\frac{1}{2}}+cE^{+\frac{1}{2}}+dE\right)/E.$$

This expression for the cross section and the $dE/d(\rho x)$ parameters are then put into the program ASTRFT which regenerates the yield curve and calculates χ^2 as a test for goodness of fit. If it is necessary to include single strong resonances the program RES is able to fit the "resonance step" in the yield function and to extract the resonance strength. ASTRFT is also able to accept the data from a resonance as well as up to five sets of cross-section parameters if it is necessary to break the yield curve into smaller intervals in energy for a good fit using ASTRO. The program RATES calculates the cross sections as a function of energy, calculates the values of

Table A4-I

Thermonuclear reaction rates as a function of temperature in billions of Kelvins (T_9) fit to the form

$$N_A\langle ov \rangle = \frac{\exp(A+BT_9^{-1/3}+CT_9^{-1})}{T_9^{3/2}}$$

Reaction	A	B	C	Range of validity
$^{58}Ni(p,\gamma)^{59}Cu$	24.445	-24.380	-1.528	$2 \leq T_9 \leq 4$
$^{60}Ni(p,\gamma)^{61}Cu$	21.995	-14.225	-9.859	$1.5 \leq T_9 \leq 4$
$^{61}Ni(p,\gamma)^{62}Cu$	27.395	-22.956	-4.635	$1.5 \leq T_9 \leq 5$
$^{28}Si(p,\gamma)^{29}P$	15.727	-4.815	-15.234	$2 \leq T_9 \leq 8$
$^{50}Cr(p,\gamma)^{51}Mn$	22.866	-17.677	-4.294	$1.5 \leq T_9 \leq 6$
$^{54}Fe(p,\gamma)^{55}Co$	27.538	-31.484	+6.697	$2.5 \leq T_9 \leq 5$
$^{64}Zn(p,\gamma)^{65}Ga$	25.567	-21.052	-7.521	$2 \leq T_9 \leq 7$
$^{67}Zn(p,\gamma)^{68}Ga$	24.198	-15.855	-10.141	$2 \leq T_9 \leq 7$
$^{68}Zn(p,n)^{68}Ga$	28.05	-10.463	-42.39	$3 \leq T_9 \leq 7$
$^{70}Ge(p,\gamma)^{71}As$	30.403	-27.859	-6.857	$2 \leq T_9 \leq 7$
$^{72}Ge(p,\gamma)^{73}As$	27.168	-19.602	-18.395	$3 \leq T_9 \leq 7$
$^{74}Ge(p,n)^{74}As$	27.367	-9.354	-39.324	$2 \leq T_9 \leq 7$
$^{76}Ge(p,n)^{76}As$	36.098	-32.872	-8.707	$2 \leq T_9 \leq 7$
$^{92}Mo(p,\gamma)^{93}Tc$	32.689	-38.769	-1.184	$3 \leq T_9 \leq 6$
$^{92}Mo(p,\gamma)^{93m}Tc$	30.755	-36.298	-3.112	$2 \leq T_9 \leq 7$
$^{95}Mo(p,n)^{95}Tc$	33.167	-29.973	-17.793	$4 \leq T_9 \leq 5$
$^{95}Mo(p,n)^{95m}Tc$	35.572	-33.794	-14.453	$4 \leq T_9 \leq 5$
$^{95}Mo(p,\gamma)^{96}Tc$	25.767	-21.425	-12.376	$2 \leq T_9 \leq 7$
$^{95}Mo(p,\gamma)^{96m}Tc$	20.759	-12.716	-17.864	$3 \leq T_9 \leq 7$
$^{96}Mo(p,n)^{96}Tc$	27.101	-11.386	-42.448	$2 \leq T_9 \leq 7$
$^{96}Mo(p,n)^{96m}Tc$	25.917	-10.399	-43.287	$2 \leq T_9 \leq 7$
$^{98}Mo(p,\gamma)^{99}Tc$	25.815	-16.671	-15.249	$2 \leq T_9 \leq 7$
$^{100}Mo(p,\gamma)^{101}Tc$	28.373	-32.931	-10.217	$3 \leq T_9 \leq 6$

$N_A\langle \sigma v \rangle$ over the specified range in T_9 and least squares fits these values to obtain the parameters A, B, and C such as those shown in Table A4-I. An example of what is available from the output of these programs is the yield and cross-section plot for the $^{92}Mo(p,\gamma)^{93}Tc$ reaction shown in fig. A4-1.

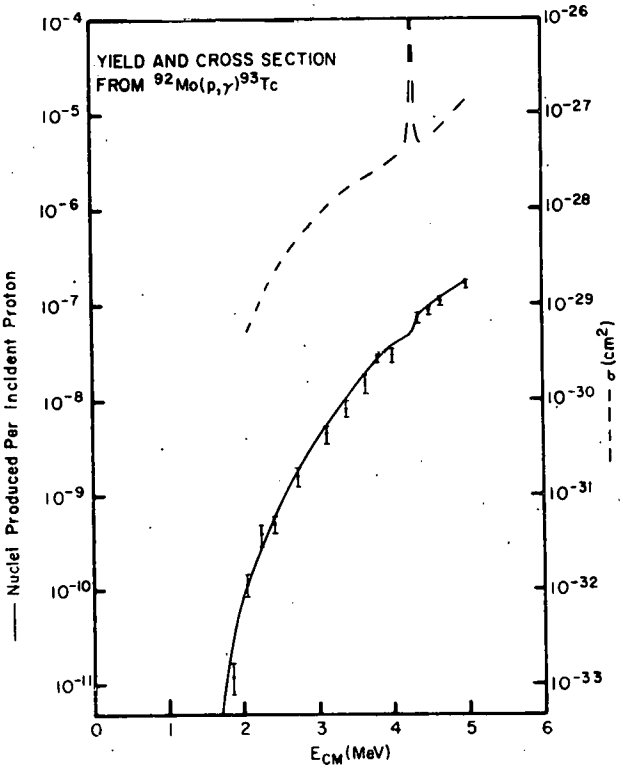

Fig. A4-1. A composite plot of the yield for the $^{92}Mo(p,\gamma)^{93}Tc$ reaction and the cross section that is derived from the analysis over the energy region of the measurements. The analysis method is discussed in the text.

The program COMB combines the programs ASTRFT and RATES, so that these can be run either separately or together depending on which is more convenient. Finally, the program ABC can be used to find the $N_A\langle \sigma v \rangle$ parameters A, B, and C from the input of rates calculated by hand or selected from the output of RATES.

At this stage, the general program of measurements is standardized and only the individual attention that each target nucleus requires keeps the measurements from becoming routine. We shall continue the measurements as rapidly as the manpower and funding will allow us.

b. Nuclear Data Project - R. L. Bunting (Nuclear Information Research Associate) and J. J. Kraushaar

September 1, 1974, brings to an end the nuclear data compilation project sponsored by the National Science Foundation through the National Academy of Sciences - National Research Council Committee on Nuclear Science. This laboratory's contributions to this effort are summarized below.

i. Nuclear Data Sheets for A=136[1]

The 1961 version of the Nuclear Data Sheets for A=136 has been revised according to experimental data received before September 1, 1973. Selected experimental data, discussions for J^{π} assignments, and detailed level schemes are presented.

Additional data now detail the decays of ^{136}Te, ^{136}Pr, and ^{136}Nd. The level structure for ^{136}Xe, ^{136}Ba, ^{136}Ce, ^{136}Pr, and ^{136}Nd are improved significantly. The low-lying levels of ^{136}Ba are very well established. Additional information on the higher excitations in ^{136}Ba is needed, possibly through more definitive ^{135}Ba(n,γ)^{136}Ba experiments. The relative positions of the isomers in ^{136}I and the details of the level structure for ^{136}La and ^{136}Cs are still unknown.

Areas of continuing experimental interest are the decays of ^{136m}I, ^{136}Nd, and ^{136}Pm, and the quasirotational levels of ^{136}Ce and ^{136}Nd. The level structure of ^{136}Xe(^{136}Pr) may be subject to major revision in the near future as is suggested by some recent unpublished data. These new decay data were not included in this evaluation because of their preliminary nature.

The levels of ^{136}La are under investigation at this laboratory as part of a continuing study of the spin-multiplet couplings in odd-odd nuclei.

The compilers would like to thank F. Ajzenberg-Selove and R. L. Auble for critical readings of the preliminary drafts of the A=136 manuscript. Special thanks also is extended to R. L. Auble for assistance in preparing the figures presented and N. A. Iverson, who aided in locating the necessary reference material.

---

[1] Nuclear Data Sheets 13 (1974) 191.

ii. Nuclear Data Sheets for A=137

The 1961 version of Nuclear Data Sheets for A=137 has been revised according to experimental data received before July 1, 1974. The preliminary manuscript is being revised as of this writing. The

following conclusions will remain unchanged.

In all cases the present revision represents a significant addition to the existing version. The decays of ^{137}I and ^{137}Xe are currently being reinvestigated with improved Ge(Li) detectors and may constitute an added-in-proof section. The data for the ^{137}Cs β^- decay is now very well determined and continued efforts along this line should be discouraged unless significant advances are made in instrumentation. The $^{136}Ba(n,\gamma)^{137}Ba$ reaction is virtually unstudied and additional data would be beneficial. The data for the decays of ^{137}Ce and ^{137m}Ce, although widely referenced, are still unpublished. The γ-ray energies and intensities associated with the Ce decays need to be restudied for improved accuracy and validity. The decays of ^{137}Pr and ^{137}Ce were the subject of recent comprehensive investigations.

The compilers would like to thank F. Ajzenberg-Selove and R. L. Auble for critical readings of the preliminary drafts of the A=137 manuscript. Special thanks also is extended to R. L. Auble for assistance in preparing the figures presented and N. A. Iverson, who aided in locating the necessary reference material.

c. Natural Occurring Radioactivity in Oil Shale - S. Allen, J. J. Kraushaar, and J. B. Martin

The development of the oil shale resources, principally in the Piceance Basis in Colorado, poses a number of stresses on the environment that should be thoroughly evaluated. There is little information available concerning the occurrence of natural radioactivity in the shale and essentially no information on the dispersal of the radioactivity upon retorting the shale to produce the oil and the spent shale.

A modest effort was initiated during the summer to start a measurement program that would make data available for an assessment of the problem. The heavily shielded 3 inch x 3 inch NaI detector in the Health Physics Laboratory was used. A container was devised that holds a sample of the material so that the top and sides of the detector have about 1½ inches of material surrounding it. The use of these large amounts of sample material provided more than ample counts in the spectra above background for samples that range up to about 5 ppm in uranium and thorium for a typical 800 minute run. Several calibration samples for both thorium and uranium were developed.

The output of the pulse height analyzer was arranged so that the punched tape output was compatible with the PDP-9 computer, and in this way the various fitting and subtraction routines available for that computer could be used directly in analyzing the data. By observation of the relative intensities of several of the gamma-rays from the daughter activities of ^{238}U and ^{232}Th some information was also obtained on disequilibrium.

The measurement program has just begun with the analysis of

samples of oil shale, oil, and spent shale obtained from the U.S. Bureau of Mines facility in Laramie. It is hoped that a number of additional samples, particularly from Anvil Point, can be obtained and analyzed in the near future. Radioactivity in the typical surface material (soil, etc.) present in an undisturbed region in the Piceance Basin will also be measured.

d. Radioactive Products from Boron-Burning CTR Reactors - R. J. Peterson, C. S. Zaidins, N. A. Roughton, M. J. Fritts and C. J. Hansen

A reaction proposed for power-generating CTR reactors is $^{11}B(p,\alpha)2\alpha$, Q=+8.59 MeV, with the major advantage of involving no radioactive species and producing no neutrons to induce radioactivity.[1] Any isotopic contamination of ^{10}B will, however, produce

1) $^{10}B(p,\alpha)^{7}Be$ 53 day

2) $^{10}B(p,\gamma)^{11}C$ 20 min

To evaluate this radioactivity problem, the reaction rates for these reactions are desired at temperatures near 3×10^9 deg. These have been measured in the same manner as has been reported in this and previous progress reports for nucleosynthesis measurements.

Natural boron targets were bombarded with protons from the cyclotron at energies from 0.25 to 3.0 MeV, and one point at 75 keV was taken with the ion-implantation accelerator of the Electrical Engineering Department. The ^{7}Be and ^{11}C yields were determined by their radioactivities and the yield curves measured. This is shown as fig. A4-2.

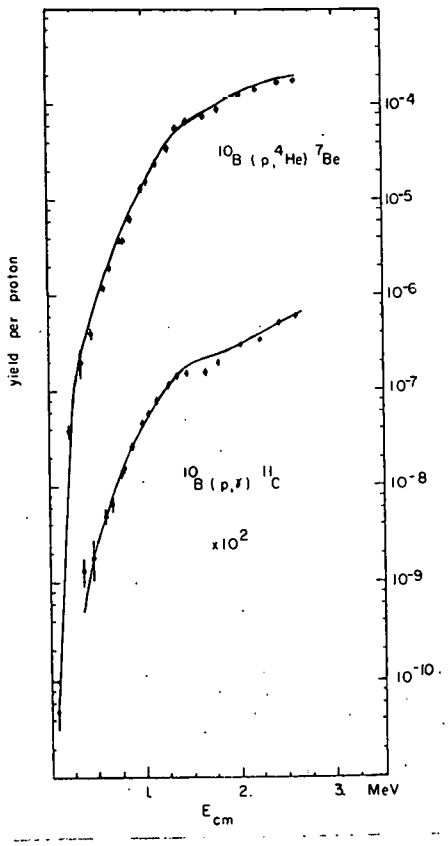

Fig. A4-2. The yield per proton incident upon ^{10}B for ^{7}Be and ^{11}C. Note the small yield of ^{7}Be at the lowest proton energy. The curve is a numerical fit used in the analysis.

The known resonances are broad, and only a smooth fit was made, shown as the solid line. Note the lowest energy point for ^{7}Be. The cross section was unfolded from these data, and combined with a thermal distribution of proton energies to obtain the reaction rates shown in fig. A4-3. These are in just the form required for calculating the ^{7}Be and ^{11}C yields from a given reactor. These results have been submitted for publication.

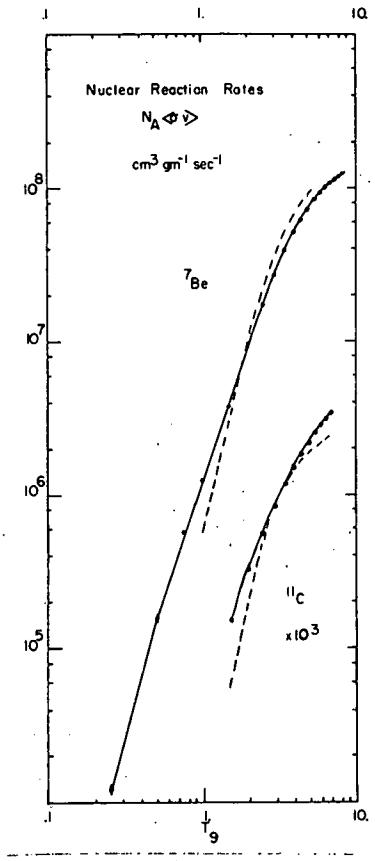

Fig. A4-3. The nuclear reaction rates for producing ^{7}Be and ^{11}C are displayed for various temperatures. The solid curve is a numerical fit, and the dashed curves represent the previously assumed values.

---

[1] T. Weaver, G. Zimmerman, and L. Wood, Lawrence Livermore Laboratory, UCRL 74938.

e. Radiobiological Characteristics of D+D Neutrons - F. M. Edwards, H. W. Fielding, J. J. Kraushaar, and M. Monce, in collaboration with K. A. Weaver of the University of Washington, Seattle.

Studies of the physical characteristics of fast neutron beams produced by 17.3 MeV deuterons incident on both beryllium and deuterium targets have been completed. Results indicate that a deuterium gas target offers significant advantages in average energy and dose rate.

i. Theoretical Calculation of Spectra and Yields from Deuterium Gas (K. A. Weaver)

Neutron spectra and yields were calculated for an incident deuteron energy corresponding to our maximum energy deuterons after passage through the gas target entrance foil, 16.8 MeV. Calculations were carried out for both a 5.8 MeV thick target and a totally stopping target.

The deuteron-deuteron interaction produces neutrons by two mechanisms: $D(d,n)^3He$ (Q value 3.268 MeV) and D(d,np)D (deuteron breakup: Q value -2.225 MeV).

The yield of neutrons from the $D(d,n)^3He$ reaction may be calculated from

$$\frac{dY}{dE_n} = \frac{N_o}{qW_A} \left(\frac{dE_d}{d(\rho x)}\right)^{-1} \frac{dE_d}{dE_n} \sigma(\theta=0°,\ E_d \rightarrow E_n)$$

where DY/dE_n = yield of neutrons per steradian per microcoulomb per MeV with energy E_n at 0° from the $D(d,n)^3He$ reaction

N_o = Avagadro's number (6.023×10^{23})

q = 1.602×10^{-13} μcoul.

W_A = 2.014 gm/mole

$dE/d(\rho x)$ = mass stopping power of deuterons in deuterium (MeV cm^2/gm)

dE_d/dE_n = incremental change in deuteron energy corresponding to incremental change in neutron energy (from kinematics)

σ = cross section in mb/(sr·MeV) for production of neutrons at 0° from deuterons of energy E_d by the $D(d,n)^3He$ reaction

For neutron production from deuteron breakup

$$Y(E_n) = \frac{N_o}{qW_A} \int_{E_{min}}^{E_{max}} \sigma(\theta=0°, E_d, E_n) \left(\frac{dE}{d(\rho x)}\right)^{-1} dE_d$$

where $Y(E_n)$ = yield of neutrons per sr per μC per MeV at 0° with energy E_n produced by all suitable deuteron energies E_d

σ = cross section in mb/(sr·MeV) for production of neutrons at 0° with energy E_n by deuterons of energy E_d due to breakup

The other parameters are as above and the integral is carried out over all contributing deuteron energies. $D(d,n)^3He$ cross sections were obtained from measurements made by Brill *et al.*[1]; cross sections for the breakup reaction were obtained from data reported by Rybakov *et al.*[2] and by Weaver *et al.*[3]; while the shape of the breakup neutron spectrum was estimated from the spectra measured by Lefevre *et al.*[4] and by Weaver *et al.*[3] The energy spread of the $D(d,n)^3He$ neutrons and the position of the high-energy edge of the breakup spectrum were calculated from particle kinematics.

The resulting spectra were integrated over neutron energy to obtain total neutron yields. The average energy and dose rate were calculated using the formulae

$$\bar{E}_n = \left(\int_0^{E_{n\,max}} Y(E_n)dE_n \right)^{-1} \int_0^{E_{n\,max}} Y(E_n)E_n dE_n$$

and

$$\Phi\left(\frac{rads}{\mu c}\right) = r^{-2} \int_0^{E_{n\,max}} Y(E_n)\frac{K(E_n)}{100}\, dE_n$$

where r is the source-to-skin distance, Y is the yield as calculated above and K is the kerma/fluence value for tissue at neutron energy E_n as tabulated in ICRU 13.[5]

The spectra calculated for 5.8 MeV thick and totally stopping targets are shown in fig. A4-4. The 5.8 MeV thick target has a total

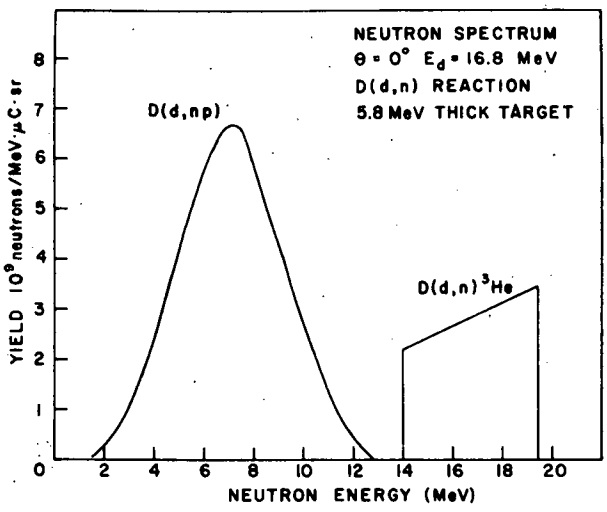

Fig. A4-4. Calculated neutron energy spectra for 16.8 MeV deuterons on totally stopping and 5.8 MeV thick deuterium targets.

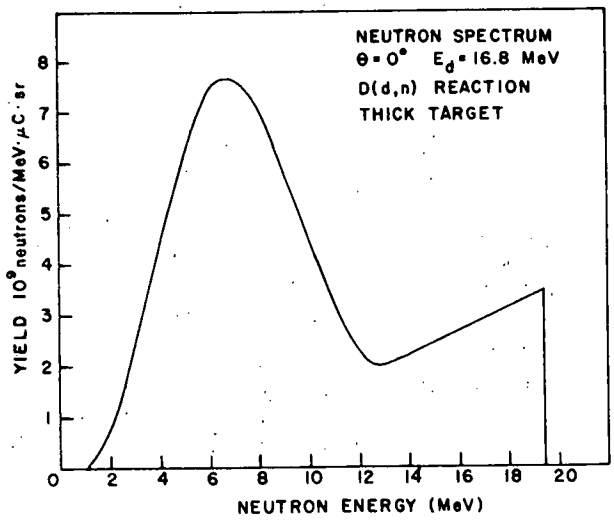

yield of 5.1 x 10^{10} neutrons/μC·sr with an average energy of 10.8 MeV. The calculated dose rate at an SSD of one meter is 0.027 rads/μC. The totally stopping target has a total yield of 6.9x 10^{10} neutrons/μC·sr with an average energy of 9.5 MeV. The calculated dose rate at an SSD of one meter is 0.037 rads/μC.

ii. Time-of-Flight Data

Two targets were used in this experiment. The beryllium target was simply a 1 cm. thick ^{9}Be plate which was water cooled by a backing plate. The deuterium gas target consisted of a gas cell with a water cooling jacket. The beam entered through a 0.001" Havar foil which was water cooled at the edges. Transmission through the foil degraded the 17.3 MeV deuteron beam by about 0.5 MeV. The target was long enough to be totally stopping at a pressure of 560 psi. Standard TOF techniques were used in conjunction with pulse shape discrimination to obtain neutron time-of-flight spectra. A bias of 1/2 x the Compton edge energy of ^{60}Co was set on the linear signal so that neutron events of energies of less than 2 MeV were rejected.

A comparison of neutron TOF spectra for equal integrated beam on target is shown in fig. A4-5 for totally stopping ^{9}Be, deuterium and 5.8 MeV thick deuterium targets. An approximate energy scale is also shown. It should be noted that since the efficiency of the scintillator depends on neutron energy, the true maximum of the breakup peak occurs at a lower energy than indicated in the TOF spectra (actually occurring at about 7 MeV for ^{9}Be and 6.5 MeV for D). However, it is immediately evident that the deuterium target yields both a higher average energy and a higher flux of neutrons.

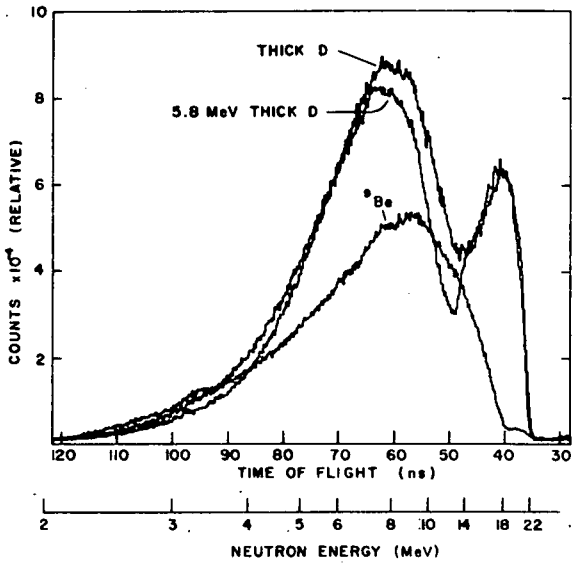

Fig. A4-5. Comparison of TOF spectra for 5.8 MeV thick deuterium, totally stopping deuterium and totally stopping beryllium targets. Spectra are normalized to equal integrated charge on target.

Comparison of the TOF spectra with theoretical calculations is difficult for two reasons. First, the absolute normalization of the spectrum with respect to integrated charge is nearly impossible since beam currents of less than a nanoamp had to be used to obtain sufficiently low counting rates. At these beam currents the background in the integrator and currents from upstream slit scattering are greater than the beam on target. Second, the thick target distorts the TOF spectra due to the incident beam slowing down in the target and the subsequent variation in flight path with deuteron energy. For example, in the case of the 5.8 MeV thick deuterium target it takes the beam about 6 ns to traverse the target, while the flight path (in the spectra shown here) varied from 2.46 to 2.23 meters. For the direct $D(d,n)^3He$ part of the spectra these effects may be calculated with not much difficulty. However, the calculation is more complex for the breakup peak and consequently was only approximated here. The theoretical neutron spectrum of dY/dE vs. E was converted to dY/dt vs. t with these thick target effects and a 2 ns Gaussian resolution function folded in. The spectrum was also multiplied by the detector efficiency which was experimentally determined using monoenergetic neutrons. A comparison of theory to experiment normalized to the $D(d,n)^3He$ peak (since absolute charge normalization was impossible as discussed above) is shown in fig. A4-6 for the 5.8 MeV thick target. The agreement is quite reasonable but not exact, partly due to approximations in our thick target corrections.

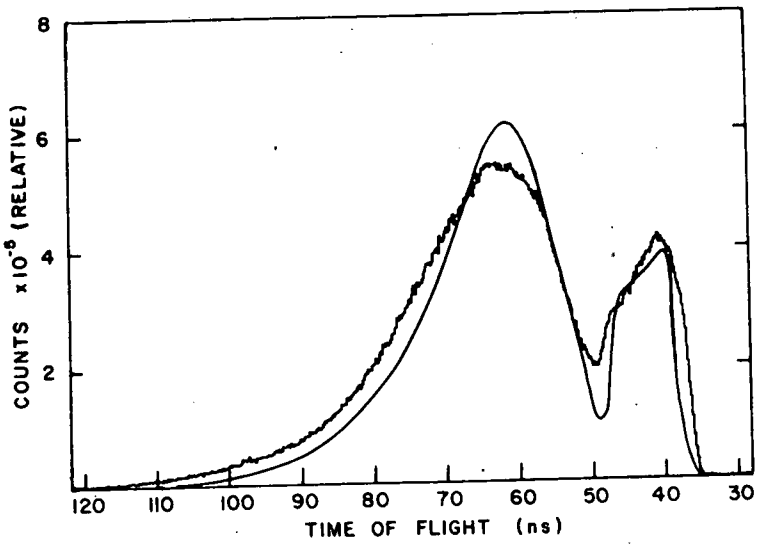

Fig. A4-6. Comparison of 5.8 MeV thick deuterium target TOF spectrum with the theoretically calculated spectrum. The calculated spectrum has been converted to a time spectrum and multiplied by the detector efficiency, with thick target effect approximately included. The curves are normalized to the $D(d,n)^3He$ peak.

iii. Bonner Sphere Data

Since the TOF method is, in this case, difficult to normalize and was insensitive to neutrons below 2 MeV it is desirable to obtain flux spectra over a broad energy range. The Bonner Spectrometer[6] achieves this broad energy range capability at the sacrifice of resolution. It also has the disadvantage of detecting neutrons not from the primary beam, for instance neutrons scattered from nearby shielding.

The spectrometer used in this experiment[7] consists of a small $^{6}Li(Eu)$ scintillator positioned at the center of polyethylene moderating spheres with diameters of 2, 2.5, 3, 4, 5, 8 and 12 inches.

Program NFLS,[7] which uses a least squares fitting routine to fit the data, calculated total neutron flux density, average neutron energy and plotted the integral neutron flux density spectrum from 0.01 eV to 20 MeV.

The Bonner Spectrometer gave an average energy of 4 MeV for the ^{9}Be target and 7.6 MeV for the 5.8 MeV thick deuterium target. The average energies are lower than indicated by TOF results due to the slowing of some neutrons by scattering off of the collimator. When spectra are taken from targets mounted far from any shielding or collimators, values closer to the indicated 7MeV (^{9}Be) and 11 MeV (D) are obtained. Total flux measurements were also obtained and converted to total yields. In the case of the 5.8 MeV thick deuterium target a total yield of 4.7×10^{10} neutrons/μC was calculated. This is close to the predicted value of 5.2×10^{10} neutrons per μC, the discrepancy probably being due to the problem of what source-to-detector distance should be used with a target 20 cm long. For the ^{9}Be target a total yield of 3.1×10^{10} neutrons/μC was measured. Thus the deuterium target yields nearly 1.5 times as many neutrons for the same amount of integrated beam.

iv. Linear Energy Transfer (LET) Spectra

The neutron beams produced by the two targets may also be compared in LET spectra. Commercially available instruments of the Rossi type are a convenient means of obtaining these spectra. The counter used in this experiment was an EG & G LET-½ 0.5 inch spherical proportional counter with tissue equivalent walls 0.1 inches thick. The chamber was filled with tissue equivalent (TE) gas of composition 55.4% propane, 39.4% carbon dioxide and 5.2% nitrogen. A pressure of 35 mm Hg was used to simulate a biologically sensitive volume of tissue density having a diameter of approximately one micron. The chamber was operated at a bias of +550 VDC. An internal ^{241}Am alpha source allows calibration of the spectra. Several computer codes exist which convert the raw pulse height spectra to LET spectra.[8] We used code TEPC, which is a version of a program used by the MD Anderson group in Texas as modified by P. Heinze and others.[9]

One often used method of presenting the data is a plot of fractional dose distribution, D(LET) multiplied by LET. This plot makes the high LET events more readily apparent. A plot of LET*D(LET) vs. LET for the 5.8 MeV thick deuterium and beryllium targets is shown in fig. A4-7. The familiar proton recoil peak (about 80 keV/μ) and alpha recoil peak (about 200 keV/μ) are readily apparent. It is obvious from the plot that the deuterium target yields more high-LET events. The program also calculates the fraction of the dose above the proton and alpha edges. For the deuterium target 13% of the dose was above the proton edge and 6% was above the alpha edge, while for the beryllium target 9% of the dose was above the proton edge and 4% was above the alpha edge. The computer code calculated total dose rates for the two targets which were within 10% agreement with measurements taken with an ionization chamber presented below.

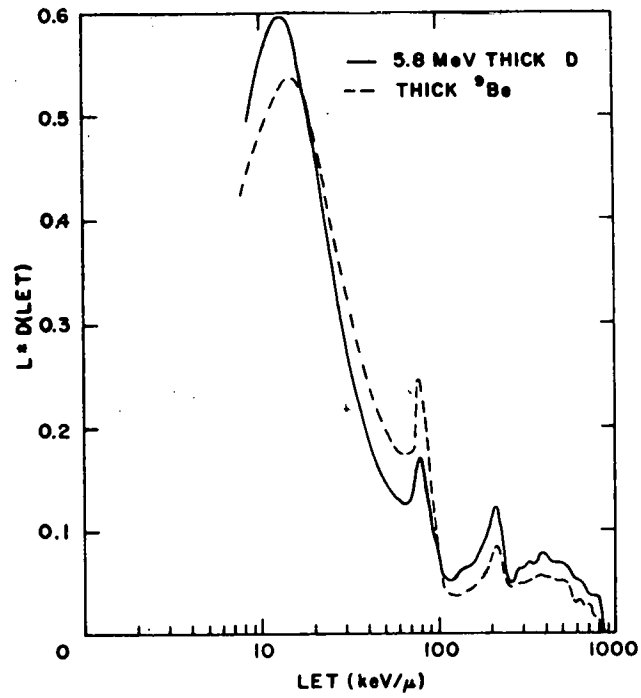

Fig. A4-7. Comparison of the two targets with respect to LET*D(LET) plotted versus LET.

v. Ionization Chamber Data

In order to compare dose rate and depth dose properties of the two neutron beams, measurements were taken with a standard type ionization chamber. We used an EG & G IC-18 three terminal ionization chamber of 0.1 cc volume having 0.06 in. thick tissue equivalent walls. The chamber was biased to +250 VDC and data were taken with both room air and TE gas. The current was measured with a Keithly 610B electrometer. The dose was calculated from the Bragg-Gray

equation:

$$\text{Neutron Dose} = (^{60}\text{Co Coul/Rad})^{-1} \frac{W_p}{W_e} \cdot \frac{S_p}{S_e} \cdot Q_{IC}$$

where (^{60}Co Coul/Rad) is the ^{60}Co calibration of the chamber, W_e and W_p are the eV/ion pair values for electrons and a combination of protons and alphas representing the charged recoils from the neutron interactions and S_p and S_e are the stopping powers of protons and electrons respectively. Q_{IC} is the charge collected in the chamber as measured by the electrometer and corrected for temperature and pressure. The values of W_p, W_e, S_p, and S_e for air and TE gas were those used by the University of Washington group.[10]

	W_p(eV/ip)	W_e(eV/ip)	S_p	S_e
Room Air	35.8	33.7	1.188	1.133
TE Gas	30.4	29.3	1.013	0.994

Measurements were taken for a fixed amount of integrated beam on target and values of Rads/μC were calculated. The ionization chamber was immersed in a 30 cm square phantom filled with tissue equivalent liquid of composition 58.2% distilled water, 34.3% glycerol and 7.5% urea, which has a density of 1.1 gm/cc.

On axis depth vs. dose for the two targets is plotted in fig. A4-8, for a 5 cm. diameter circular field with an SSD of 110 cm. The entrance doses for the beryllium and deuterium targets

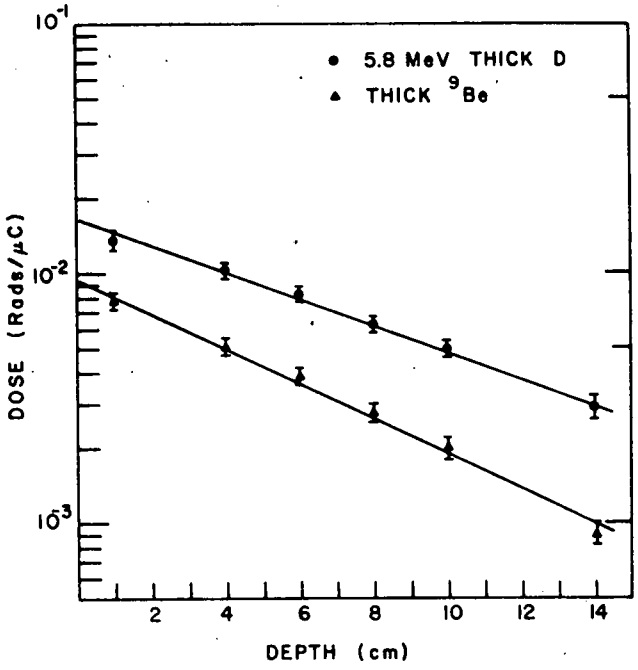

Fig. A4-8. On axis depth-dose plot for a 5 cm diameter circular field at an SSD of 110 cm.

are 0.95×10^{-2} Rads/μC and 1.7×10^{-2} Rads/μC respectively. For this SSD the theoretically calculated dose is 2.2×10^{-2} Rads/μC. Part of the discrepancy is due to field size effects. It is also evident that the dose falls off more slowly for the deuterium target due to its higher average energy. Thus the deuterium target yields about 80% more dose with slightly better depth-dose properties than the beryllium target.

vi. Conclusion

The 5.8 MeV thick deuterium gas target yields a fast neutron beam 50% greater in average energy and 80% higher in dose rate than a fast neutron beam produced by a thick beryllium target. A greater dose rate is obtainable with a totally stopping deuterium target at a slight sacrifice in average energy. One problem with the gas target used here is its length which leads to problems in defining an SSD. This difficulty can easily be overcome by increasing the pressure and decreasing the gas temperature thus allowing a shorter length.

---

1 O. D. Brill, V. M. Pankratov, and V. P. Rudkov, Atomnaya Energiya 16 (1964) 141.
2 B. V. Rybakov, V. A. Sidorov, and N. A. Vlasov, Nucl. Phys. 23 (1961) 491.
3 K. A. Weaver, J. D. Anderson, H. H. Barschall, and J. C. Davis, Nucl. Sci. and Engr. 52 (1973) 35.
4 H. W. Lefevre, R. R. Borchers, and C. H. Poppe, Phys. Rev. 128 (1962) 1328.
5 Neutron Fluence, Neutron Spectra, and Kerma, International Commission of Radiation Units and Measures Report No. 13, Washington, D. C., 1969.
6 R. L. Bramblett, R. I. Ewing, and T. W. Bonner, Nucl. Inst. & Meth. 9 (1960) 1.
7 J. B. Martin and C. S. Zaidins, Univ. of Colo., to be published.
8 W. H. Grant, G. D. Oliver, and B. A. Mitchell, Health Physics 22 (1972) 351.
9 Stanley Johnsen, Univ. of Calif., Davis, private communication.
10 Juri Eenmaa, Univ. of Washington, private communication.

f. Stable Isotope Tracers - H. Rudolph, R. A. Ristinen, M. J. Fritts, C. Solomons (CU Medical School -Denver), and S. Christensen

i. ^{48}Ca

Attempts have been made to utilize ^{48}Ca as a stable isotope tracer for situations in which radioactive tracers would either be prohibited or undesirable, e.g., calcium metabolism studies in children. The ^{48}Ca is identified through the (p,n) reaction and subsequent off-line counting of the 44 hour ^{48}Sc activity produced.

A typical spectrum from a blood serum sample is shown in fig. A4-9. These data were obtained using a 20 cc Ge(Li) detector with a counting time of 20 minutes one day after bombardment with 9 MeV protons. The ^{48}Sc activity is represented by the 983, 1037, and 1312 keV lines which form a cascade in the decay to ^{48}Ti. Activity from ^{44}Sc decay is seen in the 1497 keV line. These data were not taken in a low-level counting area.

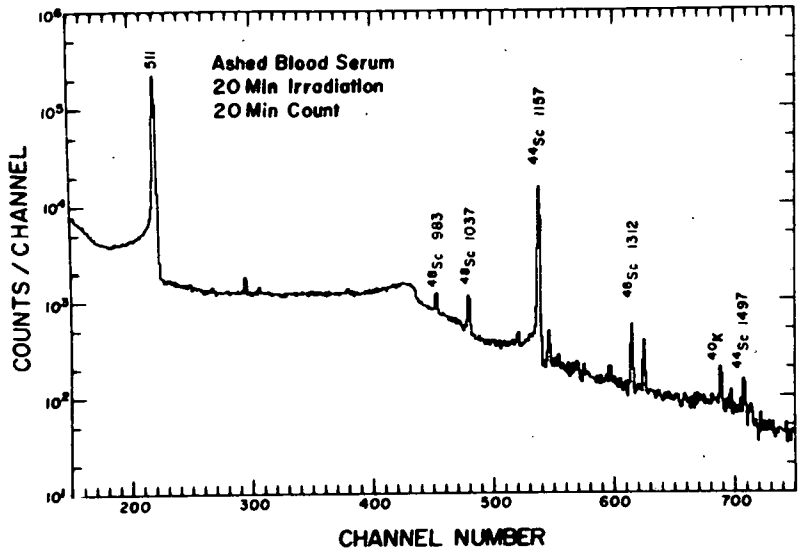

Fig. A4-9. A gamma-ray spectrum from a blood serum sample activated by the $^{48}Ca(p,n)^{48}Sc$ reaction.

Both absolute and isotopic ratio techniques have been investigated for the ^{48}Ca tracer. The absolute measurements proved to have the poorer reproducibility due primarily to losses of target material during handling. Isotopic ratios, however, can be measured quite accurately. The raw ratios listed in table A4-II for naturally abundant samples have an RMS deviation from the mean of ~4%. In

Table A4-II. $^{48}Ca:^{44}Ca$ Ratios

Sample	Ratio[a]
$CaCl_2$	.1067 ± .0024
$CaCl_2$	.1087 ± .0024
$CaCl_2$	.1067 ± .0031
$CaCl_2$	.1157 ± .0032
Blood Serum	.1150 ± .0047

Mean = .1106 ± .0046

[a] Ratios are of absolute yields 6 hr. after irradiation.

order to provide an increase in the ^{48}Ca content of the body fluids of a child by 12%, only $\lesssim$ 0.3 mg of ^{48}Ca need be injected. Hence, one or two milligrams would give clearly discernible results. Currently, feasibility studies with rats are underway which should also determine the number and frequency of blood samples to be taken.

ii. ^{13}C

The ^{13}C content of biological material is detected by the yield from the $^{13}C(\alpha,n)^{16}N$ reaction. The seven second activity thus produced leads to beta decay branches to the 6.13 and 7.11 MeV states of ^{16}O. The gamma decay of these states to the ground state is readily observable and free from contaminant γ-rays. For typical human tissue samples, all detector events corresponding to an energy $\geq$3.5 MeV show the characteristic half-life of ^{16}N decay.

^{13}C is measured relative to the ^{12}C content of the sample, where ^{12}C is seen by the $^{12}C(\alpha,p)^{15}O$ reaction. Since only 511 keV gamma rays are associated with the 122 second positron decay of ^{15}O, the data are multiscaled into sixteen 32 sec timing groups. The ^{15}O component of the 511 line may then be separated from other contributions, e.g., the decay of ^{17}F from the $^{14}N(\alpha,n)^{17}F$ reaction. The ratio of all detector events greater than 3.5 MeV in the first group to the fitted ^{15}O activity thus gives the ^{13}C:^{12}C ratio. Furthermore, ratios of these isotopes to ^{14}N can also be obtained. Spectra from two analyzer groups are shown in fig. A4-10.

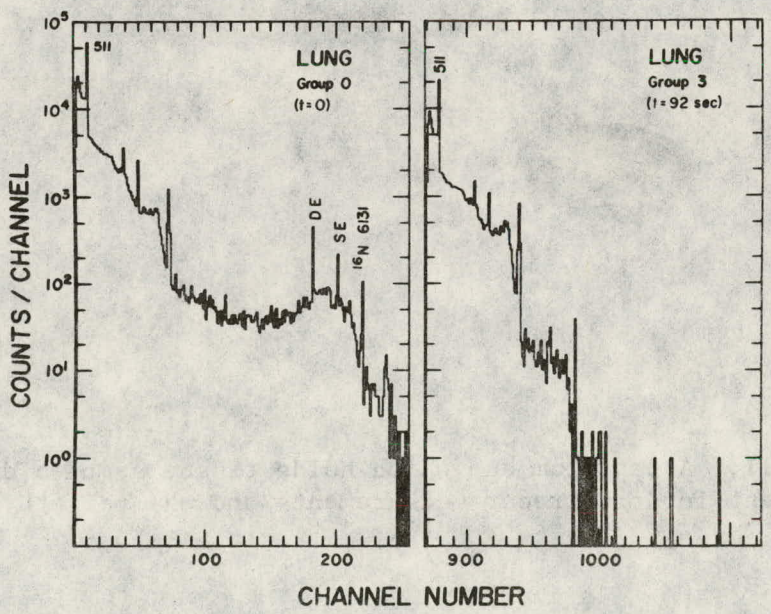

Fig. A4-10. Delayed gamma-ray spectra taken shortly after bombardment of lung tissue with 17 MeV alphas and after a 92 second delay.

Samples are made by pressing ~20 mg of dry tissue into a tantalum cup. This cup is then placed in a polyethylene rabbit fitted with a tantalum shield to prevent beam from spraying onto the polyethylene (see fig. A4-11). The target is bombarded for 128 seconds with 17 MeV alphas and then transferred by a fast shuttle system to a remote counting area. The irradiation, transfer, and multiscaling cycle is continued for four or more cycles.

Currently, the reproducibility of the ratio is poor, only ±10%. However, statistically the measurements should be good to 2-3%. The problem appears to be in the fitting of the ^{15}O activity, and efforts are underway to improve these procedures.

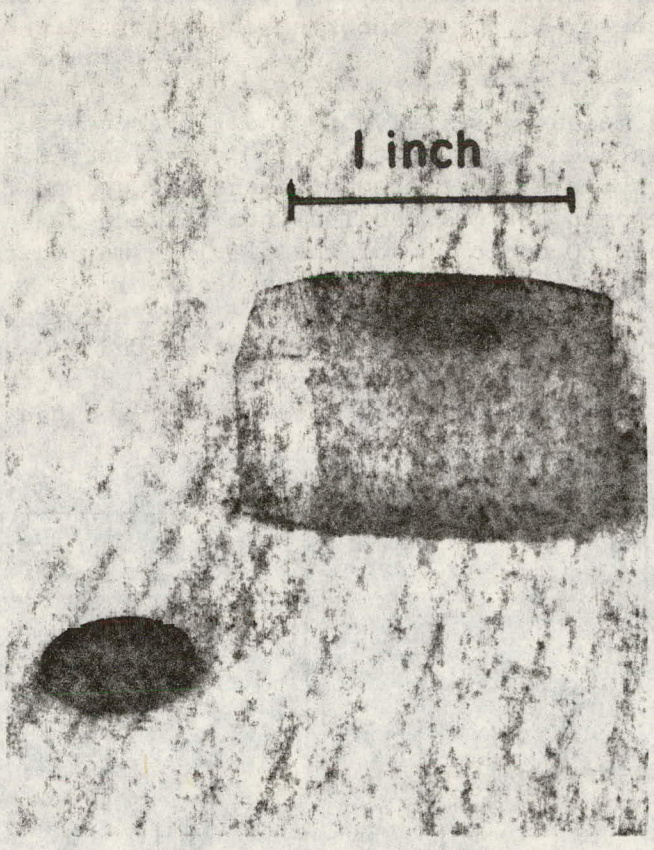

Fig. A4-11. A tantalum cup which holds tissue samples during a bombardment for ^{13}C tracer measurements and the polyethylene rabbit.

g. Neuron Damage by Alpha Particles - J. T. Lett and E. Power (CSU), R. A. Ristinen and W. R. Smythe

The NASA sponsored project to study the effect of cosmic radiation on the brain is being continued by Professor J. T. Lett's group in the Department of Radiology and Radiation Biology at Colorado State University. This laboratory is continuing its collaboration on the alpha-particle experiments. The CSU group is also doing experiments with relativistic heavy ions from the Bevalac at the Lawrence Berkeley Laboratory.

The purpose of the experiments is to determine quantitatively the amount of damage caused by heavily ionizing particles passing through non-dividing cells such as neurons. Such cells cannot be replaced by cell division, and damage to the brain and nervous system of an astronaut by cosmic rays on a prolonged space flight is presumably cumulative and must be assessed before long deep-space manned flights are attempted.

The alpha-particle experiments consist of the irradiation of living neuron cells in the retina of a rabbit. The living cells are obtained by quickly removing the retina from the eye of the rabbit immediately after killing the rabbit. The irradiation is usually accomplished within five minutes of the rabbit's death. After irradiation the retina is frozen in liquid nitrogen. Subsequently the DNA is extracted from the nuclei of the neurons and is unstranded and a molecular weight distribution of the DNA fragments is obtained by use of a zonal-rotor ultracentrifuge.

The initial irradiations were conducted with fluxes of 10^5 to 10^8 alphas/cm^2 at an energy of 15 MeV. Preliminary results led to a desire to have measurements at higher energy and higher fluxes. The initial method used to produce the alpha fluxes involved the use of Rutherford scattering from a gold foil, but this method was not suitable for the higher energies and fluxes, so a new approach was used. The cyclotron beam swinger was used to prepare a beam of alpha particles traveling vertically downward with a cross section approximately 7 mm x 25 mm. An approximately uniform flux was obtained by mounting the retina on a rotating table during irradiation. With this arrangement the retinas were irradiated with 34 MeV alpha particles at fluxes varying from 10^6 to 10^{12} alphas/cm^2 in an irradiation time of about 3 minutes. The results of this bombardment are now being analyzed.

h. Solar Cell Irradiations - R. A. Ristinen and W. R. Smythe

For the second year proton irradiations of solar cells were performed for Ball Brothers Research Corporation. These solar cells are

used as sun sensors to keep some instruments on a satellite accurately pointed at the sun. In two separate cyclotron runs a total of more than ninety cells were exposed to 4.6 MeV protons at an integrated flux of 3×10^{11} protons/cm^2. This irradiation is intended to "age" the cells so that the particle radiation which they will experience in space will not produce an appreciable reduction in their efficiency. The first such cells which were irradiated in this laboratory are expected to fly on a satellite late this year.

5. X-ray Fluorescence Trace Element Analysis - A. C. Alfrey, R. A. Ristinen, H. Rudolph, W. R. Smythe, and J. W. V. Trish

a. Introduction

Following the work of Johansson[1] which demonstrated the fact that proton induced x-rays provided a very sensitive means of detecting and identifying small quantities of elements, this laboratory investigated the applicability of the method to the determination of trace elements in small (0.3 mg) samples of various materials. Investigations of the variation of sensitivity with particle type and energy were carried out. Subsequently, the use of a filtered bremsstrahlung x-ray beam to excite the targets was investigated and found to be equally good for many purposes, and economically more attractive.

Development of the techniques and apparatus for this method of trace element analysis has been continued by working on actual trace element problems in medicine and environmental science. The immediate objective of this work is to develop the x-ray fluorescence technique, and to determine the extent to which it is a useful tool in these areas. The ultimate objective is to export the developed technology to laboratories and hospitals, assuming that it does turn out to be the valuable tool which presently it appears to be.

b. The Molybdenum Project

In June of 1972, an interdisciplinary study of molybdenum in the environment was begun jointly by the University of Colorado and Colorado State University. This study was funded by NSF-RANN and included researchers from geology, biology, chemistry, physics, civil engineering, medicine, agronomy, and animal science. The CU Nuclear Physics Laboratory participated as one of two analytical facilities, the other being a chemical analysis facility.

A good example of an application of x-ray fluorescence analysis to the molybdenum study project is the survey of trace element concentrations in tissues of wildlife carried out by Professor Eldon Kienholz of CSU. He submitted liver and kidney samples from trout, robins, pika, marmot, beaver, deer, sheep, etc. The samples were ashed, targets were prepared and the spectra were analyzed for ten elements: K, Ca, Mn, Fe, Cu, Zn, Sr, Zr, Mo, and Cd. Fish planted in live traps for 14 days in different streams showed striking differences in liver and kidney trace element content. These differences were most pronounced for molybdenum, potassium, copper, and zinc. Another interesting observation by Professor Kienholz was that pika collected in the research area had surprisingly high levels of cadmium which indicates that there may be some cadmium toxicity in pika in Colorado. This observation illustrates one of the most important aspects of the x-ray fluorescence method; it is a broad range method which discloses the presence of significant quantities of most elements of atomic number greater than about 18.

It is anticipated that the study of molybednum in the environment will be completed in June of 1975.

c. Hemodialysis

The study of trace element abnormalities among dialyzed and non-dialyzed uremics, which is a collaboration with Dr. Allen C. Alfrey, Chief of the Renal Section of the Denver V.A. Hospital, is continuing. Several abnormalities have been discovered, as was discussed in last year's Progress Report. Among these abnormalities was noted a striking deficiency of rubidium in the skeletal muscle of dialyzed uremics. In the past year considerable elucidation of the causes of this deficiency has been accomplished. It has been shown that the blood loses rubidium in passing through the artifical kidney. This loss occurs from the serum but not immediately from the erythrocytes. The artificial kidney appears to be very efficient at removing rubidium from blood serum. Blood entering the artificial kidney with a measured serum rubidium level of 60±7 parts per billion emerges with a serum rubidium level of less than 5 ppb. After six hours of dialysis, the patient's serum rubidium level has dropped a factor of two or more. Although rubidium seems to be ubiquitous in human tissues, little or nothing is understood about its physiological function. Prevention of rubidium depletion by the addition of rubidium to the dialysate is being attempted. Preliminary clinical results are encouraging but not yet definitive. Clinical tests of rubidium repletion are continuing at the Denver V. A. Hospital. This work is now being supported in part by a contract with the National Institute of Arthritis, Metabolism, and Digestive Diseases.

d. Oil Shale

The recently increased awareness of energy problems has greatly accelerated developments in the oil shale industry. In order to see what trace element problems might occur with the large scale mining of oil shale. A very preliminary trace element analysis of an oil shale sample has been made and is shown in fig. A5-1.

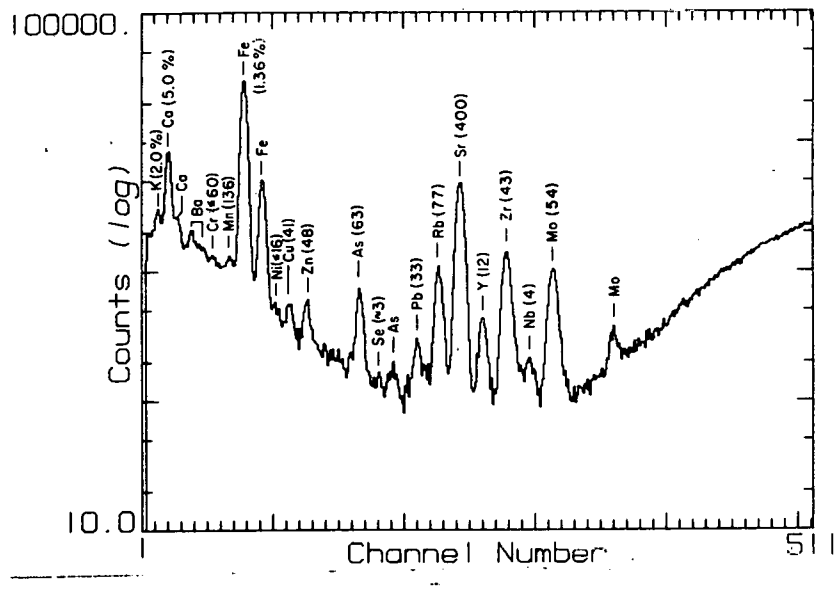

Fig. A5-1. X-ray fluorescence spectrum of a 248 μg sample of crushed oil shale. The elemental concentrations are given in parts per million, except for K, Ca, and Fe, which are given in percent. The sample was irradiated with the filtered bremsstrahlung beam from a tungsten anode x-ray tube operated at 55 kilovolts and 10 mA for a live time of 20 minutes. The fluorescent x-rays were detected with a Kevex model 3000 lithium drifted silicon detector of 3 mm thickness.

e. Software and Hardware Developments

The software programs for data taking and for computer control of the automated target changer and x-ray set have been completed and put to use. This PDP 8/E based data handling system stores two 512 channel spectra in core storage, displays one of them, and can quickly store (or retrieve) spectra on a DEC tape file. A program has been developed so that the PDP-9 computer can read the PDP-8 DEC tapes, which permits the use of the PDP-9 program "SPECTR" to analyze the x-ray spectra. A 256k word disk is on order for the PDP-8/E so that in the future it will be possible to use it to analyze the x-ray spectra.

A new x-ray collimator has been developed for the automated sample changer, which has significantly lowered background radiation levels at the detector. In particular the background lead "L" lines, with which the "old" system was afflicted, have been eliminated. The new collimator system now has no lines in its background spectrum, except for a very small copper K_α line, which corresponds to a copper background of a few parts per million. If this line is not removed by improvement of the collimator, it will be handled by background subtraction.

As soon as the collimator development project is completed the automated sample changer system will be calibrated and put into routine use. It will then be possible to load the changer with 32 targets and the computer will run the system automatically overnight. The computer will position the target, turn on the x-ray set, store the data, time the run, turn off the x-ray set, transfer the data to DEC tape and proceed to the next sample.

---

[1] T. B. Johansson, R. Akselsson, and S. A. E. Johansson, Nucl. Inst. and Meth. 84 (1970) 141.

B. Intermediate Energy Physics

1. The $^{7}Li(^{3}He,\pi^{-})^{10}C$ Reaction - M. E. Rickey, R. E. Anderson, and J. J. Kraushaar (Univ. of Colo.), and H. W. Baer and J. Carrol (Lawrence Berkeley Laboratory, Univ. of Calif.)

Observation of the $^{7}Li(^{3}He,\pi^{-})^{10}C$ reaction would be valuable for two reasons, the first of which is the reaction mechanism and nuclear physics information which might be obtained. Secondly, with the possible advent of cancer therapy using π^{-} bombardments, it would be useful to find a more efficient method of π^{-} production and this reaction is one of the possibilities.

The present method of π^{-} production via the (p,π^{-}) reaction suffers from a low cross section as well as a rather flat angular distribution. On the other hand, the (p,π^{+}) reaction proceeds with a reasonably high cross-section and it also has the highly peaked angular distribution necessary for efficient transport of the emitted pions to a separate facility. It was expected that the analogous (n,π^{-}) reaction would proceed with characteristics similar to those of the (p,π^{+}) reaction. Since high energy neutron beams are not readily available, it was hoped that the collision of the two complex nuclei might yield the (n,π^{-}) reaction through the "quasifree" interaction of the neutrons in the projectile with the nucleons in the target.

Projectiles which might suggest themselves for such a study are deuterons, ^{3}He, and α-particles. Helium-3 ions are particularly attractive since they can be accelerated to higher energies in a given cyclotron. Furthermore, the $(^{3}He,\pi^{-})$ reaction has the unusual property of increasing the number of protons in the target nucleus by three. A number of very interesting proton-rich nuclei far from the line of stability can be produced in this way. For the present experiment we restricted our attention to reactions that produced radioactive nuclei with a convenient half-life and gamma-ray decay properties in order to optimize the sensitivity of the experiment. It was finally decided to attempt to measure the $^{7}Li(^{3}He,\pi^{-})^{10}C$ production cross-section as a function of bombarding energy from threshold up to as high an energy as could be conveniently obtained.

The residual ^{10}C nucleus decays to the first excited state of ^{10}B with a half-life of 19.5 sec and a branching ratio of 98%. Subsequently the ^{10}B decays with the emission of a 0.720 MeV γ ray, and the characteristic half-life and energy of the gamma ray provide a unique signature for the decay of ^{10}C. A fast rabbit system and associated electronics was constructed at this laboratory. The ^{7}Li and ^{6}Li targets of approximately 1 cm thickness were purchased from Oak Ridge National Laboratory. Three 16-hour days of beam time were provided by the scheduling committee for the Lawrence Berkeley Laboratory 184-inch cyclotron.

Two rather heavily shielded Ge(Li) gamma-ray detectors were located outside of the shielded area of the 184-inch cyclotron at

the counting station of the rabbit system. One detector (30 cc) was used to determine the half-life of gamma rays by routing signals sequentially into four 256 channel subgroups of a pulse height analyzer. The time devoted to each subgroup could be varied but was fixed at 10 seconds for observation of the ^{10}C activity. The other detector was used with a 1024 channel pulse height analyzer for observation of a more complete gamma-ray spectrum to monitor lines from various other radioactive nuclei produced.

A set of copper absorbers were fabricated and installed with a collimator just upstream of the target so that the 1140 MeV ^{3}He ions from the cyclotron could be reduced to the desired energies. An ionization chamber was constructed and placed just downstream from the target and a charge integration system provided. The equipment was transported to Berkeley and, along with some items borrowed from various groups, was installed and calibrated in a two-day period prior to the three-day run. Bombardments of ^{6}Li, ^{7}Li, ^{9}Be, polyethylene, teflon, ^{27}Al and copper targets were carried out at 1140, 830, 730, and 450 MeV.

Since background production of ^{10}C via spallation of heavy impurities in the target could not be detected directly, a ^{6}Li target was also bombarded. Though ^{10}C could not be produced directly from the ^{6}Li this method should reproduce the impurity production in the ^{7}Li target since the two targets were fabricated using identical procedures. The difference of the ^{7}Li and ^{6}Li target yields would then provide the $^{7}Li(^{3}He,\pi^{-})^{10}C$ cross-section at each energy. The only methods of background production not identically accounted for with this method are various two-step processes. Such a process might be elastic (or inelastic) ^{3}He scattering from ^{7}Li followed by the $^{7}Li(^{7}Li,4n)^{10}C$ reaction. It was hoped that the cross-sections for these processes might be small enough to be neglected, or that they were at least partially compensated for in the bombardment of the ^{6}Li target. The most troublesome contaminant was the ^{10}C produced in the 0.002 inch polyethylene wrapper on the Li targets. The ^{10}C production resulting from ^{12}C bombardment by ^{3}He was quite copious at the energies studied.

Because of the high backgrounds encountered, the final result depended on the difference of two large, approximately equal numbers. Only the data at $T(^{3}He)$=1140 MeV yielded results which were not statistically insignificant and that result was 90±90 nb total cross-section for the $^{7}Li(^{3}He,\pi^{-})^{10}C$ (particle stable states) reaction. This result is tentative and more measurements are being considered for the future.

The inherent problems of using the activation method for the detection of low cross-section reactions may in fact discourage further attempts. In addition to the $^{7}Li(^{7}Li,4n)^{10}C$ reaction one could have $^{6}Li(^{6}Li,2n)^{10}C$ take place in the ^{6}Li target and this latter reaction most likely would have a greater cross section

than the former. For this reason, the subtraction of the yields from the two targets may lead to an underestimation of the cross-section. There are further complications such as the $^{6}Li(^{7}Li,3n)^{10}C$ and $^{7}Li(^{6}Li,3n)^{10}C$ reactions which would be difficult to evaluate with any precision. Since two-step reaction yields are dependent on the target thickness some attempt could be made at determining the yields as a function of target thickness.

The identification of the gamma rays from the other targets has permitted a number of ^{3}He reactions on heavy nuclei to be observed and work is continuing on extraction of some useful information from these results.

Though the total cross section for $^{7}Li(^{3}He,\pi^{-})^{10}C$ reaction obtained in this experiment appears quite small at best, the results are not totally discouraging. If a total cross-section of about 100 nb could be conclusively established, the next step would be to observe the $^{7}Li(^{3}He,\pi^{-})^{10}C$ reaction directly with a pion spectrometer to see if the angular distribution is highly peaked in some region. If these conditions are met, then the results speak well for using the ^{3}He projectile in order to produce negative pions for use in medical therapy for cancer patients.

We are indebted to a number of people both in Boulder and Berkeley for help in providing equipment and facilities that made the experiment possible. We are especially indebted to L. A. Erb for the design and construction of the electronics and A. K. Wiles for the construction of the mechanical parts of the rabbit system. In Berkeley we are indebted to A. Smith and J. McCaslin for making activation measurements that permitted calibration of the ionization chamber. We also with to thank R. Pehl, N. Jacobs, and D. Lee for loaning us equipment and Leal Kanstein and others at the 184-inch cyclotron for help in setting up and using their facilities.

2. Production of ^{10}C by the Bombardment of ^{9}Be with Protons from 300 to 740 MeV - M. E. Rickey, J. J. Kraushaar, and R. E. Anderson (Univ. of Colo.), and H. W. Baer and J. Carrol (Lawrence Berkeley Laboratory, Univ. of Calif.)

In an effort to measure the total cross-section for the $^{9}Be(p,\pi^{-})^{10}C$ reaction, the facilities, apparatus, and techniques described in the previous section were used. The activation technique appeared capable of providing a convenient method for determining cross sections that are difficult to measure using standard counting methods and it was hoped that data at a series of proton energies could be obtained from the 184-inch cyclotron.

Measurements of ^{10}C activity produced in a 1 cm thick ^{9}Be target were made using the 740, 600, 480, and 300 MeV proton beams obtained from the Berkeley 184-inch cyclotron. The results of these measurements are shown in fig. B1 where the cross-sections

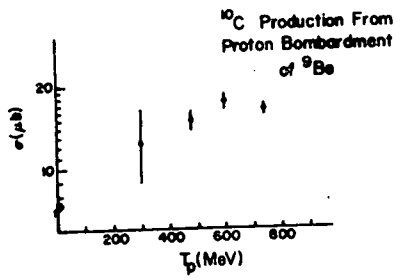

Fig. B1. The cross-sections for the production of ^{10}C by proton bombardment of ^{9}Be.

were calculated assuming the activity resulted from the $^{9}Be(p,\pi^-)^{10}C$ reaction. While extensive analysis demonstrated that spallation of heavy impurities could account for only a very small part of the observed activity, the results were much larger than those inferred by direct observation of π^- spectra resulting[1,2] from 185 and 600 MeV proton bombardment of ^{9}Be. The Uppsala data[1] at 185 MeV implies a total cross-section for the first two states of ^{10}C (i.e., the particle stable states) of about 50 nb while the CERN data[2] at 600 MeV implies a total cross section of 20 nb. The CERN measurement is thus about 10^3 times smaller than that of the present work.

There are several processes which could resolve this discrepancy. First, there could be competing processes which produce more than one pion, such as the $^{9}Be(p,\pi^-\pi^\circ)^{10}C$ or the $^{9}Be(p,\pi^-\pi^+\pi^-)^{10}C$ reactions. These reactions would leave the emerging π^- particles with much less energy and hence the CERN cross-sections would be lower than those measured in the present work. However, multiple pion production involving more than two pions is energetically forbidden for all but the 600 and 740 MeV runs, while theoretical calculations[3] assuming only single pion production do a reasonable job of reproducing the magnitudes of π^- production cross sections at 730 MeV.

Another process which does not require the presence of multiple pions in the exit channel also appears capable of explaining the large cross-sections seen. This process would involve α-particle production via the $^{9}Be(p,d)^{8}Be \rightarrow 2\alpha$ or $^{9}Be(p,\alpha)^{6}Li$ reactions followed by the $^{9}Be(\alpha,3n)^{10}C$ reaction. The calculation of the expected production rate of ^{10}C through this process is quite complex. First of all, there is no information presently available which gives the total cross-section for the (p,α) or (p,d) reactions of the energies of interest. The $(\alpha,3n)$ total cross-section is not known at any energy let alone the integrated total cross-section over the entire range of alpha energies. The effective target thickness is different for the alphas produced in the (p,d) reaction than for those produced in the (p,α) reaction. In addition, the angle of emission in the reaction gives a wide range of final alpha energies which must be considered. The alphas emitted following the

(p,α) reaction are expected to be predominantly forward peaked and highly energetic enough to penetrate the target completely (this implies that $E_\alpha \geq 170$ MeV). The situation is more complex in the case of the $^{9}Be(p,d)^{8}Be \rightarrow 2\alpha$ reaction since the alphas generally have much less energy.

An estimate of the production rate of ^{10}C may be made if one assumes the not unreasonable value of 16 mb for the total cross-section for both the $^{9}Be(p,\alpha)$ and $^{9}Be(\alpha,3n)$ reactions at T_p=740 MeV. In addition, since the $^{9}Be(p,\alpha)$ reaction takes place uniformly throughout the target, an effective target thickness equal to 1/2 the actual target thickness is assumed in calculating the ^{10}C production rate due to the latter reaction. The alpha production due to the $^{9}Be(p,d)^{8}Be \rightarrow 2\alpha$ reaction is neglected. The results of such a calculation show that 100% of the observed ^{10}C activity may be accounted for.

This suggests that activation measurements used to measure cross-sections[4] such as $^{13}C(\pi^+,\pi^\circ)^{13}N$ can be very difficult to analyze properly. In this latter case, copious quantities of protons might be expected from the $^{13}C(\pi^+,p)$ reaction and the subsequent $^{13}C(p,n)^{13}N$ reaction could add to the yield from the $^{13}C(\pi^+,\pi^\circ)^{13}N$ reaction in a manner that would be hard to evaluate.

---

1 S. Dahlgren, P. Grafström, B. Höistad, and A. Asberg, Nucl. Phys. A204 (1973) 53.

2 J. Rohlin, K. Gabathuler, N. W. Tanner, C. R. Cox, and J. J. Domingo, Phys. Lett. 40B (1972) 539.

3 M. M. Sternheim and R. R. Silbar, Phys. Rev. D 6 (1972) 3117.

4 M. Zaider, J. Alster, D. Asberg, S. Cochavi, M. A. Moinester, and A. I. Yavin, Proceedings of International Conference on Intermediate Energy Physics, Uppsala, 1973.

3. EPICS Taut Wire System - N. Ensslin and S. Greene

A taut wire system is being assembled at LAMPF to monitor the alignment of the EPICS channel and spectrometer. The sensitivity needed is on the order of 1 mil. For example, random displacements of 8 mils in all four channel magnets would shift the beam spot about 2 mm.

Such displacements can be measured by passing a taut wire through the center of four pickup coils arranged as shown in fig. B2. An AC current on the wire will induce signals in the coils. If two opposing coils are wired together so that their signals tend to cancel, then the phase and amplitude of the difference signal is proportional to the displacement of the wire from the center. The phase is converted into a DC voltage, which is then read by an analog-to-digital converter. Four coils mounted as shown make up one point along the wire.

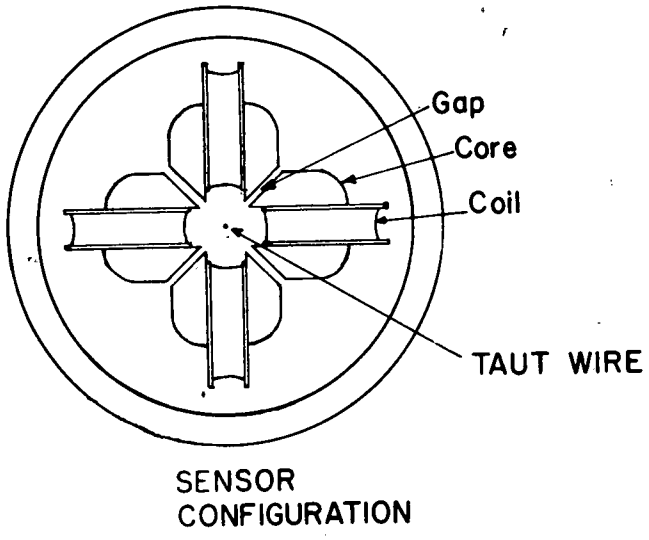

Fig. B2. Taut wire configuration superimposed on a schematic of the EPICS channel.

Ten taut wires, with six sensor units along each wire, will be installed on the EPICS channel and spectrometer. A tentative layout of the wires and sensors along the four channel magnet is shown in fig. B3. The sensors will be attached to the magnets, and the ends of the taut wire will be rigidly clamped with respect to the floor. This layout should make it possible to measure all possible translations and rotations of the channel magnets with some redundancy.

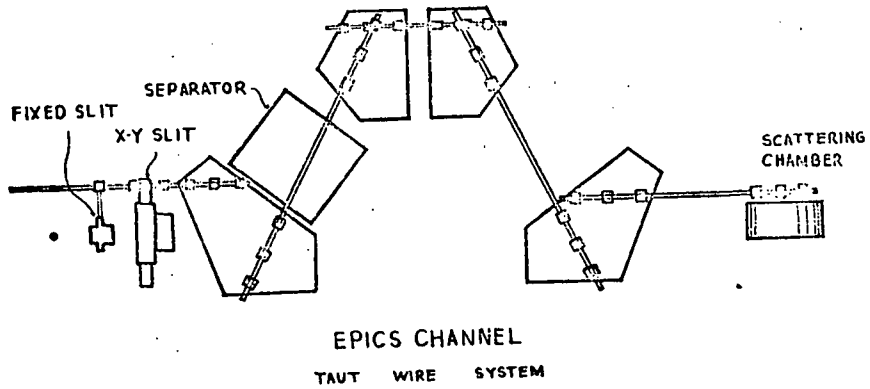

Fig. B3. Axial view of taut-wire sensor pad.

The electronics for the entire taut wire system and a computer readout program have been completed. The first taut wire is now assembled and undergoing testing in position on Bending Magnet 1. Operating experience with this wire has led to some re-design of the mounting assemblies to facilitate installation. Other changes are being made to improve sturdiness and long-term stability, since some of the wires will be inaccessible after they are installed. Assembly of the other taut wires should begin soon. Many of the parts have already been mass-produced at the Nuclear Physics Laboratory shop at Colorado and at the Physics Department shop of New Mexico State University.

4. Slit Scattering in the EPICS Beam Line - N. Ensslin

The Monte Carlo calculation of slit scattering in the EPICS channel and spectrometer at LAMPF, described in the 1973 Progress Report, has been completed. The calculation predicts the expected backgrounds of muons, protons, and slit-scattered pions.

The simulation of the EPICS channel optics was improved substantially over that described last year. The horizontal focussing produced by fringe fields and the effects of optical aberrations are now included. Under these conditions the backgrounds at the scattering target are predicted to be 25% muons, 0.3% protons, and 0.6% slit-scattered pions. The muons will not scatter into the spectrometer, and protons are easily distinguishable by other means. Most of the slit-scattered pions strike the scattering target so close to the correct position that the spectrometer will not be able to distinguish them from good events. Thus it should be possible to ignore all backgrounds generated in the channel.

The decay of pions into muons inside the spectrometer will generate additional backgrounds. In simulating this process it was found possible to reject most muons because their flight paths did not extrapolate back to the target. The remainder constitute a background of about 7%. This background is concentrated primarily in two satellite peaks, one at 1-2% higher energy than the pion peak, and one directly under it. The latter peak will make absolute cross-section measurements uncertain by perhaps 0.1 to 0.5%. The predicted background of slit-scattered pions, 0.2%, is so small that there does not appear to be any need for low-Z liners or veto counters on the spectrometer pole faces.

5. Construction for LAMPF - R. J. Peterson and A. K. Wiles

A number of items for HRS and EPICS have been built in our machine shop. These include

1) The drive mechanisms for the EPICS spectrometer.
2) A large number of components for the taut-wire systems.

3) Prototype target frames for HRS.
4) A frame and box for a spare helical MWPC for the EPICS spectrometer.

Projects currently in the shop include the vacuum cans and flanges for the quadrupole triplet in the EPICS spectrometer and a prototype trim magnet for the EPICS channel. This latter will also be field-mapped in Boulder.

C. Apparatus and Facility Development

1. The Magnetic Spectrograph System - D. E. Prull, B. W. Ridley, R. A. Emigh, E. W. Stoub, R. A. Ristinen, R. R. Sercely, and L. R. McKissick

a. Introduction

The operating principles and basic design features of the magnetic spectrograph system have been described in previous reports.[1-3] The completed system is shown schematically in fig. C1-1. During the past year two multipole trim magnets were installed, and the shielding cave was completed. A new helical cathode proportional chamber (HCPC) was built and is currently being used as the position sensitive detector.

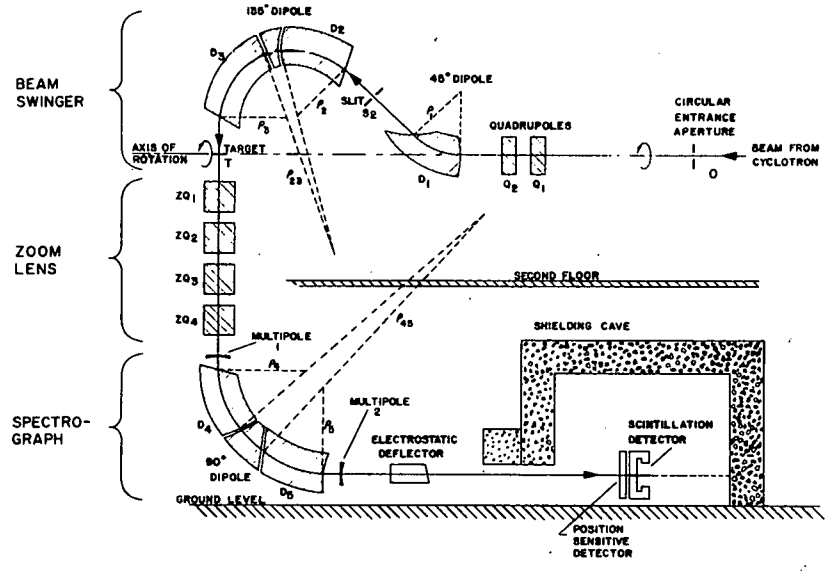

Fig. C1-1. Schematic of the magnetic spectrograph system.

The system has been used extensively without large unforeseen problems. Many of the experiments described in section A of this report have used the system.

b. General Operation

With the aid of the computer code OPTICS,[3] the experimental setup of the magnetic spectrograph system is routine. In combination with field mapping data and the empirical calibrations described later in this section, the basic design parameters of the system are used to calculate the currents required for the beam transport elements on the 0° beam line and on the beam swinger. Typically 60% to 80% of the extracted cyclotron beam is placed on target.

The currents required in each of the four zoom lens quadrupole magnets, the spectrograph magnet, and the two multipole trim magnets depend on the dispersion matching requirements and the kinematics of the reaction under investigation. The values of these currents are also calculated by OPTICS. In general, the resolution cannot be improved by further adjustment of any of these currents.

Particle identification is normally achieved by using the HCPC as a transmission (ΔE) detector and the plastic scintillator as an E detector. The computer code PLATES (described in section II-C-5), is a valuable aid in identifying peaks in the pulse height spectra of the anode and scintillator signals. This code calculates the pulse amplitudes for all the common reaction products from either the target or from specified contaminants in the target. Only those reaction products whose magnetic rigidities are within the acceptance band of the spectrograph are considered. The electrostatic deflection plates can be used to physically separate different particle groups when particle identification based only on detector amplitudes is marginal.

The first long HCPC[3] used with the system had a "thickness" of nearly 60 mg/cm^2 (equivalent carbon). In some experiments, the particle identification scheme described above was defeated since the HCPC was not a transmission detector and no scintillator signals were available. The new chamber, with a thickness less than 10 mg per cm^2, has permitted studies of reactions such as $^{120}Sn(^{3}He,^{7}Be)^{116}Cd$ which were not possible with the first detector.

c. Experimental Calibration

i. Zoom Lens

The first-order beam optics design of the magnetic spectrograph system predicts the field gradients required in each of the four zoom lens quadrupoles. In the dispersion plane, a variable magnification at a fixed image position is needed. An experimental check of the system provided evidence that the "true" image position was not fixed when the quadrupoles were set at the first-order predictions.

A strip of gold foil one mm. wide was placed in the target position to provide an "object" for the zoom lens and spectrograph. This narrow strip provided a monokinetic beam of elastically scattered particles, thus eliminating the need for dispersion matching. The width of the "image" of this strip target at the detector was measured as a function of both the first-order zoom lens image position and magnification.

The first-order image position z, as measured from the spectrograph magnet, which yielded the smallest peak width at the detector is given by:

$$z = 1.52\ m_x^2 + 177.55\ (cm)$$

where m_x is the magnification. This result has been included in the code OPTICS.

ii. Multipole Trim Magnets

When the magnification M_x of the zoom lens is changed significantly from 0.89 (the magnification for zero Q-value reactions), chromatic aberrations are introduced in the virtual image of the target. This causes the focal plane angle of the spectrograph to decrease and changes the plane to a curved surface. The multipole trim magnets (described in a previous report[3] are needed to keep the focal surface a plane at a fixed orientation. Multipole 2 (see fig. C1-1) is used to correct for the chromatic aberrations caused by the zoom lens. Similarly, multipole 1 is used to correct for the spherical aberrations introduced by the use of multipole 2.

These multipole trim magnets were calibrated by using a strip gold target and minimizing the width of the "image" at the detector. The currents in the four zoom lens quadrupole magnets and the spectrograph magnet were varied in order to place the image at five different positions along the detector. The currents in the multipole magnets were adjusted to minimize the peak width at these five positions simultaneously. This procedure was repeated for various zoom lens magnifications and the resulting calibration has been included in OPTICS.

d. Present Status and Development

i. Solid Angle

Beam optics calculations have shown that the angular acceptance in the dispersion plane of the zoom lens and spectrograph varies with position along the target as well as being a function of zoom lens magnification and position along the focal plane. Preliminary experimental studies have verified these calculations. Experiments are currently being planned to measure these effects and provide the calibrations necessary for accurate data reduction.

ii. Focal Plane Detection

The 62 cm Helical Cathode Proportional Chamber (HCPC) detection system described in last year's Progress Report has been in routine use for more than one year as a (ΔE,E,x) detector in the focal plane of the magnetic spectrometer. Typically, the detector contribution to the observed line width is no more than 1.0 mm when operated at the limit of proportionality.

A computer code has been written which calculates the shape and amplitude of cathode voltage pulses. Since the relevant physical parameters are included in this code, the performance of new geometries or new gases can be tested by computer simulation. Also included in this description is an expression for the best resolution that can be achieved from HCPC detectors, Δx, given by

$$\Delta x = K \cdot G \cdot \left(\frac{V_{noise}}{V_{signal}}\right) \cdot \exp\left(+\tfrac{1}{2}\alpha\right)$$

where

K = constant
G = anode-cathode gap
V_{noise} = pre-amp noise (output)
V_{signal} = cathode signal (pre-amp output)
α = helix attenuation coefficient (one pass)

The constant K depends in detail on the timing system used. For example, a calculated value for constant fraction timing is about 12.1, while an experimental value for leading edge timing is about 16.5.

iii. Scattering Chamber Progress

The combined function scattering chamber (charged particle measurements and time-of-flight experiments) is fully designed with approximately 75% of the drawings completed. Machine shop work on the main body is just starting due to outside vendor delays in rolling the plate. The remotely controlled target ladder sub-assembly for this chamber will be completed as soon as possible and used in the present chamber for beam mapping.

---

[1] University of Colorado, NPL Progress Report (1971) 106.
[2] University of Colorado, NPL Progress Report (1972) 96.
[3] University of Colorado, NPL Progress Report (1973) 71.

2. Rabbit, Ram, and Plunger Summary - M. J. Fritts and C. S. Zaidins

A summary of all the "folklore", data sheets, etc., for the system of multiscaling at the CU cyclotron was written during the past year. In the course of the writing of this report, several modifications were made in order to bring the various aspects of the system into a greater degree of standardization. The most extensive change was made to the plunger, which is used to detect β-delayed particles in the cave scattering chamber. The plunger logic is now the same as the ram logic.

The items which are covered in the summary constitute a large number of activities which are controlled by what was originally called the rabbit system. As there are now a relatively large number of experiments using these activities, we felt it was important to have a single document which enables the user to see the system as a whole and still include fairly detailed instructions on the operation of a particular function of the system.

The discussion includes the following activities: multi-channel scaling, multi-spectral scaling, single spectrum analysis, rabbiting, ramming (see last year's annual Progress Report), and

plunging. In addition there are sections on the basic system design, experimental configurations, circuits, and data analysis. Anyone interested in the write-up should ask for "Of Rabbits, Rams, and Plungers: or Multiscaling at the CU Cyclotron". This is the first entry in the Frit-Zaid preprint series, a series which joins with other noted series to Aid the experimental physicist.

3. Nuclides Produced from 18 MeV Proton Bombardment of Havar Foil - M. J. Fritts

The experiment on the decay of ^{36}K, discussed in section II-A-2-b, was performed using a gas target with Havar foil windows and a proton beam of 18 MeV. The resulting γ-ray spectra exhibited copious contaminant peaks. Since many suspected ^{36}K transitions involved γ-rays falling on these contaminant peaks, a detailed study of these spectra was undertaken. This information was thought to be of general interest as well, because of the widespread use of Havar in such experiments.

Table C3-I lists nuclides produced in the Havar, identified through their characteristic γ-spectra. Identification was made on the basis of energies, relative intensities and decay (or non-decay) of the γ-rays involved. Also listed are the half-lives of each nuclide, the reaction believed responsible for its production, the center-of-mass energy available to the light product and the proton Coulomb barrier if applicable. The list also includes nuclides produced from the bombardment of brass, since the Havar foil was mounted on a brass washer. Table C3-II lists the composition of Havar, broken down by nuclide for comparison.

The ^{36}K experiment used the Rabbit System to cycle the target every 3.44 sec for a two-day period. The run continued uninterrupted except for roughly seven minute pauses to dump data, and background runs taken for three hours in the middle of the experiment and for five hours at its end. As a check on the γ-ray assignments, an expression was derived relating the total counts in a peak in the "rabbited" spectra to the counts in a corresponding peak in the five-hour background spectrum as a function of the half-life of the nuclide produced. This expression included the effects of the pause for the background spectrum and a first order correction to variations in beam current over the two-day run. This expression is plotted as the solid line in fig. C3-1. Also shown in the figure are the corresponding ratios found from normalizations for all peaks arising from the decay of that nuclide for both the "rabbited" and background spectra.

The assignments shown in table C3-I account in intensity for nearly all the peaks found in all spectra to within 10-15%, except for peaks attributable to other sources. Table C3-III shows background peaks due to other contaminants. All other peaks identified are due to reactions on the target gas.

TABLE C3-I. Contaminants due to Havar and brass.

Nuclide	$\tau_{1/2}$	Reaction	$E_{c.m.}$ (MeV)	Proton Coulomb Barrier (MeV)
^{64}Ga	2.6 m	$^{64}Zn(p,n)$	9.9	---
^{66}Ga	9.4 h	$^{66}Zn(p,n)$	11.8	---
^{68}Ga	68.3 m	$^{68}Zn(p,n)$	24.2	---
		$[^{67}Zn(p,\gamma)]$	14.0	---
^{52}Mn	5.67 d	$^{52}Cr(p,n)$	12.2	---
^{52m}Mn	21.3 m	$^{52}Cr(p,n)$	11.8	---
^{50}Mn	1.75 m	$^{50}Cr(p,n)$	9.3	---
^{60}Cu	23 m	$^{60}Ni(p,n)$	10.8	---
^{55}Co	18 h	$^{54}Fe(p,\gamma)$	22.7	---
^{56}Co	77.3 d	$^{56}Fe(p,n)$	12.3	---
^{58}Co	71.3 d	$^{59}Co(p,d)$	9.5	6.9
		$^{58}Fe(p,n)$	24.6	---
		$[^{57}Fe(p,\gamma)]$	14.6	---
^{57}Ni	35.9 h	$^{58}Ni(p,d)$	7.7	7.0
^{63}Zn	38.8 m	$^{63}Cu(p,n)$	13.6	---
^{92}Tc	4.4 m	$^{92}Mo(p,n)$	9.0	---
^{93}Tc	2.75 h	$^{92}Mo(p,\gamma)$	21.9	---
^{93m}Tc	43.5 m	$^{92}Mo(p,\gamma)$	21.5	---
^{94}Tc	293 m	$^{94}Mo(p,n)$	12.8	---
^{94m}Tc	52 m	$^{94}Mo(p,n)$	12.7	---
^{95}Tc	20 h	$^{95}Mo(p,n)$	15.4	---
		$[^{94}Mo(p,\gamma)]$	22.7	---
^{96}Tc	4.28 d	$^{96}Mo(p,n)$	14.1	---
		$[^{95}Mo(p,\gamma)]$	23.3	---
^{182}Re	12.7 h	$^{182}W(p,n)$	14.4	---

TABLE C3-II. Constituents of Havar by nuclide.

Nuclide (%)	Sum
$^{59}Cr(42.50)$	42.5%
$^{50}Cr(0.86)$, $^{52}Cr(16.75)$, $^{53}Cr(1.91)$, $^{54}Cr(0.48)$	20.0%
$^{54}Fe(1.04)$, $^{56}Fe(16.37)$, $^{57}Fe(0.39)$, $^{58}Fe(.06)$	17.86%
$^{58}Ni(8.88)$, $^{60}Ni(3.39)$, $^{61}Ni(0.15)$, $^{62}Ni(0.47)$, $^{64}Ni(0.12)$	13.00%
$^{180}W(.004)$, $^{182}W(.739)$, $^{183}W(.403)$, $^{184}W(.858)$, $^{186}W(.795)$	2.80%
$^{92}Mo(.319)$, $^{94}Mo(.181)$, $^{95}Mo(.314)$, $^{96}Mo(.331)$, $^{97}Mo(.189)$, $^{98}Mo(.476)$, $^{100}Mo(.193)$	2.00%
$^{55}Mn(1.60)$	1.60%
$^{12}C(.198)$, $^{13}C(.002)$	0.20%
$^{9}Be(.04)$	0.04%

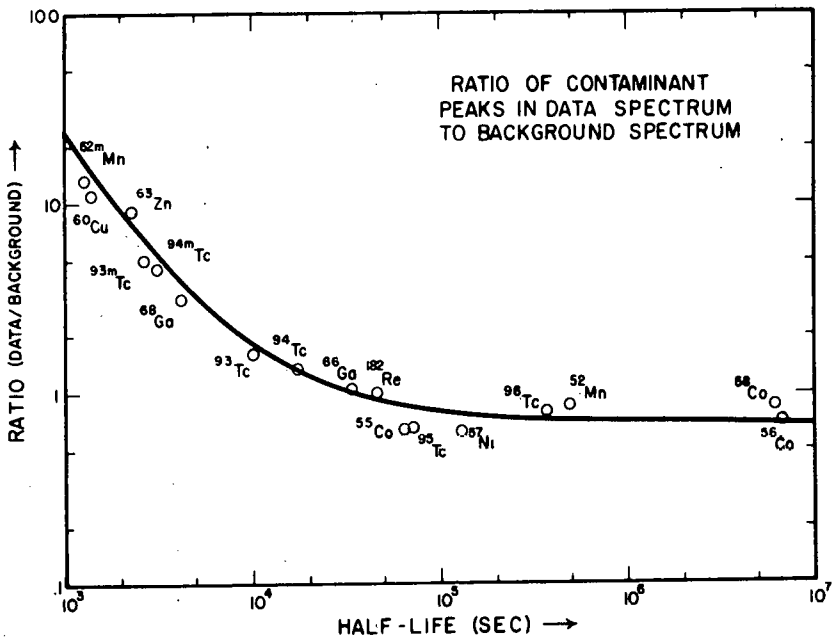

Fig. C3-1. Ratios of peak area in the data spectrum to corresponding peak area in the background spectrum for contaminant nuclei as a function of half-life. The solid curve is the prediction including a first order correction for variation in beam intensity during the run.

TABLE C3-III. Background contaminants.

Nuclide	$T_{1/2}$	Reaction	$E_{c.m.}$	Proton Coulomb Barrier
^{40}K	1.28 x 10^9 y	---	---	---
^{124}Sb	60.2 d	---	---	---
^{122}Sb	2.72 d	---	---	---
^{14}O	70.5 s	^{14}N(p,n)	10.8	---
^{16}N	7.11 s	^{16}O(n,p)?	---	---

Table C3-IV lists possible contaminants which cannot be positively excluded because of overlap with other peaks. However, their contribution, if any, would be small.

TABLE C3-IV. Other possible Havar or brass contaminants.

Nuclide	$\tau_{1/2}$	Reaction	$E_{c.m.}$	Proton Coulomb Barrier
^{65}Zn	243.8 d	$^{65}Cu(p,n)$	15.6	---
^{51}Mn	45.9 m	$^{50}Cr(p,\gamma)$	22.9	---
^{70}Ga	21.1 m	$^{70}Zn(p,n)$	16.3	---
^{182m}Re	64 h	$^{182}W(p,n)$	14.4	---

Finally, there remain a few unsolved puzzles. Peaks at 4807, 3272, 3000, and 1935 keV have $\gtrsim$ 30% of their area unaccounted for, with the 4807 showing evidence of decay with $\tau_{1/2} \lesssim 2$ sec. No serious attempts were made to find assignments for peaks at 623, 614, 584, 575, and 412 keV because of the very large background and relative low intensity of the peaks.

4. Efficiency of the 34 cc Ge(Li) Detector - M. J. Fritts and P. D. Ingalls

Relative full energy peak (FEP), single escape peak (SEP), and double escape peak (DEP) efficiencies were determined for the Nuclear Diodes 34 cc Ge(Li) detector (#L-888). The low energy portion of the FEP curve was determined from measured γ-ray transitions following ^{56}Co decay, using well known relative intensities.[1] Known γ-cascades[2] at proton capture resonances in the $^{23}Na(p,\gamma)$ reaction were used to obtain the FEP, SEP, and DEP efficiencies at high energies relative to the low energy portion of the FEP curve. The ratios R''(≡DEP/FEP), R'(≡SEP/FEP) and R(≡DEP/SEP), determined from intense transitions in the decays of ^{66}Ga, ^{64}Ga, ^{60}Cu, ^{56}Co, ^{57}Ni, and ^{36}K were used to establish other regions of the DEP and SEP curves.

The measurements were performed for a specific geometry, using shielding to enhance high energy γ-rays relative to low energy ones. The front face of a 2.5 cm thick collimator (3/4" hole) was positioned 1.75 cm from the center of the source or target. A 5.1 cm lucite β^+ stopper and a 2.4 cm lead hardener were positioned just behind the

collimator. The aluminum can of the Ge(Li) detector was aligned on the axis determined by the centers of the source and collimator hole, and placed immediately behind the hardener. Since the detector efficiency at low energies is a strong function of the shielding, the curves derived from these experiments should be used only for duplicate geometries, or if the effects of shielding and geometry are properly accounted for.

The measured FEP efficiency values obtained from the ^{56}Co decay were extracted from peak areas assuming linear background. Peaks falling on Compton edges were discarded. The resulting values were fitted to a smooth curve covering an energy range of 847 to 3550 keV.

The ^{23}Na proton capture reaction at the 1417 and 1318 keV resonances provides data on the 13052 → 4123 → 1369 keV and 12957 → 1369 → 0 keV cascades, respectively. The values obtained from the smoothed low energy curve at 2754 and 1369 keV then provide relative efficiencies at 8929 and 11588 keV, respectively, from the known branching ratios.[2]

The behavior of the FEP curve in the intermediate region (expected to be nearly linear) was checked using efficiency curves published for other coaxial detectors.[3] Efficiency data on a 31 cc and a 38 cc detector were corrected for differences in shielding and interpolated to a 34 cc detector. The resulting curve was found to pass through all the error bars on our measured data, and was therefore used to obtain the final FEP curve shown in fig. C4-1.

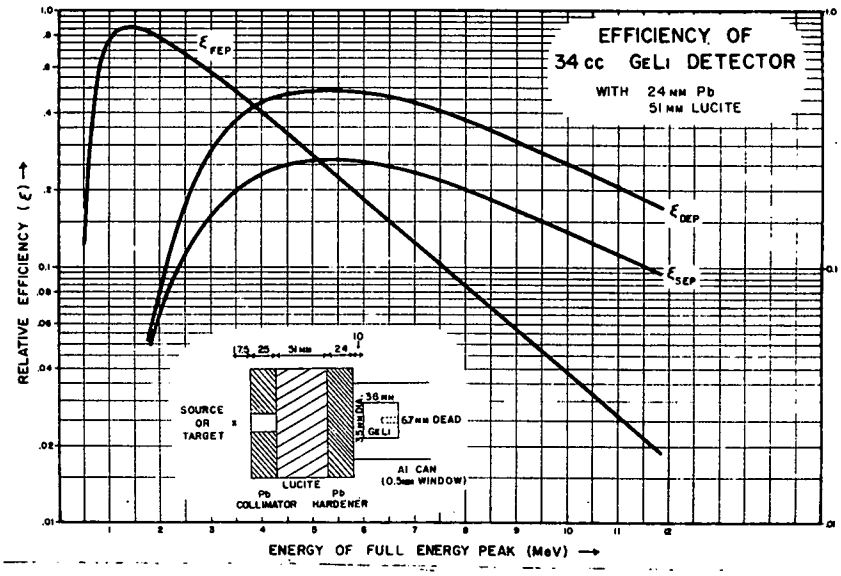

Fig. C4-1. Relative full energy peak (FEP), single escape peak (SEP), and double escape peak efficiencies for the 34 cc Ge(Li) detector as a function of full energy peak energy.

The ratios R'', R', and R obtained from γ-rays seen in the ^{66}Ga, ^{64}Ga, ^{60}Cu, ^{56}Co, ^{57}Ni, and ^{36}K decay were plotted along with the resonance data and fitted to smoother curves. The ratio R was used only as a check on the data, since this ratio is nearly constant over the entire energy region.

Interpolated curves for R'' and R' were again obtained from those in ref. 3, and were found to fall within 3% of all the smoothed measured data! This is extremely good agreement, since fairly good statistics were available for several ^{36}K transitions. These curves were then used to obtain the final SEP and DEP efficiency curves shown in fig. C4-1.

Errors on the FEP curve vary with energy extending from 3% at the region of the ^{56}Co data, through 4.5% at 5500 keV, 10% at 8500 keV, to 15% at 11500 keV. Below 900 keV the error rises extremely fast, since it is based solely on the behavior of the interpolated curves. The DEP and SEP curves are good only to 10% for most regions, and greater when the FEP curves are greater.

---

[1] D. C. Camp and G. L. Meredith, Nucl. Phys. A166 (1971) 349.
[2] B. P. Singh and H. C. Evans, Nucl. Instr. and Meth. 97 (1971) 475.
[3] H. Seyfarth et al., Nucl. Instr. and Meth. 105 (1972) 301.

5. Computer Program Development

a. MEXTAB - D. E. Prull

A library subroutine which reads an atomic mass excess table and returns the mass excess and uncertainty of a specific isotope to the calling program has been developed for use on the PDP-9 computer. The table is based on data due to A. H. Wapstra and N. B. Gove[1] and currently contains the mass excess for 1770 isotopes. On the first call, the subroutine reads the table from the disk into a common block reserved by the calling program. Successive calls then access this common block.

---

[1] A. H. Wapstra and N. B. Gove, Nuclear Data Tables 9 (1971) 267 and private communication.

b. QTABLE - D. E. Prull

A program to tabulate nuclear reaction Q-values has been written for the PDP-9 computer. The only input to the program is the target nucleus. The output is a table listing the Q-value, residual nucleus, and the uncertainty of the Q-value (computed quadratically) for 48 possible reactions. The mass excess information is provided by the subroutine MEXTAB.

c. PLATES - D. E. Prull

A program to provide information needed for particle identification when using the magnetic spectrograph system[1] has been written for the PDP-9 computer. The input to the program is a description of the experimental setup, including the reaction under investigation, the kinetic energy of the beam, the scattering angle, and the gas pressure in the multiwire proportional chamber. Using relativistic kinematics and the Q-values obtained from the subroutine MEXTAB, the program determines the reaction products whose magnetic rigidities are within the input acceptance band of the spectrometer. For these reaction products, the program computes and lists the energy loss in the anode region of the detector and the energy deposited in the backup plastic scintillator. In addition, the transverse deflection provided by the electrostatic deflection plates and the range of excitation levels in the residual nucleus are also listed.

---

[1] University of Colorado, NPL Progress Report (1973) 71.

d. BEAM - D. E. Prull

A first-order beam optics program has been developed for the PDP-9 computer. The program describes the beam envelope and gives the 5 x 5 transfer matrix at the end of each element in a specified beam transport system. One of the options available is a plot of the phase space accepted as determined by baffles and slits located along the transport system. No variation of field strengths is attempted in the present version since memory requirements already necessitate a complex overlay structure for the program.

e. Software for the XRF System - H. Rudolph

Program XRF has been written for the PDP-8/E computer which controls the operation of the x-ray fluorescence system. The major tasks performed by the program are the operation of peripheral devices (x-ray tube power supply, 32-position sample changer and analog-to-digital converter), data acquisition and dumping of data onto magnetic tape.

XRF is written almost entirely in SABR code. Machine language has been used wherever it has been necessary or more convenient. The program itself resides in field 0 of the PDP-8 memory, while field 1 is used primarily as storage. Two 512 channel memory groups are provided. Each channel consists of two 12-bit words, and hence a maximum of 1.6×10^7 counts may be stored in each channel.

Both manual and automatic modes of operation are possible. The program starts initially in manual mode, and the automatic sequencing can be called at any time. Control of program flow is obtained by the LA-30 DECwriter and the 12-bit switch register. A

series of 18 two-character commands may be entered via the LA-30. These control the labeling and manipulation of the data, the sample changer and x-ray set. Data acquisition and display are governed by the switch register settings.

When the automatic sequencing in XRF is called, all necessary data are requested by messages printed on the LA-30. Appropriate checks are made on the status of all devices necessary for automatic operation, and error messages are printed to warn the operator to correct the status of each device. While samples are being run, a continual check is made. If a failure occurs, the automatic mode is aborted with a message signifying that error which occurred. The successful run of a sample is also signified, so that a complete picture of the automatic run may be obtained.

f. SETN - D. E. Prull

A program has been written to read DECtapes written by program XRF on a PDP-8E computer and write the data on PDP-9 DECtapes in the workingfile format used by SPECTR. A maximum of 25 runs can be transferred in less than five minutes. The previous method which used paper tapes required about two hours for 25 runs.

g. REGRES - M. L. Munger

A program to calibrate charged particle spectra has been written for the PDP-9 computer. The calibration is carried out in an n^{th} order polynomial regression of energy against channel. Forsythe[1] has shown that there is a set of "orthogonal" polynomials which enables us to obtain the regression coefficients without solving a system of simultaneous equations. Input allows for bootstrapping the calibration if peaks are known in only a small region of the spectrum. Output gives CHI**2 up to 9^{th} order and a calibration overlay plot which allows one to read off peak kinetic energies.

---

[1] G. E. Forsythe, J. Soc. Indust. Appl. Math., 5 (1957) 74-88.

6. Electronics Maintenance and Development - Lee A. Erb

a. Cyclotron

i. Main Magnet M.G. Set

Regulation problems were experienced with the main magnet current. The problem was tracked down to unusually high M.G. set commutator noise which swamped the regulator. The commutator was machined and new brushes were installed. This action has reduced the noise to an acceptable level. However, the generator has a limited life and a replacement supply should be considered soon.

ii. RF System

A dee stem finger stock failure occurred this year. This has been the first such failure in a decade. It seems that contact surface cleanliness is of utmost importance under high RF current conditions. The dee stem had acquired a thin coating of brown residue which probably contributed to the finger stock failure.

iii. Shim Coil Supplies

The two dual shim coil supplies ordered from Transrex of Torrance, California, have been delivered. Step-start provisions were eliminated from the manufacturing specifications for cost reduction purposes. The step-start feature has been added here at a minor additional cost. The only problems encountered were parts delivery and access to the barn area to work on the supplies.

iv. Vault Air Conditioner

Contactor replacement was necessary on the vault air conditioner compressor. High starting currents were causing contact failures. Insufficient margin of safety was used in selecting the contactors during manufacture.

b. Beam Handling

i. RF Interlocks

The increasing lack of reliability of the neutron monitoring system has necessitated a re-design of the vacuum valve status link in the RF-peronnsel safety interlock chain. Access to some areas now requires both a low indicated neutron level and multiple valve closures.

ii. Neutron Monitors

A study is under way to improve our neutron monitoring system. The moderated BF_3 detector tubes now in service have deteriorated significantly. We are looking into the possibility of incorporating both neutron and gamma detectors in the same sensing system calibrated relative to tissue damage.

iii. 135° Swinger Magnet Supply

A failure occurred in a winding of the rectifier transformer of the 135° magnet power supply. The supply was designed for 0-750 amps at 0-40 volts output utilizing a tapped auto transformer to adjust the input line voltage in order to reduce regulator transistor power dissipation. As an alternative to rewinding the transformer, the auto transformer and rectifier transformer were replaced by a surplus Titan missile silo power supply. This supply is voltage regulated from 20 to 40 volts by use of a saturable reactor regulator.

Its control circuit was modified to maintain a conservative voltage drop across the regulator transistors. This feature insures that the transistor power dissipation will remain well below that of the original design and therefore increase its reliability. Final packaging of this configuration has been delayed by almost continuous use of the supply.

c. Data Processing

i. PDP-9 Computer

The PDP-9 computer has been operating fairly reliably this past year. Wear and tear effects are becoming visible on the line printer, card reader, and teletype units. These will need replacement within the next few years.

ii. ND-50/50 Pulse Height Analyzer

The Nuclear Data ND-50/50 pulse height analyzer interfaced to the PDP-9 continues to be a workhorse for data collection. The only difficulty experienced this year was intermittent failure of many of the miniature toggle switches on control panels. These have been replaced when needed.

d. Experimental Support

i. Energy-Loss Spectrometer

The electronics required for a spare position sensitive proportional counter for the spectrometer have been built. This includes helix and anode wire preamps and coincidence scintillator P.M. tube electronics.

ii. Time-of-Flight

The 30-meter flight path station has been completed. The detectors and support electronics are housed in a cement-block shed constructed west of the beam swinger. The flight path is through a hole cut in the concrete shielding wall. A full set of high voltage, fast and slow signal, and control cables have been installed as well as building power and cooling.

iii. X-ray Fluorescence System

The in-lab constructed interfaces for the PDP-8E control computer have been installed and are working. The software for the automatic system is running. This system reduces the manpower required to analyze trace element samples and allows more time to be devoted to sample mounting. Data reduction is also streamlined by the elimination of punched paper tape data storage.

iv. BART II Experiment Control

A versatile experiment controller, named BART II, was built for

use on the lab's pion experiment conducted this year at Berkeley. The system configuration is 1, a master sequence controller and timer; 2, a target transport system; 3, PHA control; and 4, cyclotron irradiate control. All time states are controllable in 1/10 second increments so as to be adaptable to many experimental conditions.

The target transport system was vaguely similar to the Bay Area Rapid Transit (BART) system, hence its BART II designation.

v. General Purpose NIM Modules

We continue to manufacture special function NIM modules which are not available on the commercial market.

7. Neutron Flux Survey of Environs - M. D. Otis, J. B. Martin, C. D. Zafiratos, C. S. Zaidins, and F. M. Edwards

On November 4, 1973, a survey of the neutron flux in the environs of the cyclotron was conducted. The results of an earlier neutron survey have been reported in a previous Progress Report (1968). This second survey was felt to be necessary because completion of the beam swinger led to a possibly significant change in the neutron flux near the Nuclear Physics Laboratory. Two effects due to this change in geometry were of interest: 1) changes in dose rates at the fence and at distant locations due to the new neutron source at the beam swinger target box, and 2) the effect, on neutron flux rates of changing the angle of the swinger. The relative numbers of neutrons produced by carbon and beryllium targets were also of interest.

It was established early in the survey that the beryllium target produced more neutrons by a factor of 30 than did the carbon target. Since the neutrons from carbon were too few for accurate measurement at the fence, beryllium was used for all distant measurements. It has been assumed that this factor of 30 is accurate at all swinger angles and beam currents, so that extrapolation can be made from beryllium back to the carbon Faraday-cup which is more typical of routine cyclotron operations.

Measurements were taken with the swinger at 0 degrees and 125 degrees. It was felt that these two angles offer the greatest differences in geometry relative to the shield wall. The 125 degree angle, moreover, offers the greatest potential for increased dose rates in the direction of occupied buildings.

The effect of the angle of the swinger proved to be quite small. Count rates at the fence line and in the control room changed by factors of 10 to 30 percent when the swinger was moved from 0 degrees to 125 degrees. As the errors in measurement are close to 10 percent, the effect of swinger angle, although easily detected, is not easily quantified.

Dose rates in mRem/hr-μa were calculated for both targets and both angles, assuming that the beryllium scaling factors between 0 degrees and 125 degrees hold also for carbon. The dose rates thus calculated indicate that the fence rather than the control room receives the limiting dose. However, a yearly average of 10^5 μa hours using 27 MeV protons and a carbon target would not exceed 0.5 Rem/year at the fence.

There was not enough time during this survey to map the dose rate within the building itself. Because the flux shows a tendency to increase as one moves out of the immediate shadow of the shielding concrete wall, such a mapping would be of some interest. The flux in the control room adjacent to this wall, which is currently used as the limiting factor in the interlocked neutron monitoring system, may not deliver the most significant dose. While the differences may not be large, they are probably worth measuring at some future date, particularly in view of the planned development of a new interlocked neutron-gamma monitoring system.

8. The Response of a Mariner-Jupiter-Saturn Photo-Polarimeter Spectrometer to Energetic Protons - W. R. Smythe, R. A. Ristinen; N. Taylor - LASP

A deep-space probe of the Mariner series, designed for a mission to Jupiter and Saturn, will include a photo-polarimeter spectrometer. This spectrometer is under development by the Laboratory of Atmospheric and Space Physics of this university. This spectrometer must function reliably during the four-year flight beginning in 1977, and must record optical spectra in the presence of charged-particle fluxes to be encountered, particularly in the Jovian Radiation Belts. In order to provide a laboratory test of the system which would be indicative of photomultiplier tube performance in the vicinity of Jupiter, the photocathode end of the spectrometer's photomultiplier was irradiated with a uniform flux ($10^5/cm^2/sec$) of 27 MeV protons. The resultant photometer count rate was observed for various photomultiplier gains. Preliminary results indicate that many pulses result for each incident proton, possibly due to multiple fluorescent excitations in the tube assembly with lifetimes appreciably longer than the 50 nanosecond pulse pair resolution time of the detection circuitry.

9. Calibration of Neutron Detectors - H. W. Fielding, F. M. Edwards, and R. E. Anderson

A set of five 8" diameter x 2" thick NE-224 scintillation detectors were constructed for (^{3}He,n) reaction studies. These detectors were to be used at higher neutron energies and higher bias settings than the 8" x 1" detectors we had used in (p,n) studies. Accordingly, it was decided to directly measure their efficiencies rather than attempting to scale the measured efficiencies of the thinner detectors.

In addition to the large detectors, a small 2" x 2" detector used for medical physics experiments was to be calibrated. In all, it was desired to calibrate the small detector over the range 2 MeV $\leq E_n \leq$ 21 MeV and the large detectors over the range 21 MeV $\leq E_n \leq$ 33 MeV.

Neutrons were obtained from the $^3H(p,n)$ and $^3H(d,n)$ reactions with Q values of -0.8 MeV and +17 MeV, respectively. The proton and deuteron beams were obtained from the Los Alamos F.N. Tandem Van de Graaff. The energy of neutrons available thus ranged between 2 and 33 MeV with the exception of the interval between 15 MeV and 20 MeV.

A standard recoil telescope[1] was used to provide an absolute measure of the neutron flux irradiating our detectors. The telescope utilized a thin polyethylene radiator (12 mg/cm^2 to 52 mg/cm^2) exposed to the neutron flux at 0°. The recoiling protons were detected in a ΔE-E telescope consisting of a surface barrier transmission detector and a scintillation detector. The (n,p) cross-sections were evaluated using the method[2] of Hansen and Smith. Knowing the geometries for the recoil telescope and our detector, the radiator thickness and the (n,p) cross-sections, the efficiency of our detector could be evaluated.

The results obtained for the large detectors for 20 MeV $\leq E_n \leq$ 33 MeV are shown in fig. C9-1. The two bias levels

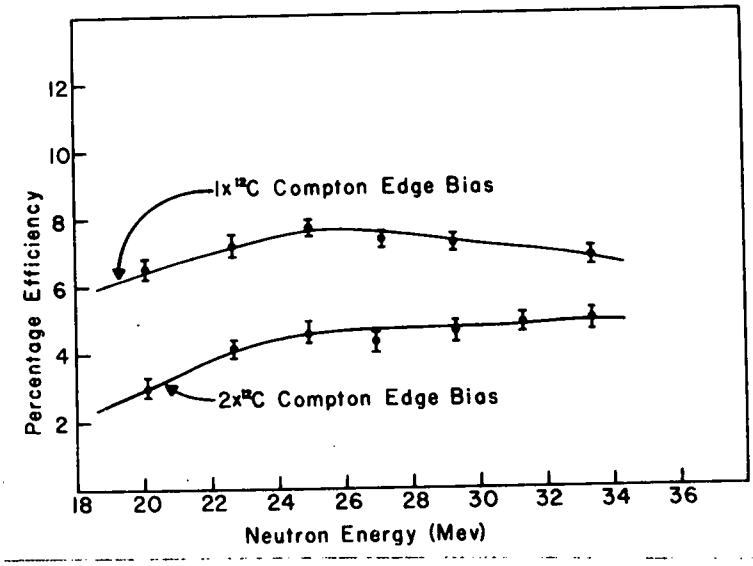

Fig. C9-1. Neutron detection efficiencies of a 2" x 8" NE-224 scintillation detector for two bias settings.

used are defined in terms of the Compton distribution produced in our detectors by the 4.43 MeV ^{12}C γ-ray produced by a Pu-Be source. The 1 x ^{12}C level is set at the half-height of this Compton edge and the gain is doubled for the 2 x ^{12}C setting.

This method of bias setting is reproducible to ±2% and the 2 x ^{12}C setting corresponds to a neutron energy near 15 MeV.

Although not shown here, results were also obtained for the 2" x 2" detector for bias settings of 1 x ^{60}Co and ½ x ^{60}Co.

The authors express their appreciation to R. K. Smith, R. F. Bentley, C. E. Moss, D. Drake, and the operating staff of the Los Alamos Tandem Van de Graaff facility.

---

[1] Supplied by R. K. Smith.

[2] R. K. Smith, private communication and G. E. Hansen and R. K. Smith, to be published.

D. Cyclotron Operation - A. B. Phillips

Operation for the period 1 September 1973 to 31 August 1974 is covered below. Table D-I shows hours of cyclotron operation by purpose. Table D-II shows hours of operation by type of particle accelerated. The 22-hour difference between the totals on the two tables represents time spent in tests of cyclotron components.

Of the 8760 hours in the year, the cyclotron was in use for 5721 hours, or 65% of the year. Actual beam-on-target time was 4399 hours, or 77% of cyclotron running time.

Cyclotron runs for outside users were 4 hours for Ball Bros. Research Corporation, Boulder, Colorado, and 38 hours in collaboration with Colorado State University, Ft. Collins, Colorado.

The cyclotron was out of commission for a total of 852 hours or 9.7% of the year. 255 hours were used for scheduled maintenance, 89 hours for scheduled repairs, and 508 hours for non-scheduled repairs.

Of the scheduled repair time, 40 hours were used to install a new cooling water tower. The old tower rusted out after 12 years of operation. The new tower, with 30% greater capacity, and no rustable parts, should last for the rest of the cyclotron lifetime.

The major non-scheduled repairs were 224 hours spent on failure of finger contacts on the RF short and 146 hours spent on repairing a water leak, caused by stray cyclotron beam, on the top of the RF liner inside the cyclotron. Included in the 852 hours for repairs is 56 hours for repairing a power supply on the energy-loss spectrometer. While this is not strictly a cyclotron repair, the time was lost from the operating schedule.

An attempt is being made to anticipate what parts of the cyclotron are most apt to break down due to age or wear. To this end, spare units are being accumulated. For instance, when a vacuum baffle refrigeration unit broke down, it was replaced in 4 hours instead of an estimated 4 days, which would have been needed to find and buy a replacement on an emergency basis.

In review, the cyclotron has either been in use or ready for use an estimated 85% of the year. Over the years, the two week annual maintenance period, a complete shut-down, has paid for itself by eliminating practically all of the potential small break-downs and a good many major break-downs.

Table D-III is a list of scheduled visitors to the laboratory during the period.

TABLE D-1

Hours of Cyclotron Operation - Purpose

Month	Cyclotron Development & Test	Research		Radionuclide Production		Subtotal Hrs/mo.
		Staff	Collaborate	Staff	Outside & Collaborate	
Sept. 73	3	510	---	---	---	513
Oct. 73	---	382	---	---	---	382
Nov. 73	7	486	---	---	---	493
Dec. 73	---	320	---	---	---	320
Jan. 74	---	400	---	---	---	400
Feb. 74	---	643	---	---	---	643
Mar. 74	---	658	---	---	---	658
Apr. 74	---	304	32	---	---	336
May 74	9T	305	---	---	---	314
June 74	13T	551	---	---	---	564
July 74	11	519	10	---	---	540
Aug. 74	1	557	---	---	---	558
Totals	22+22T	5635	42	---	---	5721

TABLE D-II

Hours of Cyclotron Operation - Particle

Month	Protons 0.25-27 MeV	Deuterons 7-17 MeV	H_2^+	^3He 16-41 MeV	^4He 3-36 MeV	Other	Sub-Total Hrs/mo.
Sept. 73	407	---	---	56	50	---	513
Oct. 73	105	66	---	105	106	---	382
Nov. 73	148	14	---	259	72	---	493
Dec. 73	154	---	---	66	100	---	320
Jan. 74	118	130	---	116	36	---	400
Feb. 74	69	18	---	508	48	---	643
Mar. 74	105	146	---	381	26	---	658
Apr. 74	32	42	---	149	113	---	336
May 74	128	69	---	91	17	---	314
June 74	101	113	---	302	35	---	564
July 74	127	---	---	360	53	---	540
Aug. 74	415	14	---	92	37	---	558
Totals	1909	612	---	2485	693	---	5699

TABLE D-III

Scheduled Visitors - 9/1/73 to 8/31/74

Date	No.	From
9-17-73	6	Colorado College, Colorado Springs, Colo.
10-2-73	30	C.U. class, Modern Physics
10-8-73	14	Flat Valley High School physics class, Kersey, Colorado
10-10-73	26	C.U. class, Physics 207
11-1-73	5	C.U. Molybdenum Project personnel
11-3-73	12	C.U. Denver Center physics class
11-10-73	15	C.U. ΣπΣ tour for high school students
12-1-73	26	C.U. Denver Center physics class
12-8-73	10	Cub Scouts, Boulder, Colorado
2-23-74	100	C.U. Engr. Dept. - Jr. Acad. of Science
3-12-74	110	C.U. class, Physics 112
3-15-74	8	C.U. class, Physics 560
4-22-74	13	C.U. class, Physical Sciences 102
4-23-74	20	C.U. class, Physical Sciences 102
5-8-74	18	High school physics class, Niwot, Colo.
6-17-74	18	Physics class, Colo. School of Mines, Golden, Colorado
7-22-74	55	High School Honors Conf., U. of Wyoming, Laramie, Wyoming
8-19-74	12	C.U. class
	498	

E. Outside Users of Cyclotron Facilities

The Nuclear Physics Laboratory has continued to encourage outside groups to make use of the cyclotron facility for educational or research purposes. These uses have included service irradiations, collaborative research, and educational tours of the laboratory.

The cooperative program with the University of Wyoming has continued. One of Professor Kunselman's graduate students, Mr. Harry Fielding, has completed his thesis research studies of the (^{3}He,n) reaction at this laboratory. Those (^{3}He,n) studies are reported in section II-A-3.

Professor Martin Rickey has spent the past year as a visiting professor in the Department of Physics. He has collaborated with J. J. Kraushaar and R. E. Anderson in the pion production studies reported in section II-B.

Professor W. P. Alford of the University of Ontario spent one week with us this summer during which he collaborated in (^{3}He,n) reaction studies reported in section II-A-3.

Professor S. D. Schery, formerly of Kenyon College in Gambier, Ohio, and now with Texas A & M at Galveston, Texas, spent two months at the laboratory and collaborated in the precision (p,n) studies described in section II-A-3.

Professor Joseph Comfort of Ohio University spent two weeks at the laboratory and also collaborated in the (p,n) studies described in section II-A-3.

Three staff members of the Los Alamos Scientific Laboratory--N. Stein, E. R. Flynn, and J. Sherman--collaborated in (^{3}He,t) studies described in section II-A-1-c.

Solar cell irradiations for Ball Brothers Research Corporation are described in section II-A-4.

For the fifth year we have provided volunteer time and laboratory facilities to students in the Hispano Summer Program of the Department of Physics and Astrophysics. This program works with selected Hispano students between their sophomore and junior years from Denver's North High School. The goal of the program is to acquaint these students with the possibilities and realities of higher education through a series of seminars, lectures, field trips, and laboratory work for one month. Our participation consisted of supplying lab space and instructors for eight of the students for 20 afternoon lab sessions. Various students and faculty volunteered time for this program.

There are, of course, a number of classes that visit the laboratory every year and these visitors are listed in the preceding section of this report.

III. THEORETICAL PROGRAM

A. Analysis of the $^{12}C(p,d)^{11}C$ Reaction at 700 MeV - E. Rost

An experimental group at Saclay, France, measured outgoing deuterons from a ^{12}C target excited by 700 MeV protons with sufficient energy resolution (about 50 keV) to resolve several discrete states. While at Saclay for the 1973-74 academic year, I collaborated with this group in analyzing the resulting $^{12}C(p,d)^{11}C$ angular distributions. This analysis was unusual because of the high energy (and consequently high momentum transfer) involved which required a number of approximations and/or special techniques. The results showed that nuclear two-step processes involving the 2^+ excitation of the ^{12}C target nucleus were important and could explain the rather large relative yield of the $5/2^-$ and $7/2^-$ states in ^{11}C. Qualitative agreement with the data was found for the relative magnitudes of the states excited although the data showed less structure than that predicted by a simple neutron pickup process. The possibility of observing N^* (i.e. excited nucleon) pickup was investigated and work along these lines is still in progress. A paper reporting the $^{12}C(p,d)^{11}C$ experiment and analysis has been accepted for publication in Physics Letters.

B. Baryon Resonance Transfer in Nuclear Reactions - E. Rost

The existence of the Saturne synchro-cyclotron data in the 1 GeV energy region (see previous section) stimulated theoretical investigations of the possibility of directly observing excited baryon components in the nucleus by pickup experiments. I was extremely fortunate to be able to collaborate with Leonard Kisslinger, who was visiting Orsay, France, at the same time I was at Saclay. Together with Richard Schaeffer of Saclay we calculated as best we could the effects of N^* admixtures in the nucleus and a joint paper on the subject is in preparation. The conclusion is that the baryon resonance degrees of freedom should be included for momentum transfers of 2 F^{-1} or greater and their effect can be comparable with ordinary nucleon transfer in some cases. The application of these ideas to the analysis of the Saclay data is in progress and future results from LAMPF are eagerly awaited.

C. N^* Admixtures in the Deuteron - E. Rost

In calculating N^* pickup in a nuclear reaction such as (p,d), one needs a rather accurate wave function for the relative N-N^* motion in the deuteron. In particular, the quantity

$$D_*(\Delta) = \left[\frac{\hbar^2\Delta^2}{2\mu_{NN^*}} + M\text{-}M_*\right] (4\pi)^{\frac{1}{2}} \int_0^\infty r^2 dr\, u_*(r)\, j_L(\Delta r)$$

is required for momenta Δ in the region 2-4 fm^{-1} and the cross-section is proportional to the square of this quantity. Here

$u_*(r)$ is the radial part of the relative N-N^* motion and must be calculated very accurately to give a reliable integral for D_*. A bound state coupled channel program was constructed for the deuteron with three channels; the usual ^3S and ^3D, and a N-N^* channel with arbitrary L and S. The computational difficulties were considerable due to the different scales involved (the "normal" deuteron components have a range ~4 fm, the N^* component range is about 0.2 fm) and the instabilities that occur in such a system. Nevertheless, an efficient and reliable integration-iteration scheme was developed and is currently being exploited. For the initial results presented in table III-I the couplings for the N-N parts were obtained from the Hamada-Johnston potential[1] renormalized by a strength λ in the presence of a given N^*. The N-N^* couplings are given by Jena[2] and use a generalized OPEP potential model. Finally, an incoherent sum over all N^*'s yields a probability of 1.2% in the deuteron.

TABLE III-I. Results of coupled channel calculations for the deuteron including a NN^* component. The NN interaction is $\lambda V_{\text{Hamada-Johnston}}$; the NN^* interaction is obtained in an OPEP model.

Partition	L	S	λ	% D	% N^*	$D_*(2.6\ \text{fm}^{-1})$ MeV-$\text{fm}^{3/2}$
$NN^*(1470)$	0	1	0.97	7.4	0.12	3.1
	2	1	0.96	6.4	0.10	8.0
$NN^*(1520)$	1	1	1.00	7.1	0.0002	0.3
	1	2	0.95	7.5	0.09	7.5
	3	2	0.93	6.1	0.11	5.1
$NN^*(1688)$	2	2	1.00	7.1	0.0001	0.2
	2	3	0.86	8.4	0.22	7.0
	4	3	0.81	4.8	0.21	2.1
$NN^*(1710)$	1	0	1.00	7.0	0.006	1.3
	1	1	0.94	6.8	0.19	9.8
$NN^*(1535)$	1	0	1.00	7.1	0.001	0.6
	1	1	0.99	7.0	0.05	5.1
$NN^*(1670)$	1	2	1.00	7.1	0.002	1.0
	3	2	1.00	7.1	0.002	0.5
	3	3	0.98	6.9	0.03	2.4
$NN^*(1780)$	0	1	0.99	7.1	0.02	1.4
	2	1	0.99	6.9	0.02	3.1
$NN^*(1860)$	0	1	1.00	7.1	0.0002	0.2
	2	1	1.00	7.1	0.0007	0.5
	2	2	0.99	7.0	0.01	2.3

[1] T. Hamada and I. D. Johnston, Nucl. Phys. 34 (1962) 382.
[2] S. Jena, Ph.D. Thesis, Carnegie-Mellon Univ., 1973.

D. Pion-Nucleus Scattering Calculations - M. Iverson and E. Rost

Pion-nucleus scattering was studied using a local potential which differs from the standard Kisslinger non-local potential in that it contains a term proportional to the Laplacian of the density rather than the derivative term which occurs in the Kisslinger potential. This allows one to use an efficient integration routine and substantially reduces the machine time required for a DWBA calculation involving pions. This modified potential was compared directly with the Kisslinger potential by transforming the latter so as to eliminate the derivative term. The local potential was found to give as good fits to the data.

In a recent paper, Kisslinger[1] suggested a new "almost local" potential which differs from his original potential by an additional term resulting from a Lorentz transformation of the pion-nucleon interaction from the pion-nucleon to the pion-nucleus center of mass system. The additional term, proportional to the Laplacian of the density, was added to the computer code[2] which calculates elastic scattering of pions on nuclei.

Theoretical calculations were performed to assist a LAMPF users group headed by Dr. Thornton Fisher of Lockheed in an experiment they are scheduled to do involving pion scattering from an aligned ^{165}Ho target. The calculations required modification of the calculation of inelastic scattering[3] of pions on nuclei so as to include elastic scattering from rotational nuclei with quadrupole deformations. The program calculates the scattering from either aligned or unaligned targets and allows for the possibility that the parameters describing the neutron distribution (including the deformation) may differ from those for the proton distribution. Fisher plans to use the results of his experiment to obtain information on the relative neutron and proton distributions and deformations in a strongly deformed nucleus.

---

[1] L. S. Kisslinger and F. Tabakin, Phys. Rev. C 9 (1974) 188.
[2] G. W. Edwards, PINUCLI, computer code.
[3] G. W. Edwards, Pionic DWUCK, computer code.

E. Pion Absorption in Complex Nuclei - D. A. Sparrow

One fundamental difference between nuclear reactions induced by pions and those induced by nucleons is the possibility of true absorption of the pion as it traverses the nucleus. An understanding of these absorption processes will be needed in order to construct a reliable reaction theory for the analysis of pion induced nuclear reactions. Unfortunately, these processes are not observable in the two-body system, and must therefore be understood through the analysis of reactions with complex targets.

In the absence of extensive pion absorption data, the most promising reaction is pion production by high energy nucleons. These experiments[1,2] have been analyzed quite successfully using a semi-classical model.[3] Recently it has been shown that the production cross-sections are sufficiently sensitive to the pion absorption rates to allow determination of these rates as a function of energy.[4]

Work at Colorado has focussed on improving the analysis of these experiments by including the effects of pion energy loss due to quasi-elastic scattering. Furthermore, it has been shown that such knock-out reactions may have an important effect on pion absorption cross-sections. Work in progress includes developing a model for this reaction which will allow a more precise determination of the absorption rate as both absorption and quasi-elastic cross-sections become available. A preliminary report on these developments was given at the Pittsburgh meeting of the APS.

---

1 D. R. F. Cochran, Phys. Rev. D 6 (1972) 3085.
2 K. O. Oganesyan, Soviet Phys. JETP 27 (1968) 679.
3 R. R. Silbar and M. M. Sternheim, Phys. Rev. C 8 (1973) 492.
4 D. A. Sparrow, M. M. Sternheim, and R. R. Silbar, submitted to Phys. Rev. C, July, 1974.

F. On Two-Step Processes via Particle Transfer Channels - P. D. Kunz

The calculation of second order processes in nuclear reactions involving intermediate states of different fragmentation has been examined carefully. The particular case investigated is the two-nucleon transfer reaction in which the second order term is considered to be a sequential transfer of the two particles. This term is difficult to calculate since one of the transfers involves an intrinsically non-zero range interaction and hence must in principle be calculated via a full finite range calculation. However, by making a post-prior interchange of the interaction, one can approximate the single transfer terms with the zero-range approximation and the second order term may be calculated directly by a coupled channels code such as CHUCK.

Although the post-prior matrix element equality is valid in a first order DWBA theory, it is not in a second order process since the intermediate state is off the energy shell and one is then left with a large correction term which must be evaluated. By some canonical algebraic manipulations we have reduced the correction term due to the post-prior interchange to a form which exactly cancels the first order term, i.e. the one describing the two particle transferred in a single step. Thus the first two terms of the series are reduced to a single second order term.[1]

However, the calculation of this amplitude is not without difficulties in that to recover the full amplitude one must sum the amplitudes over the complete set of intermediate states of the system for both the intermediate projectile and nucleus. While, in practice, only a few nuclear states are included because of selection rules, the set of continuum projectile states must be considered.

In the case of the (p,t) reaction proceeding via the deuteron, much of the sum rule strength for the sequential pick-up is accounted for by the deuteron ground state so that one might try using just the deuteron ground state in the two-step term. In order to be consistent one must use only the deuteron ground state in the correction term thus nullifying the exact cancellation between it and the first order term. Estimates of the correction term for the deuteron ground state show that it has the same form and is somewhat larger but of opposite sign to the first order term.[1,2] This suggests that one can use an empirical approach of calculating the second order term for only the deuteron ground state and using the strength and sign of the first order term as an adjustable parameter. This procedure seems to give a more systematic fit to the two-nucleon transfer data.[3,4]

---

[1] P. D. Kunz and E. Rost, Phys. Lett. 47B (1973) 136.
[2] T. Udagawa, H. H. Walter, and W. R. Coker, Phys. Rev. Lett. 31 (1973) 507.
[3] N. B. de Takacsy, to be published.
[4] W. R. Coker, T. Udagawa, and J. R. Comfort, to be published.

G. The Two-Step Method Applied to (p,t) Reactions - P. D. Kunz and J. R. Shepard

The problem of fitting (p,t) cross-sections in the mass region 40-60 is well known.[1,2] The ^{50}Ti(p,t) data at 23 MeV has been rather well fit with the modified two-step procedure described in the preceding section. It would be interesting to see if this procedure is valid over a wide energy range. We will use the 19, 23, and 27 MeV ^{50}Ti(p,t) data taken here at the University of Colorado, along with some data for the same reaction at 35 and 52.5 MeV taken at the Crocker Nuclear Physics Laboratory at the University of California at Davis, and some 40 MeV data from the Institute for Nuclear Science at Grenoble, France. Preliminary results for the 23 MeV, 35 MeV, and 52.5 MeV data are encouraging for a consistent fitting of both the strength and shape of the (p,t) angular distribution depending only upon the single parameter, the magnitude of the one-step contributions.

---

[1] H. W. Baer et al., Phys. Rev. Lett. 25 (1970) 1035.
[2] J. R. Shepard et al., Phys. Lett. 40B (1972) 95.

H. A Reanalysis of the $^{12}C(d,\tau)^{11}B$ Reaction at 80 MeV - P. D. Kunz and E. Rost

A recent paper[1] from the Jülich group claimed that their measurements of the $^{12}C(d,\tau)^{11}B$ reaction at 80 MeV supported a positive deformation for ^{11}B. This result was very surprising since ^{12}C is known to have a large, negative deformation and the simple shell model ideas that ^{11}B is roughly a $p_{3/2}$ hole coupled to the ^{12}C core would be completely erroneous. We have repeated the analysis using the conventional techniques of the coupled channels Born approximation and find that the data are not inconsistent with ^{11}B having the same deformation as ^{12}C. Several inconsistencies in the Jülich analysis were found and were pointed out in a paper submitted for publication in Physics Letters.

---

[1] O. Aspelund, D. Ingham, A. Dajaloeis, H. Kelleter, and C. Mayer-Böricke, Phys. Lett. 50B (1974) 441.

I. Multistep Contributions to (p,n) Reactions to Isobaric Analog States - P. D. Kunz and L. D. Rickertsen

Last year we reported calculations of the (p,n) reactions for a number of targets and several proton energies. The calculations which explicitly included the microscopic charge-exchange as well as the (p,d)(d,n) transition to second order in the interaction were able to give a good account of shapes of angular distributions using a 1 fm^{-1} range Yukawa effective interaction with a strength which was nearly the same for almost every nucleus and which had a very weak energy dependence. The calculations ignored the knock-on exchange which is known to have little effect on the shape of these angular distributions and which essentially renormalize the charge-exchange strength upward by about 20%.[1]

The calculations were not sensitive to the energy of the intermediate deuteron channels nor to reasonable changes of the optical potentials in any channel (with the exception of the absorption in the outgoing neutron channel).

Over the past year we have investigated other relevant questions concerning the role of the higher-order contributions to this reaction, including:

a) Higher order terms. Including the interaction only to 2nd order is equivalent to a 2nd order DWBA when the coupling back into any channel is neglected and the elastic scattering is provided by one optical model potential. It can be argued that the Born series may in fact diverge. We have calculated terms to third order in the interaction, including coupling back into the elastic channel, and find them to be negligible when compared to the large first-order term which presently provides the best fit to the data.

b) Correlations in target wavefunctions. In general, calculations of transitions to the analog states are insensitive to the configurations assumed for the (elastic channel) ground states. Large scale correlations in these wavefunctions may provide a correction, however, not because the transitions calculated do not correspond exactly to those of the actual reaction, but because additional strength can be obtained through two-step transitions forbidden for the simpler ground states. We have found such effects to be small except when the target is strongly correlated. When the deviations from the simple picture can be described by the collective model, explicit inclusion of the contributions due to these correlations provides an effective interaction which is consistent with spherical nuclei. For example, accounting for the collectivity in ^{26}Mg (and the analog nucleus) in the rotational model, fitting inelastic transition strengths to experiment and using the charge-exchange interaction appropriate for heavier nuclei (and including the (p,d)(d,n) two-step process for the spherical part of the wavefunction), excellent agreement with shape and magnitude of the (p,n) angular distribution was obtained.

c) The role of the deuteron continuum. In the representation of the coupled equations we use, it is possible, in principle, to account for every two-step process by expanding all possible intermediate states in the basis states of a single fragmentation. The actual number of states is restricted by the selection rules which generally apply to the matrix elements of the nucleon-nucleon interaction. In the previously reported work we have included the complete set of states for the target but have neglected explicit contributions due to the excited states of the intermediate projectile. We have attempted to include the deuteron breakup states in the (p,d)(d,n) process following the method of Johnson and Soper.[2] By breaking up the continuum into a discrete number of cells and taking all states in a cell at a single average energy, the interaction can be diagonalized to produce approximate eigenfunctions and overlap, D_o, for the pickup to this state. The number of cells can be increased and the procedure repeated until convergence is obtained. Calculations including these states, the folded deuteron optical potentials of Johnson and Soper,[2] and the transition strength to these states produced fits inferior to those obtained by ignoring them, reflecting the approximate nature of the procedure. Calculations repeated using only the deuteron bound state function, which we know very well, but the summed D_o strength obtained from the continuum calculation provided somewhat better fits and required a larger charge-exchange force to fit the data than was needed when the continuum was neglected altogether. The interference of the two-step process with the one-step is still destructive. The values obtained from these later calculations are shown in the table. The inclusion of knock-on exchange will probably reduce these values by about 20%.

---

[1] A. Galonsky, MSU preprint, 1973.
[2] R. C. Johnson and P. J. R. Soper, Phys. Rev. C 1 (1970) 976.

TABLE III-II. Charge exchange strengths to fit data.

Target (E_p=22 MeV)	Charge Exchange Only (MeV)	Charge Exchange + (p,d)(d,n) + Realistic g.s. Wavefunctions (MeV)	Charge Exchange + (p,d)(d,n) (Including continuum strength) (MeV)
^{26}Mg	26.2	33.0	---
^{40}Ar	21.7	36.3	---
^{48}Ca	20.0	33.0	---
^{54}Fe	20.4	32.3	38.2
^{56}Fe	18.5	33.0	39.0
^{58}Ni	17.9	33.0	---
^{64}Zn	18.2	32.6	---
^{90}Zr	19-32.5	33.4	---
^{96}Zr	16.9	32.8	---
^{120}Sn	17.1	33.8	---
^{208}Pb (26 MeV)	15.8 ±20%	31.0 ±10%	---

J. Comparison of the (α,^{3}He) and (α,t) Reactions on ^{24}Mg - L. D. Rickertsen and P. D. Kunz

It has been of interest for some time to study isospin breaking in direct nuclear reactions in order to sort out the effects due to Coulomb scattering from those involving, for example, Q value differences. The best place to look for such effects is in transitions forbidden by isospin selection rules. However, efforts to study ratios of cross-sections of mirror reactions which, in the absence of Coulomb effects and isospin breaking, are simply related to ratios of isospin Clebsch-Gordan coefficients have also been pursued. In the one-nucleon transfer reactions, it has not been easy to account for the deviations from simple isospin-conserving predictions in DWBA calculations largely because of the sensitivity to optical parameters. Last year we reported initial DWBA calculations for the (α,t) and (α,^{3}He) transitions from the ^{24}Mg ground state to mirror levels in ^{25}Mg and ^{25}Al. These detailed calculations reveal that: a) the DWBA alone is unable to account for the experimental or the theoretical ratios, and b) calculations explicitly including inelastic excitations in the initial and final nuclei reproduce the theoretical ratios reasonably well but the experimental angular distributions and ratios to a lesser extent.

The calculations need to be pursued further to ascertain whether the modest discrepancy is real or only apparent but at

present we can say that the latter calculations are not at all sensitive to optical parameters so that this aspect of the problem is not likely to be a factor. Finite range and non-locality effects have not yet been investigated.

K. Computer Codes - P. D. Kunz

The most recent version of DWUCK, a DWBA code, has been made ready for export. The instruction manual is nearly finished and the code should be ready for other nuclear physics groups to use.

A finite range version of DWUCK is under development. The advantages over other codes should be the speed of computation and more efficient computing organization so that the mass storage requirements of the program should be considerably reduced. Also, preliminary indications show that the size of core storage needed for the program should be modest so that the program can be adapted to smaller computers.

IV. PUBLICATIONS AND REPORTS

A. Published Articles

Widths of Analog States in Heavy Elements from (p,n) Spectra. H. W. Fielding, S. D. Schery, D. A. Lind, and C. D. Zafiratos, Phys. Rev. C 10 (1974).

Radius of the Neutron Distribution in ^{208}Pb from (p,n) Quasi-Elastic Scattering. S. D. Schery, D. A. Lind, and C. D. Zafiratos, Phys. Rev. C 9 (1974) 416.

Study of the ^{56}Fe(p,n)^{56}Co Reaction to the Anti-Analog State. H. W. Fielding, L. D. Rickertsen, P. D. Kunz, D. A. Lind, and C. D. Zafiratos, Phys. Rev. Lett. 33 (1974) 226.

A Diffraction Spectrometer for Studies of Particle Excited Radiative Transitions. J. H. Jett, N. S. P. King, D. A. Lind, and P. Henning, Nucl. Inst. and Meth. 114 (1974) 301.

Data Simulation Techniques for Reactions of the Form X(a,b,c)Y. M. J. Fritts, Nucl. Inst. and Meth. 117 (1974) 415.

Thick-Target Measurements of the (p,γ) Stellar Reaction Rates on the Nuclides ^{12}C, ^{29}Si, ^{46}Ti, ^{42}Ti and ^{56}Fe. N. A. Roughton, C. J. Hansen, M. J. Fritts, R. G. Peterson, and C. S. Zaidins, The Astrophysical Journal 188 (1974) 595.

Neutron-Proton Shell Model Multiplets in ^{88}Y and ^{90}Y from a Study of the (α,nγ) Reaction. H. W. Baer, R. L. Bunting, J. E. Glenn, and J. J. Kraushaar, Nucl. Phys. A128 (1974) 355.

Short-Lived Radioactivity Induced in Ge(Li) Gamma-Ray Detectors by Neutrons. R. L. Bunting and J. J. Kraushaar, Nucl. Inst. and Meth. 118 (1974) 565.

Nuclear Data Sheets for A=136. R. L. Bunting and J. J. Kraushaar, Nucl. Data Sheets 13 (1974) 191.

Identification of Silver in a Periapical Lesion of a Tooth. E. H. Macintyre, J. K. McClatchy, H. Rudolph, and J. J. Kraushaar, Amer. Journal of Clinical Pathology 60 (1973) 613.

Charge Exchange Reactions on ^{91}Zr. P. D. Ingalls and H. Rudolph, Nucl. Phys. A220 (1974) 191.

Inelastic Scattering Studies on ^{50}Cr. R. J. Peterson and E. W. Stoub, Nucl. Phys. A218 (1974) 109.

Microscopic Calculations for (p,n) Reactions to Isobaric Analog States. L. D. Rickertsen and P. D. Kunz, Phys. Lett. 47B (1973) 11.

On Two-Step Processes via Particle Transfer Channels. P. D. Kunz and E. Rost, Phys. Lett. 47B (1973) 136.

Micoscopic Analysis of (p,n) Reactions. P. D. Kunz, L. D. Rickertsen, and G. W. Hoffmann, Phys. Rev. C 9 (1974) 1659.

Field Mapping the Dipole Magnets for the University of Colorado Energy-Loss Spectrograph. D. E. Prull and S. C. Schery, Nucl. Inst. and Meth. 115 (1974) 339.

B. Articles Submitted for Publication

A Comparison of Fast Neutron Beams Provided by 17.3 MeV Deuterons Incident on Beryllium and Deuterium Targets. F. M. Edwards, H. W. Fielding, J. J. Kraushaar, and K. A. Weaver, submitted to Medical Physics.

The (p,n) Reaction to the Isobaric Analog State in High-Z Elements at 25.8 MeV. S. D. Schery, D. A. Lind, H. W. Fielding, and C. D. Zafiratos, accepted by Nucl. Phys.

Comparison of Activation and Direct Measurement Yields for the $^{13}C(p,n)^{13}N$ (g.s.) Reaction. D. A. Lind, R. J. Peterson, and H. W. Fielding, submitted to Physical Review.

A Study of the $^{106}Pd(p,d)^{105}Pd$ and $^{106}Pd(^{3}He,d)^{107}Ag$ Reactions. R. E. Anderson, R. L. Bunting, J. D. Burch, S. R. Chinn, J. J. Kraushaar, R. J. Peterson, D. E. Prull, B. W. Ridley, and R. A. Ristinen, submitted to Nucl. Phys.

Level Structure of ^{106}Ag. R. E. Anderson, R. L. Bunting, J. D. Burch, S. R. Chinn, J. J. Kraushaar, R. J. Peterson, D. E. Prull, B. W. Ridley, and R. A. Ristinen, submitted to Nucl. Phys.

Two-Step Processes in the (h,t) Reaction to the Analog and Anti-Analog States in ^{56}Co. L. D. Rickertsen, M. J. Schneider, H. Rudolph, J. J. Kraushaar, and W. R. Zimmerman, submitted to Phys. Lett.

The Decay of ^{36}K. M. J. Fritts, submitted to Phys. Rev.

A Method for Energy-Loss and Range Calculations Based on Empirical Approximations. C. S. Zaidins, submitted to Nucl. Inst. and Meth.

Stellar Reaction Rates for Proton Captures on ^{28}Si, ^{50}Cr, ^{54}Fe, ^{58}Ni, ^{60}Ni, and ^{61}Ni. N. A. Roughton, M. J. Fritts, R. J. Peterson, C. S. Zaidins, and C. J. Hansen, submitted to The Astrophysical Journal.

(^{3}He,2n) Excitation Functions for Some Light Nuclei. C. E. Moss and C. S. Zaidins, submitted to Nucl. Phys.

A Study of the Higher Excited States of ^{10}Be from the ^{9}Be(d,p)^{10}Be Reaction. R. E. Anderson, J. J. Kraushaar, M. E. Rickey, and W. R. Zimmerman, submitted to Nucl. Phys.

Study of Unbound Levels in ^{10}C via ^{10}Be(^{3}He,t). M. J. Schneider, B. W. Ridley, M. E. Rickey, and J. J. Kraushaar, submitted to Phys. Rev.

Nuclear Data Sheets for A=137. R. L. Bunting, submitted to Nuclear Data Sheets.

Weak Absorption Effects in the ^{48}Ca(^{16}O,^{15}N)^{49}Sc Reaction. M. J. Schneider, J. V. Maher, T. J. Lewis, J. C. Peng, C. M. Cheng, and H. S. Song, submitted to Phys. Rev.

Radioactive Products from Boron CTR Reactors. R. J. Peterson, C. S. Zaidins, M. J. Fritts, N. A. Roughton, and C. J. Hansen, submitted to Journal of Nuclear Energy.

The Direct (p,α) Pickup Reaction on the Even Isotopes of Zr. R. J. Peterson and H. Rudolph, submitted to Nucl. Phys.

On the Analysis of the ^{12}C(d,τ)^{11}B Reaction at 80 MeV. P. D. Kunz and E. Rost, submitted to Nucl. Phys.

The ^{12}C(p,d)^{11}C Reaction at 700 MeV. S. D. Baker et al. (Saturne Experimental Group) and E. Rost, accepted for publication in Phys. Lett.

The (^{3}He,α) Reaction at 216 MeV. E. Gerlic, J. Van de Weile, H. Langevin, J. P. Didelez, G. Duhamel, and E. Rost, submitted to Phys. Lett.

Two-Step Processes in Transfer Reactions. E. Rost, submitted to Journal de Physique.

Proton Spectroscopy of ^{105}Ag from the (^{3}He,d) Reaction. R. E. Anderson and J. J. Kraushaar, submitted to Nucl. Phys.

C. Published Abstracts and Conference Presentations

Analysis of the (p,n) Reaction to the Isobaric Analog State of ^{208}Pb in Terms of a Nuclear Matter Distribution Model. S. D. Schery, D. A. Lind, and C. D. Zafiratos, Bull. Am. Phys. Soc. 19 (1974) 60.

Investigation of the (^{3}He,n) Reaction on ^{48}Ti, ^{56}Fe, ^{60}Ni, and ^{64}Zn. H. W. Fielding, P. G. Brabeck, R. E. Anderson, D. A. Lind, and C. D. Zafiratos, Bull. Am. Phys. Soc. 19 (1974) 545.

The (^{3}He,n) Reaction on ^{46}Ti, ^{57}Fe, ^{68}Zn, ^{70}Ge, and ^{72}Ge at 25.5 MeV. H. W. Fielding, R. E. Anderson, M. F. Edwards, D. A. Lind, and C. D. Zafiratos, Bull. Am. Phys. Soc. 19 (1974) 644.

The (^{3}He,n) Reaction on ^{90}Zr, ^{92}Zr, ^{94}Zr, ^{112}Cd, and ^{114}Cd at 25.5 MeV. H. W. Fielding, M. F. Edwards, D. A. Lind, and C. D. Zafiratos, Bull. Am. Phys. Soc. 19 (1974) 644.

The (^{3}He,n) Reaction on Isotopes of Sn, In, and Mo. H. W. Fielding, R. E. Anderson, F. M. Edwards, D. A. Lind, C. D. Zafiratos, and W. P. Alford, Abstract for Pittsburgh Meeting.

Angular Distributions for the (p,n) Reactions to the Isobaric Analog States of ^{112}Sn, ^{116}Sn, ^{124}Sn at 23 MeV. S. D. Schery, J. R. Comfort, P. G. Brabeck, D. A. Lind, and C. D. Zafiratos, Abstract for Pittsburgh Meeting.

Stable Isotope Tracing by Charged Particle Activation. H. Rudolph, R. A. Ristinen, M. J. Fritts, and S. Christensen, Bull. Am. Phys. Soc. 19 (1974) 550.

Application of Helical Cathode Proportional Chambers to the University of Colorado Energy-Loss Spectrometer. E. W. Stoub and R. A. Ristinen, Bull. Am. Phys. Soc. 19 (1974) 528.

Proton Spectroscopy of ^{105,106,107}Ag. R. E. Anderson, R. L. Bunting, J. D. Burch, S. R. Chinn, J. J. Kraushaar, R. J. Peterson, B. W. Ridley, and R. A. Ristinen, Bull. Am. Phys. Soc. 19 (1974) 474.

A Study of the ^{24}Mg(^{3}He,t)^{24}Al Reaction at $E_{^{3}He}$=38.2 MeV. Nelson Stein, E. R. Flynn, J. Sherman, R. J. Peterson, and R. A. Ristinen, Bull. Am. Phys. Soc. 19 (1974) 643.

Trace Elements and Energy Resources - Nuclear Methods Analysis at the University of Colorado Nuclear Physics Laboratory. R. A. Ristinen, invited talk at the Workshop on Nuclear Techniques for Environmental Trace Element Information Relative to Energy Production and Consumption, Tallahassee, Fla., June 23-26, 1974.

Even More Stellar Nuclear Reaction Rates by Thick Target Techniques. N. A. Roughton, M. J. Fritts, R. J. Peterson, C. S. Zaidins, and C. J. Hansen, Bull. Am. Phys. Soc. 19 (1974) 644.

Detailed Study of the (^{3}He,t) Reaction to Analog and Anti-Analog States in ^{56}Co. M. J. Schneider, H. Rudolph, L. D. Rickertsen, J. J. Kraushaar, B. W. Ridley, and W. R. Zimmerman, Bull. Am. Phys. Soc. 19 (1974) 430.

Proton Spectroscopy of ^{86}Sr and ^{88}Sr. P. G. Brabeck, M. J. Schneider, and R. E. Anderson, Bull. Am. Phys. Soc. 19 (1974) 450.

Small Angle Structure in ^{48}Ca(^{16}O,^{15}N)^{49}Sc Angular Distributions. M. J. Schneider, J. V. Maher, T. J. Lewis, J. C. Peng, C. M. Cheng, and H. S. Song, Bull. Am. Phys. Soc. 19 (1974) 503.

Study of Unbound ^{10}C Levels via $^{10}B(^{3}He,t)$. M. J. Schneider, B. W. Ridley, M. E. Rickey, and J. J. Kraushaar, Abstract for Pittsburgh meeting of APS.

Progress in Understanding the (^{3}He,t) Reaction to Excited States of ^{56}Co. L. D. Rickertsen, M. J. Schneider, H. Rudolph, J. J. Kraushaar, and W. R. Zimmerman, Bull. Am. Phys. Soc., Abstract submitted for Pittsburgh meeting of APS.

Radioactive Products from Proton Reactions on ^{10}B. R. J. Peterson, C. S. Zaidins, M. J. Fritts, C. J. Hansen, and N. A. Roughton, Abstract for Pittsburgh meeting of APS.

Short-Lived Radioactivity Induced in Ge(Li) Gamma-Ray Detectors by Neutrons. J. J. Kraushaar and R. L. Bunting, Bull. Am. Phys. Soc. 19 (1974) 529.

Nuclear Data Sheets for A=136. R. L. Bunting and J. J. Kraushaar, Bull. Am. Phys. Soc. 19 (1974) 501.

The (d,p) and (p,π^{+}) Excitations of the 11.9 MeV State in ^{10}Be. M. E. Rickey, R. E. Anderson, J. J. Kraushaar, and W. R. Zimmerman, Bull. Am. Phys. Soc. 19 (1974) 431.

More Stellar Nuclear Reaction Rates by Thick Target Techniques. N. A. Roughton, M. J. Fritts, R. J. Peterson, C. S. Zaidins, and C. J. Hansen, Bull. Am. Phys. Soc. 19 (1974) 30.

Technecium Production by Low-Energy Proton Reactions on Molybdenum. R. J. Peterson, C. S. Zaidins, C. J. Hansen, M. J. Fritts, and N. A. Roughton, Bull. Am. Phys. Soc. 19 (1974) 473.

Production of ^{10}C in ^{9}Be by 300 to 740 MeV Protons. M. E. Rickey, R. E. Anderson, J. J. Kraushaar, J. Carrol, and H. W. Baer, Abstract for the Pittsburgh meeting of the APS.

Pion-Nucleus Reactions. E. Rost, LAMPF Summer School of Pion-Nucleus Scattering, LA-5443-C, 1973.

Inelastic Scattering. E. Rost, Journées d'Etude de Physique Nucléaire a Mageuve Energie, Gif-sur-Yvette, 1973.

Effet de structure nucléaire a haute énergie. E. Rost, Mesure et interpretation des impulsions élevées dans les Noyaux, Saclay, 1974.

Recent Results in the Study of (p,n) Reactions. C. D. Zafiratos, invited talk at the Sale Lake City meeting of the APS, Bull. Am. Phys. Soc. 19 (1974) 671.

D. Thesis

Measurement of ^{3}He Spin Analyzing Power of 27 MeV Protons and 15.5 MeV ^{4}He. Randolph Howard Ware, Ph.D., 1974.

V. PERSONNEL

A. Academic and Scientific

R. E. Anderson	Research Associate
R. L. Bunting[1]	Research Associate
F. E. Cecil[2]	Research Associate
M. J. Fritts[3]	Research Associate
J. J. Kraushaar	Professor
P. D. Kunz	Professor
D. A. Lind	Professor
L. L. Nunnelley[4]	Research Associate
R. J. Peterson	Assistant Professor
L. D. Rickertsen[5]	Research Associate
M. E. Rickey[6]	Visiting Professor
B. W. Ridley	Professor
R. A. Ristinen	Professor, Chairman of Laboratory until August 1, 1974
E. S. Rost[7]	Professor
N. A. Roughton[8]	Research Associate
H. Rudolph[9]	Research Associate
M. J. Schneider	Research Associate
W. R. Smythe	Professor
D. A. Sparrow[10]	Research Associate
H. H. Wieman[11]	Research Associate
C. D. Zafiratos	Professor, Chairman of Laboratory from August 1, 1974
C. S. Zaidins	Associate Professor

B. Technical and Support Staff

R. H. Akers[12]	Electrician
R. C. Armstrong	Research Technician
J. Boyd[13]	Research Technician
E. C. DeGabain	Instrument Maker
B. A. Deobler[14]	Design Engineer
L. A. Erb	Electronics Engineer
J. L. Homan	Research Technician
L. R. McKissick[15]	Designer-Draftsman
W. G. Minor	Instrument Maker
A. B. Phillips	Cyclotron Engineer
D. E. Prull	Research Physicist
J. N. Sonnenberg	Administrative Assistant
J. W. Trish[16]	Research Technician
A. K. Wiles	Instrument Shop Foreman

C. Research Assistants

P. G. Brabeck[17]	M. S. Iverson
J. D. Burch	M. L. Munger
H. H. Chang	A. S. Rosenthal[22]
S. R. Chinn[18]	R. R. Sercely[23]
N. J. DiGiacomo[19]	E. W. Stoub[24]
S. T. Durrance[20]	R. H. Ware[25]
R. A. Emigh	W. R. Zimmerman
H. W. Fielding[21]	

D. Other Students (part-time)

S. Allen
R. Bernthal[26]
B. Briggs[27]
S. Christensen[27]
S. Christianson[26,27]
S. Depetris[27]
O. Ehrlinger
F. Greene
S. Greene
N. Iverson
L. Johnson[27]
M. Mauro[26]
R. Perko[27]
A. Randall[27]
P. Schreck[26]
O. Sharp
M. Sher[27]
S. Wilmeth[27]
K. Woellhof[26,27]
L. Zanetti[27]

Independent study project - Margaret Wacker

---

1 NIRA appointment, ended August, 1974. Now at Aerojet Nuclear, Idaho Falls, Idaho.
2 Appointment began September, 1974.
3 Appointment ended August, 1974. Now at Naval Research Laboratory, Washington, D. C.
4 Appointment began October, 1974, funded by NIH.
5 Appointment ended August, 1974. Now at Oak Ridge National Laboratory.
6 On leave from Indiana University, Bloomington, academic year 1973-74.
7 On leave 1973-74 academic year at Saclay, France.
8 Part-time appointment. Chairman, Department of Physics, Regis College, Denver, Colorado.
9 Appointment ended July, 1974. Partially funded by NSF; now at University of Pittsburgh, Pittsburgh, Pennsylvania.
10 Appointment began September, 1974.
11 Appointment began October, 1974.
12 Appointment ended January, 1974.
13 Supported by NSF grant. Appointment ended February, 1974.
14 Appointment ended February, 1974.
15 Half-time appointment, began February, 1974.
16 Supported by NSF grant. Appointment began February, 1974.
17 Appointment ended June, 1974.
18 Appointment ended August, 1974.
19 Appointment began September, 1974.
20 Appointment began September, 1974.
21 Supported by the University of Wyoming.
22 Appointment began June, 1974. Worked part-time academic year 1973-74.
23 Appointment began June, 1974.
24 Appointment ended August, 1974. Now at Colorado School of Mines, Golden, Colorado.
25 Ph.D., 1974. Now at JILA, University of Colorado, Boulder, Colorado.
26 Supported by NSF grant.
27 Appointment ended 1974.